UNIVERSITÉ DU QUÉBEC À MONTRÉAL

A FRAMEWORK TO STUDY THE POTENTIAL BENEFITS OF USING HIGH-RESOLUTION REGIONAL CLIMATE MODEL SIMULATIONS.

THESIS

PRESENTED

AS PARTIAL REQUIREMENT

FOR PHD DEGREE IN EARTH AND ATMOSPHERIC SCIENCES

BY

ALEJANDRO DI LUCA

JULY 2011

UNIVERSITÉ DU QUÉBEC À MONTRÉAL

UN CADRE POUR ÉTUDIER LES AVANTAGES POTENTIELS DE L'UTILISATION DES SIMULATIONS À HAUTE RÉSOLUTION DE MODÈLES RÉGIONAUX DU CLIMAT

THÈSE

PRÉSENTÉE

COMME EXIGENCE PARTIELLE

DU DOCTORAT EN SCIENCES DE LA TERRE ET DE L'ATMOSPHÈRE

PAR

ALEJANDRO DI LUCA

OCTOBRE 2011

REMERCIEMENTS

D'abord, je tiens à remercier mes superviseurs, René Laprise et Ramón de Elía, tout simplement parce que ce fut un plaisir d'avoir à partager l'expérience de la recherche au cours de ces cinq dernières années et parce que, grâce à leurs conseils, commentaires et nombreuses discussions, j'ai pu accomplir mon doctorat.
À René pour la précision de ses conseils, scientifiques et autres, qui m'ont énormément aidé pendant tout ce temps. Pour avoir toujours trouvé le mot juste et optimiste.
À Ramón pour sa patience et sa sagesse pour me guider. Parce qu'il m'a incité et encouragé à réfléchir sur des questions qui vont au-delà des problèmes techniques mais, qui sans doute font partie de la recherche scientifique et qui ont contribué à développer mon esprit critique. En bref, parce que plus que quiconque, il m'a montré la voie à suivre pour devenir un scientifique.

Au centre ESCER pour le soutien financier qui m'a permis de me consacrer à temps plein au doctorat et d'assister à de nombreuses conférences scientifiques qui ont enrichies mes connaissances et mes liens avec d'autres collègues.

À Georges, Abderrahim, Frédèrik et Mourad pour l'inestimable aide technique et à Delphine et Adelina qui m'ont toujours aidé à surmonter les nombreux problèmes administratifs.

À tous les collègues et amis de l'UQAM et d'Ouranos, qui ont toujours été prêts à me donner un coup de main quand j'en ai eu besoin et qui ont égayé les innombrables 5 à 7 et d'autres bons moments.

À tous les amis, qui sont les grands responsables de ces cinq dernières années très heureuses passées à Montréal.

Finalmente, agradezco profundamente a toda mi familia, particularmente a mis viejos, a Pauli y a Eugi, por estar siempre ahí : generosos, comprensivos, estimulantes y tan queribles.

CONTENTS

x

LIST OF FIGURES

LIST OF TABLES

LIST OF ACRONYMS

AOGCM	Atmospheric-Ocean General Circulation Model
AMIP-II	Atmospheric Model Intercomparison Project II
AV	Added Value
BBE	Big Brother Experiment
CC	Climate Change
CGCMs	Coupled General Circulation Models
CPC	Climate Prediction Center dataset
CRCM	Canadian Regional Climate Model
DT	Downscaling Technique
ERA40	ECMWF 40-year re-analysis data
GCM	Global Climate Model
HRD	High-Resolution Data
HRGCM	High-Resolution Global Climate Model
LAM	Limited Area Model
LBC	Lateral Boundary Condition
LRGCM	Low-Resolution Global Climate Model
MCG	Modèle de Circulation Générale
MR	Multi-Resolution approach
MRC	Modèle Régional de Climat
NARCCAP	North American Regional Climate Change Assessment Program
NARR	North American Regional Reanalysis
NCEP	National Centers for Environmental Prediction
PAV	Potential Added Value
RCM	Regional Climate Model
rPAV	Relative Potential Added Value

SD	Statistical Downscaling
SI	Sea Ice
SST	Sea Surface Temperature
UWash	University of Washington precipitation dataset
VGCM	Virtual Global Climate Model

RÉSUMÉ

La modélisation du climat à haute résolution est nécessaire aux études d'impact du climat et, de nos jours, les modèles de circulation générale (MCG) n'ont pas encore une résolution suffisante pour satisfaire ces besoins. Les modèles régionaux du climat (MRC) ont été développés dans le but de fournir des détails sur le climat à fine échelle sur des régions spécifiques de la Terre. Les MRC ont démontré leur capacité à produire de la variabilité spatiale à petite échelle qui manque dans les simulations de MCG ; pour cette raison, les MRC sont de plus en plus utilisés dans les études sur le climat actuel et futur. Malgré ce succès, les avantages découlant de la production d'une variabilité climatique de fine échelle - autres que l'effet visuel saisissant des animations réalistes - ont rarement été clairement identifiés. Les tentatives pour quantifier ces avantages, généralement désignés comme étant la valeur ajoutée (VA) des MRC, ont été relativement rares et ont prouvé que la question de la VA est très complexe.

Compte tenu de cette complexité, ce projet se concentre sur un aspect particulier de cette question : l'étude des conditions préalables que doivent satisfaire certaines statistiques climatiques pour permettre aux MRC d'ajouter de la valeur aux données utilisées comme pilote. Ces conditions sont basées sur l'idée que la VA des MRC ne peut survenir que si les statistiques climatiques d'intérêt contiennent de l'information à fine échelle qui n'est pas négligeable. Des données observées et simulées par des MRC peuvent ensuite être utilisées pour quantifier l'influence relative des fines échelles dans les statistiques climatiques, comme un proxy, pour estimer la valeur ajoutée potentielle (VAP) des MRC. Deux méthodes différentes ont été utilisées pour étudier la VAP sur l'Amérique du Nord, respectivement pour la température de surface et la précipitation. Les deux méthodes comprennent 3 étapes : l'utilisation d'une technique de décomposition pour séparer les variables atmosphériques en plusieurs échelles temporelles et spatiales, le calcul de statistiques climatiques et la définition d'une quantité pour estimer la VAP.

Pour la température, nous constatons que la VAP se dégage presque exclusivement dans des régions caractérisées par des forçages de surface importants, soit la présence de topographie de fine échelle ou de contrastes terre-mer. Par ailleurs, certains des processus qui produisent la variabilité de petite échelle semblent être liés à des mécanismes relativement simples tels que la réponse linéaire aux différentes propriétés physiques de la surface et la variation générale de la température avec l'altitude dans l'atmosphère.

Le potentiel des MRC à ajouter de la valeur dans les projections futures de la température moyenne est brièvement étudié. L'analyse montre que la variabilité de fine échelle du signal du changement climatique est généralement très faible par rapport à celle de grande échelle, ce qui suggère que peu de VA est attendue pour cette statistique climatique.

Pour les précipitations, les résultats montrent que la VAP est fortement liée à des instabilités hydrodynamiques de fine échelle. La VAP est beaucoup plus élevée sur de

courtes échelles temporelles (par exemple, pour des données sur 3 heures) et pour la saison chaude en raison de la proportion plus élevée de précipitations produites par de petits systèmes météorologiques et systèmes convectifs. Dans les régions à topographie complexe, le forçage orographique induit une composante supplémentaire de VAP, peu importe la saison ou l'échelle temporelle considérée. Les résultats montrent aussi que les MRC ont tendance à reproduire relativement bien la VAP par rapport aux observations bien qu'ils montrent une légère surestimation de la VAP en saison chaude et dans des régions montagneuses.
Les résultats démontrent l'utilité du cadre utilisé pour étudier la VAP dans le climat actuel et dans des projections futures. Il est souligné que l'étude approfondie de la VA des MRC devrait aider à comprendre comment utiliser le mieux les divers produits climatiques disponibles en appui aux études en impact et adaptation face au climat changeant.

Mots-clés : modèles régionaux du climat, valeur ajouté potentielle, Amérique du Nord, température, précipitation.

ABSTRACT

High-resolution climate information is necessary to support climate-impact assessment studies, and present-day General Circulation Models (GCMs) do not run at a resolution sufficient to satisfy these needs. Regional Climate Models (RCMs) were developed with the aim of providing fine-scale climate details over particular regions of the Earth.
RCMs have been shown capable of producing the small-scale variability lacking in GCM simulations, and for this reason RCMs are widely and increasingly used in research studies of present and future climate. Despite this success, benefits arising from resolved fine-scale variability –other than the stunning visual effect of realistic animations– have seldom been clearly identified. Attempts to quantify these benefits, generally designated as the added value (AV) of RCMs, have been relatively rare and proved that the AV issue is very complex.
In view of this complexity, the present project focuses on a particular aspect of this issue, the study of prerequisite conditions that observed and RCM-derived climate statistics of interest must satisfy for RCMs having any chance of adding value over the coarser driving data. These conditions are based on the idea that RCM's AV can arise only if climate statistics of interest contain non-negligible fine-scale information. Observed and RCM-simulated data can then be used to quantify the relative influence of fine scales in climate statistics as a proxy for estimating the *potential* added value (PAV) of RCMs.
Two different methodologies are used to investigate the PAV in near-surface temperature and precipitation respectively. Both methodologies include the use of a decomposition technique to separate atmospheric variables in several temporal and spatial scales, the computation of various climate statistics and the definition of a PAV quantity that estimates the contribution to the climate statistics coming from those small-scales represented by RCMs but absent in the driving data.
For temperature, we find that the PAV emerges almost exclusively in regions characterised by important surface forcings either due to the presence of fine-scale topography or land-water contrasts. Moreover, some of the processes leading to fine-scale variability appear to be related with relatively simple mechanisms such as the distinct physical properties of the Earth surface and the general variation of temperature with altitude in the Earth atmosphere.
The potential of RCMs to add value in the simulation of the future mean-temperature change is briefly studied. The analysis shows that the fine-scale variability of the climate change signal is generally very small compared to its large-scale part, suggesting that little AV can be expected for the time-averaged temperature.
For precipitation, results show that the PAV is strongly related with fine-scale hydrodynamic instabilities leading to much higher PAV values for short temporal scales (e.g., 3-hourly data) than for long temporal scales (16-day average data) and for warm com-

pared to cold season due to the higher proportion of precipitation falling from small-scale weather systems in the warm season. In regions of complex topography, the orographic forcing induces an extra component of PAV, no matter the season or the temporal scale considered. Results also show that RCMs tend to reproduce relatively well the PAV compared to observations although showing an overestimation of the PAV in warm season and mountainous regions.
Results demonstrate the usefulness of the framework used to study the PAV in present climate and future projections and suggest its application to investigate a broader spectrum of factors influencing AV issues, i.e. other variables, climate statistics, regions. It is highlighted that these studies should help in order to get a clearer idea on how to use the several available climate products in various applications but particularly in support of impact and adaptation studies in the context of a changing climate.

Keywords : regional climate models, potential added value, North America, temperature, precipitation.

RESUMEN

La información climática de alta resolución espacial es necesaria para realizar estudios de evaluación del impacto del clima y, hoy en día, la resolucion utilizada en simulaciones realizadas con modelos de circulación general (MCG) no es suficiente para satisfacer estas necesidades. Con el objetivo de obtener información climática de pequeña escala en regiones especificas se desarrollaron los modelos climáticos regionales (MCR). Los MCR son capaces de generar variabilidad de pequeña escala ausente en las simulaciones de los MCG y, por esta razón, los MCR han sido y son frecuentemente utilizados en estudios que investigan aspectos relacionados con el clima presente y futuro.

A pesar de este éxito, los beneficios derivados de resolver los detalles climáticos de pequeña escala rara vez han sido claramente identificados. Los intentos de cuantificar estos beneficios, generalmente designados como el valor agregado (VA) de MCR, han sido relativamente escasos y han mostrado que la cuestión del VA es muy compleja.

En vista de esta complejidad, este proyecto se centra en un aspecto particular que apunta a estudiar condiciones previas que las estadísticas climáticas de interés deben satisfacer para que los MCR tengan la posibilidad de agregar valor a los datos utilizados como piloto. Estas condiciones se basan en la idea de que los MRC pueden generar VA si y sólo si las estadísticas de interés contienen información de pequeña escala que no es despreciable. Datos observados y simulados pueden ser entonces utilizados para cuantificar la influencia relativa de escalas finas en las estadísticas del clima y así estimar el valor agregado potencial (VAP) de los MRC.

Se investiga el VAP en América del Norte utilizando dos metodologías diferentes para la temperatura de superficie y la precipitación, respectivamente. Ambas metodologías incluyen el uso de una técnica de descomposición para separar las variables atmosféricas en varias escalas temporales y espaciales, el cálculo de diversas estadísticas climáticas y la definición de variables que describen el VAP.

Para la temperatura, los resultados muestran que el VAP surge casi exclusivamente en regiones caracterizadas por forzantes de superficie, ya sea debido a la presencia de topografía de pequeña escala o por contrastes entre el mar y la tierra. Se observa que algunos de los procesos que conducen a generar la variabilidad de pequeña escala parecen estar relacionados con mecanismos relativamente simples, tales como la variación general de la temperatura con la altura en la atmósfera o la mejor discretización de los gradientes lineales. El potencial de los modelos climáticos regionales para agregar valor en la simulación de la temperatura en el futuro también se estudió brevemente. El análisis muestra que la señal del cambio de temperatura entre el presente y el futuro está principalmente dominada por la gran escala con escasa variabilidad de pequeña escala, lo que sugiere un limitado VAP para esta variable en particular.

Para la precipitación, los resultados muestran que el VAP está fuertemente relacionado

con inestabilidades hidrodinámicas de pequeña escala que inducen mayor VAP en cortas escalas temporales (por ejemplo, en datos cada 3 horas) y en la estación cálida debido a la mayor proporción de precipitación producida por sistemas de pequeña escala. En regiones de topografía compleja, el forzante orográfico induce una componente extra de VAP, sin importar la estación o la escala temporal considerada. Los resultados también muestran que los modelos climáticos regionales tienden a reproducir relativamente bien el VAP en comparación con las observaciones, aunque presentan una ligera sobreestimación del VAP en la estación cálida y algunas regiones montañosas.
Los resultados demuestran la utilidad del marco que se utiliza para estudiar el VAP en el clima actual y en las proyecciones futuras y sugieren su aplicación para investigar otros factores que influyen el valor agregado (por ejemplo, otras variables, estadísticas climáticas, regiones, etc). Se destaca que el estudio mas profundo de factores relacionados con el valor agregado debe ayudar a entender mejor la manera mas eficiente del uso de los diversos productos climáticos disponibles en diversas aplicaciones, pero en particular en apoyo de los estudios de impacto y adaptación en el contexto del cambio climático.

Palabras claves : modelos climáticos regionales, valor agregado potencial, América del Norte, temperatura, precipitatión.

INTRODUCTION

Context

Numerical modelling constitutes the only way to attempt to simulate the evolution of extremely complex non-linear systems. The Earth climate constitutes such a complex system by including several complicated dynamical sub systems (e.g., atmosphere, land surface, oceans, ice, etc), each one exerting a considerable influence on the others. Atmospheric-Ocean General Circulation Models (AOGCMs) constitute the primary and most comprehensive tools to study past, present and future climate. AOGCMs include dynamical components describing atmospheric, oceanic and land-surface processes, as well as sea ice and other components of the Earth system that influence the climate on time scales ranging from minutes to several hundred and even thousand years. AOGCMs consist of a set of coupled differential equations that are solved using some numerical scheme, subject to a set of external boundary conditions (e.g., intensity of solar irradiance) and initial conditions.

It is generally accepted that the reduced numerical truncation afforded by an increase in the horizontal and vertical resolution of the grid mesh used to discretize the differential equations in models leads to an improvement in the simulation of the climate compared to its coarser resolution version. There is, however, an implicit assumption in the last statement that the parameterizations of subgrid-scale processes have been adapted to the higher resolution, as the appropriateness of these subgrid-scale representations may be altered by changes in resolution and hence call for new physical parameterizations or a retuning of the existing ones (Boer and Lazare 1988; Pope and Stratton 2002; Knutti 2008). Assuming that the recalibration process was performed and that the model formulation was adapted to its "new" resolution, several arguments can be presented to support the expectation of an improvement in the simulated climate through an increase in resolution.

First, the enhanced resolution leads to a more accurate discretization of the differential equations that describe fundamental physical laws due to a reduction in the truncation error. This implies that, particularly for those dynamical processes that are

little affected by parameterizations, the finer resolution generally improves the simulation (Knutti 2008).

Second, new small-scale features can appear due to a variety of processes related with the finer spatial scales explicitly resolved (e.g., non-linear interactions between large and small scales, development of hydrodynamics instabilities, etc). For example, the better representation of temperature and humidity gradients can trigger smaller-scale hydrodynamic instabilities that may lead to a more realistic description of the spatio-temporal distribution patterns of precipitation.

Third, an increase in the resolution of the atmospheric grid mesh is generally accompanied by a similar increase in the resolution of surface fields such as topography, lakes, coastal regions and others. The more detailed surface forcings can modify meteorological variables locally, mainly those variables strongly influenced by the surface (e.g., 2-m temperature, humidity), but also away from the surface due to the perturbation of planetary-scale atmospheric flows. For example, in regions of complex topography, the use of a finer grid mesh would resolve small-scale near-surface temperature gradients due to the better described mountains profiles, combined with the general variation of atmospheric temperature with altitude. Another example is given by the interaction between middle-latitude synoptic precipitating systems and a higher-resolution topography. The presence of higher mountains and the potential improvement in the representation of mountain waves may enhance the rain shadow effect in the lee side of the mountains, influencing the precipitation locally but also far from the mountains due to the conservation of water in the system (e.g. Fig. 6 of Laprise et al. (2008)).

Notwithstanding the potential advantages of high-resolution meshes, in practice however, the resolution of climate models is constrained by the limited availability of computing resources. The current resolution of climate models results from a compromise between the number and length of ensemble members, the desired complexity of physical processes described (e.g., carbon cycle, atmospheric chemistry) and the variety of external forcings considered (e.g., greenhouse-gases emission scenarios) (Randall et al. 2007). For example, the current horizontal grid spacing of the atmospheric component of state-of-the-art AOGCMs is about 200 km (Randall et al. 2007).

In order to circumvent the practical impossibility of making operational high-resolution climatic simulations at the global scale, several downscaling techniques (DT) have been developed (Giorgi and Mearns 1991; Rummukainen 2010). DTs attempt to translate the large-scale, low-resolution atmospheric fields into local, high-resolution in-

formation of the climate variables of interest. A description of the different downscaling approaches can be found in Giorgi and Mearns (1991) and a more recent discussion can be found in Laprise et al. (2008) (dynamical downscaling) and Wilby et al. (2004) (statistical downscaling).

In this thesis, we concentrate on the analysis of results derived using nested, limited-area, regional climate models (RCMs). Basically, the RCM technique allows for an increase in resolution by concentrating the degrees of freedom, and hence the computational resources, over a limited region of the globe where the main interest of a user lies (Laprise et al. 2008). Technically, it consists of using time-dependent large-scale atmospheric fields and ocean surface boundary conditions to drive a high-resolution atmospheric model integrated over a limited-area domain (Giorgi et al. 2001). The atmospheric driving data are either derived from simulations of lower resolution General Circulation Models (GCMs) simulations or analyses of observations.

The concept of added value

The paradigm behind the nesting technique is that RCMs can be used as magnifying glasses to obtain regional or local details from coarse-resolution global fields either derived from reanalyses or GCM simulations (Giorgi et al. 2001; Laprise et al. 2008; Rummukainen 2010). RCMs are supposed to improve the representation of the climate compared to the driving data, generating what is generally designated as the *added value (AV)* of RCMs.

In order to illustrate the AV issue and the particular topic that is dealt with in this thesis, let us consider a hypothetical AV study (a more general example is discussed in Appendix 3.A). Lets suppose that we are trying to decide whether an RCM adds value over a GCM in the representation of some climate statistics X (e.g., time-averaged precipitation). Assuming that the metric chosen to assess model's performance is given by the squared error (SE), then the AV can be defined by

$$AV = (X_{GCM} - X_{OBS})^2 - (X_{RCM} - X_{OBS})^2 = SE_{GCM} - SE_{RCM}. \qquad (1)$$

Defined in this way, the RCM generates some AV if its SE is smaller than the GCMs one, i.e., if AV is larger than 0.

In order to gain more insight on the sources of AV, let us separate the field

according to different spatial scales and express the value of X_{OBS} as follows:

$$X_{OBS} = X^{ls}_{OBS} + X^{ss}_{OBS}, \tag{2}$$

where the super-scripts *ls* and *ss* designate, respectively, the *large scales* and *small scales* that are permitted or not by the GCM grid. Hence by definition $X^{ss}_{GCM} = 0$ and

$$X_{GCM} = X^{ls}_{GCM}. \tag{3}$$

Similarly the RCM-derived climate statistics (X_{RCM}) may be decomposed as

$$X_{RCM} = X^{ls}_{RCM} + X^{ss}_{RCM}. \tag{4}$$

Replacing Eqs. (2), (3) and (4) in Eq. (1), rearranging and neglecting covariance terms (see below and in Appendix 3.A for details), we obtain:

$$AV = AV^{ss} + AV^{ls}, \tag{5}$$

where

$$\begin{aligned} AV^{ss} &= (X^{ss}_{OBS})^2 - SE^{ss}_{RCM} \\ &= (X^{ss}_{OBS})^2 - (X^{ss}_{RCM} - X^{ss}_{OBS})^2, \end{aligned} \tag{6}$$

and

$$AV^{ls} = SE^{ls}_{GCM} - SE^{ls}_{RCM}. \tag{7}$$

That is, the AV can be approximately decomposed into a small-scale term (AV^{ss}) and a large-scale term (AV^{ls}). Three conditions must be satisfied for the RCM to generate small-scale added value ($AV^{ss} > 0$):

- the observed climate statistics X_{OBS} must contain non-negligible fine-scale information ($(X^{ss}_{OBS})^2 > 0$),
- the RCM-derived climate statistics X_{RCM} must contain non-negligible fine-scale information ($(X^{ss}_{RCM})^2 > 0$), and
- the fine-scale RCM information must have some skill, i.e. $(X^{ss}_{RCM} - X^{ss}_{OBS})^2 < (X^{ss}_{OBS})^2$.

We recall that these equations were arrived at neglecting two covariance terms; one

corresponds to assuming that large-scale errors of GCM are uncorrelated with small-scale variance of observations, and the other that large-scale and small-scale errors of RCM are uncorrelated.

This analysis suggests that a measure of the potential of RCMs to add value can be obtained by defining

$$PAV^{ss}_{OBS} = (X^{ss}_{OBS})^2. \tag{8}$$

The quantity PAV^{ss}_{OBS} is called *potential added value (PAV)* of the small scales in observations and gives an estimation of the maximum AV that an RCM can add. Assuming that $(X^{ss}_{RCM})^2$ is a good approximation of $(X^{ss}_{OBS})^2$ we can define PAV^{ss} in terms of fine-scale RCM features:

$$PAV^{ss}_{RCM} = (X^{ss}_{RCM})^2. \tag{9}$$

It is important to note that if $PAV^{ss}_{RCM} \neq PAV^{ss}_{OBS}$ then the quantity PAV^{ss}_{RCM} will under- or over- estimate the real PAV by simulating too much or too little fine-scale variability. An under/over estimation of the real PAV can be related with either positive or negative AV, depending on the values of SE^{ss}_{RCM} and $(X^{ss}_{OBS})^2$. The interests of computing PAV^{ss}_{RCM} is that it allows to estimate the PAV in those cases where we do not have any knowledge about the true climate statistics.

The term AV^{ls} in Eq. (5) represents the AV generated by an RCM due to an improvement in the large-scale part of the climate statistics X. Due to the limited domain size of RCMs, the lack of two-way interaction between the regional domain and the rest of the globe, and the lateral boundary condition issues, it is not clear whether we should expect that RCMs add value at large scales (e.g., Diaconescu et al. 2007). In this thesis, we will concentrate in the study of AV^{ss} with no explicit consideration of AV^{ls}.

Brief review of previous work

Various studies have dealt with the added value issue either by directly considering some statistics of the type shown in Eq. (1) or by using a scale decomposition method in order to analyse some specific aspect of the problem such as AV^{ss}, AV^{ls} or PAV (although not named as such). Here we will briefly describe some of them and for a recent review of AV studies the reader is referred to Feser et al. (2011).

In one of the first comparisons between the climate as simulated by an RCM

and its driving data, Giorgi et al. (1998) compared the precipitation as simulated by the National Center for Atmospheric Research (NCAR) RCM and the Australian Commonwealth Scientific and Industrial Research Organization (CSIRO) GCM over a region located in the central part of United States that includes the states of Missouri, Iowa, Nebraska and Kansas (MINK region). Comparisons of seasonal-mean precipitation in the MINK region showed large biases for both models in all seasons, and there was no clear evidence of the RCM adding value in this particular statistics. Although the MINK region is not characterized by pronounced local topographic variability, the seasonal-mean spatial correlation with observations are generally higher in the RCM than in the GCM, thus showing AV in spatial correlations. In particular, an important improvement in the spatial pattern was found in the summer season with correlations of 0.77 and -0.69 between observed and RCM- and GCM-simulated fields, respectively.

Durman et al. (2001) studied the simulated daily precipitation in a global (HadCM2) and a limited-area version (HadRCM) of the same model. The HadRCM is driven by the HadCM2 and the comparison is performed in two HadCM2 grid boxes that includes Scotland and south-east England. Comparisons between simulated and observed intensity-frequency distributions showed that, in the winter season, the HadRCM had a large positive bias in the frequencies of heavier events and performed worse than the HadCM2. On the contrary, in the summer season, the HadRCM greatly outperformed the HadCM2, particularly due to an improvement in the representation of the upper tail of the precipitation distribution.

Using a two-dimensional Fourier transform, Castro et al. (2005) computed the power spectra of several atmospheric variables simulated by the Regional Atmospheric Modeling System (RAMS) and by the National Centers for Environmental Prediction (NCEP) reanalyses used to drive the RCM. They found that the RAMS simulation underestimated the spectral power of integrated kinetic energy and moisture flux convergence at large scales. Assuming that NCEP reanalyses represent "perfect" boundary conditions, the RAMS underestimation means a subtraction of AV^{ls}. They also found that, particularly in those regions with strong surface boundary forcing, RAMS showed larger spectral power of kinetic energy and moisture flux convergence at small-scales than the coarse-mesh NCEP reanalyses data, suggesting some PAV^{ss}.

Feser (2006) assessed the AV generated by the REMO RCM over the driving NCEP reanalyses for sea level pressure and 2-m temperature in Europe. A spatial filter is used to separate simulated and observed fields into two spatial-scale ranges: medium

scales (between 550 and 250 km; AV^{ss}) and large scales (larger than about 700 km; AV^{ls}). Results showed that, when evaluating a large-scale dominated quantity such as sea level pressure, spatial patterns produced by the RCM are very similar to those obtained from the NCEP reanalysis driving data. On the other hand, when assessing near-surface temperature on medium spatial scales, the RCM outperforms the NCEP reanalyses in the representation of the seasonal-mean spatial patterns. The author suggested that the improvement arises from the better representation of physiographic data in the RCM.

Winterfeldt and Weisse (2009) evaluated the AV produced by two RCMs over the NCEP reanalyses driving data for hourly time series of instantaneous 10-m wind speeds. Using several in situ observations in the North Atlantic and North Sea during the year 1998, they found that RCMs tend to improve the representation of surface wind speeds compared to the NCEP reanalysis in coastal stations located near complex orographic features. When assessing instantaneous wind speeds and their associated frequency distributions in stations located in the "open ocean", they found that RCMs tend to perform worse than the NCEP reanalyses. Similar results were found by Sotillo et al. (2005) over open-ocean stations in the Mediterranean Sea area when assessing the AV generated by the REMO RCM over the NCEP reanalyses.

De Sales and Xue (2011) also showed that the AV of RCMs can be strongly dependent on the region of analysis and that the improvement of the representation of fine-scale topographic features can be a crucial factor in the generation of AV. They found that the better representation of the Andes Mountain Range in an RCM compared to a lower-resolution GCM is a key factor in order to improve the simulated low-level moisture fluxes and the resulting precipitation in some regions of South America.

Bresson and Laprise (2009) analyzed the atmospheric water budget over North America as simulated by the Canadian RCM by using a spatial scale-decomposition tool. In both summer and winter seasons, they found that the small spatial scale component contributes to a large part of the total temporal variability of most relevant water budget variables such as precipitation and water vapour flux divergence. Their results suggest that the representation of moist processes show a high potential for RCMs to add value over GCMs with important differences across regions (e.g., oceanic vs. continental) and seasons.

It is clear from the articles already cited that RCMs do not generate AV in an unambiguous way. Rather, the AV seems to be contingent upon a variety of factors

such as the season and time scale, the variable and the climate statistics of interest, the region of analysis, etc. These results prompted the following question: Where, when and with respect to which variables and climate statistics should one expect to find added value generated by RCMs?

Scientific objective and outline of the thesis

The main goal of this research is to investigate the potential added value at small scales (AV^{ss}) based on observations and RCM simulations in North America using a framework that allows to estimate PAV^{ss} independently in each high-resolution data set. The thesis is composed of two scientific papers each represented as a separate chapter and is structured as follows.

The first chapter, entitled "Potential for added value in precipitation simulated by high-resolution nested Regional Climate Models and observations" and published in Climate Dynamics in 2011, evaluates the PAV in seven regions across United States based on four high-resolution precipitation data sets. One reanalysis and two gridded observed datasets are used to estimate the PAV in the real climate system and RCM simulations from the North American Regional Climate Change Assessment Program (NARCAAP) are used to evaluate the PAV suggested by models. The methodology uses the multi-resolution approach in order to estimate a number of statistics at different temporal and spatial resolutions. The multi-resolution method consists in the application of numerical filters in order to aggregate the original high-resolution time-varying precipitation fields into lower-resolution temporal and spatial scales. Spatial scales vary from approximately 0.5° to 6.4° and temporal scales range between 3 hours and 16 days. The article focused in the 95th percentile computed from 20-year time series between 1981 and 2000.

The second chapter, entitled "Potential for added value in RCM-simulated surface temperature", evaluates the PAV in the temperature variable as simulated by the same NARCCAP-ensemble of RCMs used in the first article. The general framework is similar to that used in the first article, but some important methodological modifications are introduced. First, results are generalized to the North American continent and the adjacent oceans. Second, Reynolds decomposition rules are used to separate the total variance of temperature according to the contribution of large and small spatial scales and of stationary and transient processes. The variance of the original temperature field is then computed and described by four different terms including two terms that describe

the original contribution of RCMs. Finally, the article includes a brief discussion about the PAV in future climate projections, together with some results of application of the PAV framework to the temperature change signal.

Concluding remarks encompassing the main contributions of both papers along with some possible lines of added value research studies are presented in the conclusion's section.

CHAPTER I

POTENTIAL FOR ADDED VALUE IN PRECIPITATION SIMULATED BY HIGH-RESOLUTION NESTED REGIONAL CLIMATE MODELS AND OBSERVATIONS

This chapter is presented in the format of a scientific article. It was published in 2011 in the Climate Dynamics journal. The design of the research and its performance together with the analysis of data and the redaction of this article are entirely based on my work, with the co-authors involved in the supervision of all these tasks.
The detailed reference is:

Di Luca, A., de Elía R. and Laprise, R., 2011: "Potential for added value in precipitation simulated by high-resolution nested Regional Climate Models and observations". Climate Dynamics; DOI 10.1007/s00382-011-1068-3.

Alejandro Di Luca - René Laprise
Centre ESCER (Étude et Simulation du Climat à l Échelle Régionale).
Département des Sciences de la Terre et de l'Atmosphère
Université du Québec à Montréal (UQAM)
B.P. 8888, Succ. Centre-ville
Montréal (Québec) Canada H3C 3P8

Ramón de Elía
Centre ESCER (Étude et Simulation du Climat à l Échelle Régionale),
Consortium Ouranos, 550 Sherbrooke West, 19^{th} floor, West Tower,
Montréal (Québec) Canada H3A 1B9

Abstract

Regional Climate Models (RCMs) constitute the most often used method to perform affordable high-resolution regional climate simulations. The key issue in the evaluation of nested regional models is to determine whether RCM simulations improve the representation of climatic statistics compared to the driving data, that is, whether RCMs add value. In this study we examine a necessary condition that some climate statistics derived from the precipitation field must satisfy in order that the RCM technique can generate some added value: we focus on whether the climate statistics of interest contain some fine spatial-scale variability that would be absent on a coarser grid. The presence and magnitude of fine-scale precipitation variance required to adequately describe a given climate statistics will then be used to quantify the potential added value (PAV) of RCMs. Our results show that the PAV of RCMs is much higher for short temporal scales (e.g., 3-hourly data) than for long temporal scales (16-day average data) due to the filtering resulting from the time-averaging process. PAV is higher in warm season compared to cold season due to the higher proportion of precipitation falling from small-scale weather systems in the warm season. In regions of complex topography, the orographic forcing induces an extra component of PAV, no matter the season or the temporal scale considered. The PAV is also estimated using high-resolution datasets based on observations allowing the evaluation of the sensitivity of changing resolution in the real climate system. The results show that RCMs tend to reproduce relatively well the PAV compared to observations although showing an overestimation of the PAV in warm season and mountainous regions.

Keywords: regional climate model; temporal-spatial scale analysis; precipitation; added value.

1.1 Introduction

Atmospheric-Ocean General Circulation Models (AOGCMs) constitute the primary and most comprehensive tools to study future climate. However, due to the large number and complexity of processes to be represented, the long simulations needed for climate studies, and the need of ensemble simulations to provide robust statistical estimates, computational constraints severely restrict the horizontal grid mesh used in the discretized equations. Present horizontal grid intervals of the atmospheric component of AOGCMs are usually between 125 and 400 km (Randall et al. 2007); these are insufficient to resolve the fine-scale structure of several climatic processes.

The method most often used to perform affordable high-resolution regional climate simulations is the nested regional climate modelling technique; it consists of using time-dependent large-scale atmospheric fields and ocean surface boundary conditions to drive a high-resolution atmospheric model integrated over a limited-area domain (Giorgi et al. 2001). The atmospheric driving data are either derived from lower resolution General Circulation Models (GCMs) simulations or analyses of observations (reanalyses). Typical Regional Climate Models (RCMs) horizontal grids for climate simulations are about 50 km, although long-term simulations are increasingly being performed using grids of 10 km (Kanamitsu and Kanamaru 2007; Suklitsch et al. 2011). For a detailed description of potential merits and limitations of nested RCMs, refer to Laprise et al. (2008) and Rummukainen (2010). Alternative methods to obtain regional climate information also exist, such as variable-resolution global models, time-slices of high-resolution global models and empirical-statistical techniques (e.g. Christensen et al. 2007), but these will not be addressed in this paper.

RCMs have been used in a broad spectrum of applications such as the reconstruction of recent-past climate on the regional scale (e.g., Mesinger et al. 2006; Kanamitsu and Kanamaru 2007); the downscaling of low-resolution global simulations in seasonal prediction investigations (e.g., Rauscher et al. 2007; Seth et al. 2007; De Sales and Xue 2011) and the study of processes and mechanisms in the regional scale (Pielke et al. 1999; Roebber and Gyakum 2003). During the last decade, RCMs have become increasingly used for dynamical downscaling of climate-change projections (Christensen et al. 2007; and references therein), by driving RCMs with GCM-simulated climate-change projections.

In any of these applications, the RCM's objective is to simulate small-scale cli-

mate processes that are absent in the coarser resolution simulation providing the driving data. This implies that, from a practical viewpoint, the key issue in the nesting regional modelling technique evaluation is to determine whether RCM simulations improve the representation of climatic statistics compared to the driving data (Prömmel et al. 2010). Generally, studies evaluating the relative skill of RCMs and the driving fields are designated as added value (AV) studies (Bärring and Laprise 2005; Rockel et al. 2010).

Despite the great importance of identifying AV in RCM simulations, the AV issue has not received much attention till recently (Laprise 2005; Feser and von Storch 2005). In recent years, however, the AV problem received increased attention and become the main subject of several studies (Castro et al. 2005; Sotillo et al. 2005; Duffy et al. 2006; Feser 2006; Kanamitsu and Kanamaru 2007; Rauscher et al. 2007; Sanchez-Gomez et al. 2009; Winterfeldt and Weisse 2009; De Sales and Xue 2011; Prömmel et al. 2010) and a central topic in a number of workshops (Bärring and Laprise 2005; Rockel et al. 2010). Although some authors (e.g. Liang et al. 2008) believe that the existence of AV generated by the RCM downscaling technique was already demonstrated for some particular measures (e.g. reduction of precipitation biases), evidence found in a large number of articles do not tend to univocally support this view, rather suggesting that AV remains an important open question for the community.

For example, when downscaling reanalyses data, studies generally show that RCMs add value to their driving data for surface variables (e.g., surface temperature and 10-m wind speed) in regions characterized by small-scale orographic features such as mountainous regions (Feser 2006; Prömmel et al. 2010) and coastal areas (Sotillo et al. 2005; Winterfeldt and Weisse 2009); but little AV and even degradation is sometimes found in regions with no important small-scale physiographic forcings (Winterfeldt and Weisse 2009). Long-term large-scale features (i.e., general circulation) are generally reasonably well reproduced by RCMs (Feser 2006; Sanchez-Gomez et al. 2009), but degradation of large-scale fields arises when considering shorter time scales (e.g., daily mean) (Castro et al. 2005; Sanchez-Gomez et al. 2009).

Somewhat similar results are found when using GCM-simulated lateral boundary conditions (LBCs). According to Seth et al. (2007) and De Sales and Xue (2011), RCMs generally improve the simulation of precipitation compared to GCMs in regions where small-scale surface forcings are important and/or GCMs do not perform very well, but RCMs can degrade the simulated climate in those regions where GCMs perform well and/or large-scale forcings are dominant. De Sales and Xue (2011) also showed that

the AV of RCMs is strongly dependent on the region considered; in their study, the improvement on the representation of the Andes Mountain Range by the RCM compared to the GCM was a key factor to adding value to the simulation of low-level moisture fluxes and precipitation in South America.

The value added by RCMs seems to depend on a variety of factors. A key factor is related with the climatic variable considered in the assessment, understanding the term climatic variable in a broad sense as some statistical measure of a variable computed for a given season and region. So some remaining questions are: For which climate statistics should one hope to find AV from dynamical downscaling? How the AV depends on the temporal scale of the climatic variable? Where and when can some AV be found for monthly-mean values? The objective of this article is to examine these issues by making a systematic characterization of a necessary condition to be satisfied by climate statistics in order that AV be generated through the use of the RCM technique. Given that the ansatz behind the dynamical downscaling technique is that an RCM, driven by large-scale atmospheric fields at its LBC, generates fine scales that are dynamically consistent with these, this paper will focus specifically on the fine-scale information generated by the use of nested high-resolution RCM. The presence and magnitude of fine-scale variance required to adequately describe a given climate statistics will then be used to quantify the potential of RCMs to add value.

Our study will be performed using precipitation data simulated by several RCMs; this will allow to determine which of the findings are inherent to the downscaling technique and which are specific to a particular model. Datasets based on observations will also be analysed in order to highlight limitations of RCMs performance when possible as well as to indicate disagreements among observed datasets. The use of precipitation is justified because it is a variable that displays a wide range of temporal and spatial scales, and thus a variable that tends to maximize the potential AV. It is also a key variable because some of the most important societal impacts of climate change will probably result from changes in precipitation (Trenberth et al. 2003; Gutowski et al. 2007).

The paper is organized as follows. The next section discusses in more detail the issue of added value and the objectives of this article. Section 1.3 presents a brief description of the data used. Section 1.4 describes the method used to analyze the dependence of the precipitation field on various temporal and spatial scales, together with the manner in which statistics are computed. Results are presented in section 1.5

with some general results of the method and specific results of the characterization of AV as function of several parameters. Some discussion of the results and conclusions is given in section 1.6.

1.2 Added value issue

1.2.1 General Characterization

Figure 1.1 shows a diagram adapted from Orlanski (1975) and von Storch (2005) illustrating the characteristic temporal and horizontal spatial scales of atmospheric processes, together with the range of scales represented by climate models. Grey shaded areas are regions of dominant spectral power resulting from the composite of a broad range of atmospheric variables. Due to the space and time truncation, numerical models can only resolve explicitly a part of the atmospheric processes; smaller scale phenomena are at best accounted for in an average sense through the subgrid-scale parameterisations. Differences between RCM- and GCM-resolved scales can be conceptually seen in Fig. 1.1 by comparing the areas boxed in by the blue and red solid lines. These boxes were constructed using as lower limit the temporal and spatial intervals of discretization, and as the upper limit the entire computational domain and length of simulations. For a typical RCM the lower limits are located roughly at 50 km and 5 min., and the upper limit at spatial scales of 10,000 km. For a standard GCM the lower limit is here taken as 300 km and 30 min., and the upper limit as 40,000 km. It should be noted that timestep and grid spacing of models only constitute a lower limit to temporal and spatial resolution (Pielke, 1991).

Figure 1.1 highlights that the main potential advantage of an RCM over a GCM is related with the representation of spatial scales smaller than 300 km and/or temporal scales smaller than 30 min. that are absent in the GCMs. The enhanced horizontal resolution of an RCM implies some potential advantages compared to a lower resolution GCM: i) a more accurate discretization of equations; ii) a broader range of fine-spatial scales explicitly resolved; and iii) an improvement in the representation of surface forcings such as topography, lakes, coastal regions and others. Figure 1.1 also shows that scales larger than the RCM domain are not within the resolved scale interval of RCM; hence planetary scales are only felt insofar as they are provided by the driving data through the LBC.

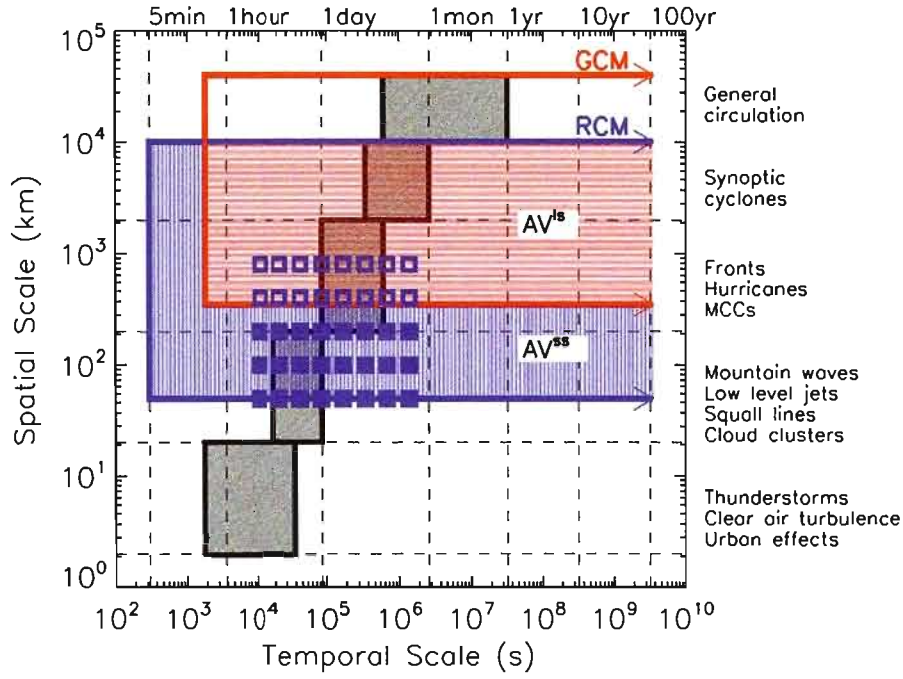

Figure 1.1 Characteristic temporal and horizontal spatial scales of atmospheric processes (in grey) and the range of scales represented in RCMs (blue line) and GCMs (red line). Light- blue and red shaded regions represent AV_{ss} (called AV1) and AV_{ls} (called AV2) respectively. Blue squares represent temporal and spatial scales of the data produced with the multi-resolution method.

The original paradigm of the nesting technique is that RCMs can be used as sophisticated magnifying glasses (MG) where the generated small scales accurately represent those that would be present in the driving data if they were not limited by resolution (Laprise et al. 2008; hereafter referred as MG hypothesis). The idea behind this hypothesis is that an RCM can be used to represent small scales that would be present in a desirable but in practice unaffordable high-resolution GCM (HRGCM). The evaluation of the MG hypothesis has been addressed without having to use observed data, through a systematic approach developed by Denis et al. (2002): the Big Brother Experiment (BBE). In its idealized version, the BBE consists in comparing two high-resolution simulations generated by using different configurations of the same model: a simulation conducted with a high-resolution global model (referred to as big brother) and a RCM simulation (referred to as little brother) run at the same resolution

and with the same discretisation and parameterisation as the big brother, but forced by low-resolution LBCs derived from filtering out the big-brother simulated fine scales. The low-resolution data resulting from filtering mimics the situation when driving an RCM from GCM data. The use of the same model, run in different configurations while using the same physics, dynamics and numerics, permits to circumvent errors due to the model itself, through the BBE perfect model approach. As a consequence, the differences between the little and the big brothers can be attributed solely to the nesting technique and to differences in LBCs due to the use of low-resolution data to drive the little brother.

A low-cost version of the BBE was obtained by replacing the HRGCM by a very large domain high-resolution RCM; it was successfully used to show that the little brother tends to replicate the magnitude and spatial distribution of small-scale climate statistics present in the big brother, at least in mid-latitude climates (see Laprise et al. 2008 and references therein). The BBE was also very useful to study the influence of a variety of parameters in RCMs setup such as the impact of the size of the domain used to run the model (e.g., Leduc and Laprise 2009) and the impact of LBC errors (Diaconescu et al. 2007).

1.2.2 Added value concept

The evaluation of the MG hypothesis with the BBE does not depend on the model performance, i.e. models skill at reproducing the observed climate, which has definite advantages as discussed above; it has also its downside. Satisfying the MG hypothesis does not imply that the high-resolution RCM-derived statistics are closer to observed statistics than those that would be produced by a low-resolution GCM; hence the conclusions are mute about whether RCM provide any real added value compared to coarser resolution GCM. Indeed, as discussed by several authors for both GCMs (Boer and Lazare 1988; Boville 1991; Boyle 1993) and RCMs (Giorgi and Marinucci 1996), higher resolution simulations do not necessarily produce results closer to the observed values, in part because the approximations in models do not converge monotonically with resolution and the performance is strongly dependent on the behaviour of parameterizations.

These days, the most popular paradigm used to evaluate RCMs is through a pragmatic consideration about their usefulness, evaluating if RCMs are able to add value (AV) to, i.e. improve, the simulation of climate statistics compared to those produced by GCMs. The AV hypothesis has important differences compared to the MG hypothesis.

First, it introduces the necessity of using observed data in its validation, thus inducing important constraints due to the scarceness of fine-scale observations and the limited number of variables (e.g., precipitation, temperature, surface pressure) available for validation. Second, the evaluation of the AV hypothesis implies the assessment of the performance of the RCM downscaling technique but also of the relative performance of the RCM and its driving data (i.e., the AV is model dependent). It is generally very difficult to determine if an improvement (degradation) of a given climate statistics comes from advantages (disadvantages) of the RCM downscaling technique or because the RCM performed better (worse) than the GCM; there may also be compensating errors between the driving data and the RCM that may result in apparent improvements, but for wrong reasons. From this viewpoint, it seems that the only way of using the AV paradigm to obtain some intrinsic characteristics of the downscaling technique is through the use of a large ensemble of RCM-GCM pairs of simulations in order to extract common behaviours.

In general, RCMs could simulate more realistic climate than the lower resolution driving data by adding value in two different ways. First by adding climate variability in scales that are not explicitly resolved by GCMs, hereafter referred to as *small-scales* added value (AV_{ss}), as indicated by the light-blue shaded region in Fig. 1.1. A second way is by improving the simulation of climate in those scales that are common to both RCMs and GCMs, hereafter referred to as *large-scales* added value (AV_{ls}), as indicated by the light-red shaded region in Fig. 1.1. The separation of AV in two components can be helpful because of the different methodological approach needed to assess both large- and fine- scales AV components. The estimation of AV coming from the additional climate variability in scales only resolved in RCM simulations (AV_{ss}) is ultimately an evaluation of the performance of RCMs to simulate small-scale variability. On the other hand, the evaluation of the improvements produced by the RCM in the range of scales resolved by both models (AV_{ls}) can be done by comparing results from the RCM and the GCM with large-scale analyses of observations to determine which one produces better performance. This classification can be complemented with the one proposed by Castro et al. (2005) in which RCM dynamical downscaling technique is separated into four distinct types according to the LBCs used to drive the RCM.

Due to the limited domain size of RCMs, the lack of two-way interaction between the regional domain and the rest of the globe, and the lateral boundary condition issues, it is not clear whether RCMs actually improve or degrade the larger scales; hence AV_{ls} has not been clearly identified and it is still a debated topic in the modelling

community (e.g., Laprise et al. 2008), although recent results indicate that there may be improvements under specific circumstances (Veljovic et al. 2010). In the following we will concentrate on AV_{ss} although it will be generally referred to as AV.

1.2.3 Potential added value concept

It is important to note that in some cases the absence of added value might be related to the failure of the assumptions from which AV is expected. For example, from Fig. 1.1 it seems clear that very little AV can be found when analyzing monthly-mean precipitation data in regions without important surface forcings because monthly scales are predominantly associated with large-spatial scales that are probably well resolved by GCMs. A necessary condition for RCMs to produce AV_{ss} is that the contribution of the simulated fine-scale details on the climate statistics of interest is not negligible. That is, if the RCM does not produce any climatic information at small scales then, by definition, there is no AV_{ss}.

The study of the relative contribution of fine scales in a given climate statistics has lead to the concept of potential added value (PAV) as discussed in Bresson and Laprise (2009). The term potential in this definition accounts for the fact that the presence of small scales is not a sufficient condition to have AV_{ss}. A simple example is an RCM that generates small scales but with little resemblance between simulated and observed patterns or amplitude. Then, we can argue that the small scales are not skilful and do not add any real value to the coarser GCM climate, even if they suggest a large PAV. Clearly however the presence of PAV in RCM simulations is a prerequisite for, although not a definite proof of, AV_{ss}.

In this article, a perfect-model approach was developed to study the PAV. The idea behind the PAV concept is that the high-resolution (e.g., 50-km grid spacing) precipitation field simulated by a RCM will be aggregated into a coarse-resolution (e.g., 300-km grid spacing) in order to generate what we can call a virtual GCM field. The important hypothesis behind this framework is that the virtual GCM can be interpreted to represent more or less the same statistics as those resulting from a climate model operating at similar grid spacing. Evidently, a virtual GCM differs from a real GCM due to a number of reasons, among them that the virtual GCM fields are influenced through the upscaling of fine-scale processes that are resolved in the high-resolution RCM simulation but would be absent in a low-resolution GCM simulation.

Di Luca (2009) compared the statistics of extremes (e.g., 95th percentile) of a virtual GCM with those of a real GCM, for the precipitation as simulated by the Canadian Global Climate Model (CGCM3) and the Canadian RCM (CRCM) driven by the CGCM3. The evaluation focused on time scales larger than a day and on spatial scales that are common to both models, i.e., the CRCM was aggregated at the CGCM3 resolution to generate virtual GCM datasets. Using as reference daily observational time series, the comparison showed that seasonal biases are of the same magnitude in the CGCM3 and the CRCM. Both models display also comparable skills to simulate the frequency and intensity of observed daily values, but the CGCM3 generally shows larger 95th percentile values. It is important to note that the performance of GCMs, under the assumption that model precipitation output represents an areal mean (see Chen and Knutson 2008 for a detailed discussion), is evaluated using observations which are always made at finer spatial resolutions than the GCMs resolutions. This implies that GCMs are evaluated and sometimes calibrated using observed statistics that are similar in nature as virtual GCM statistics, containing for example the upscale of fine-scale processes that occur in the real climate system.

The aim of this study is to develop some simple measures to characterize the PAV of the precipitation field as simulated by a number of RCMs and as represented in reanalyses and observations. The dependence of PAV on several parameters will be evaluated: the choice of the temporal scale of the data (ranging from 3-hourly to 16 days means), the region (e.g., complex topography region versus flat region), and the season (e.g., mostly convective in summer versus stratiform in winter precipitation).

1.3 Data

The potential added value as defined in the last section is dataset dependent. Four different but not independent sources of high-resolution precipitation data (HRD) are used in this study. RCM-simulations are used to evaluate the PAV suggested by models. One reanalysis and two gridded observed datasets are used to estimate the PAV of changing resolution of data in the real climate system. Observed datasets are more reliable in the conterminous United States due to the higher density of stations compared to Canada and oceanic regions and, for this reason, the region of study is located in continental United States. Particularly at fine temporal scales and over complex terrains, observed datasets cannot be fully trusted and will not be considered as a ground truth.

1.3.1 NARCCAP simulations

The RCM simulations to be used in this study are those from the North American Regional Climate Change Assessment Program (NARCAAP; http://www.narccap.ucar.edu/; Mearns et al. 2009). In NARCCAP, six RCMs were run with a horizontal grid spacing of about 50 km over similar North American domains covering Canada, United States and most of Mexico, during the 25 years between 1980 and 2004. The RCM simulations to be used are those of contemporary climate using driving data derived from the National Centers for Environmental Prediction (NCEP) Department of Energy (DOE) Atmospheric Model Intercomparison Project II (AMIP-II) global reanalysis (R-2; Kanamitsu et al. 2002). Table 2.1 gives the acronyms, full names and the modelling group of each RCM, together with the number of grid points within the computational domain of each model available for the analysis and the map projection and the number of vertical levels. The computational domain of the CRCM RCM is shown in Fig. 1.2 and a brief description of each NARCCAP RCM can be found at http://narccap.ucar.edu/data/rcm-characteristics.html.

1.3.2 CPC gridded precipitation

An interesting source of high spatial resolution precipitation data for daily and longer time scales is given by the gridded Climate Prediction Centers (CPC) product derived using stations from the Unified Raingauge Database (URD) (Higgins et al. 2000). This dataset consists of daily analyses, gridded at 0.25° by 0.25°, from over 8000 stations each day covering the period 1948 - 1998 with no missing values. The dataset covers the domain 20°-60° N, 140°-60° W over continental United States with an heterogeneous density of stations, higher in the eastern part of United States but with relatively good coverage in all continental United States.

1.3.3 UWash gridded precipitation

This daily gridded precipitation dataset was obtained from the Surface Water Modeling group at the University of Washington (UWash) from their web site at http://www.hydro.washington.edu/Lettenmaier/Data/gridded/ and is described by Maurer et al. (2002). Within the coterminous United States, it uses daily totals of precipitation from the National Oceanic and Atmospheric Administration Cooperative stations, also included in the URD database, to produce a 1/8° gridded dataset using the syner-

Table 1.1 Acronyms, full names and modelling group of RCMs involved in the NARCCAP project. Column 4 indicates the number of grid points in each RCM. Column 5 denotes the map projection and the number of vertical levels for each RCM.

RCM	Full Name	Modelling group	Domain (lon x lat)	Map projection N° of vertical levels
CRCM	Canadian Regional Climate Model (version 4.2.0)	Ouranos / UQAM	140 x 115	Polar stereographic 29
ECPC	Experimental Climate Prediction Center Regional Spectral Model	UC San Diego Scripps	123 x 104	Polar stereographic 28
HRM3	Hadley Regional Model (version 3)	Hadley Centre	155 x 130	Rotated lat - lon 19
MM5I	MM5 - PSU/NCAR mesoscale model	Iowa State University	123 x 99	Lambert conformal 23
RCM3	Regional Climate Model (version 3)	UC Santa Cruz	134 x 104	Mercator 18
WRFP	Weather Research and Forecasting model	Pacific Northwest Natl Lab	134 x 109	Lambert conformal 35

graphic mapping system algorithm of Shepard (1984). In order to better capture local variations due to complex terrain, each grid cell of the 1/8° gridded dataset is adjusted using monthly-mean values computed with the parameter-elevation regressions on independent slopes model (PRISM). PRISM (for more details see Daly et al. 1994) is an analytical model that uses statistical relations between the observed precipitation and several topographical parameters (e.g., elevation, steepness of the terrain, orientation of the slope, and others) derived from a digital elevation model (DEM) in order to provide gridded precipitation products better adapted over elevated terrains where rain gauge data are sparse. The influence of PRISM has little effect on the adjusted precipitation in flat regions and so UWash is expected to be similar to CPC in these regions.

1.3.4 NARR reanalyses

The North American Regional Reanalysis (NARR, http://www.emc.ncep.noaa.gov/mmb/rreanl/index.html) is a product created at NCEP

that combines, in a dynamically consistent way, the simulated fields by the NCEP regional Eta model (Mesinger 2000) driven at its LBCs by the R-2 reanalysis, together with numerous additional observed datasets through the use of the NCEP Data Assimilation System (Mesinger et al. 2006). NARR has a grid spacing of 32 km and 45 layers in the vertical, and reanalysis fields are available every 3 hrs between 1979 and 2003, over a large domain covering Canada, United States and Mexico. According to Mesinger et al. (2006), in addition to its higher resolution, one of the main advantages of these reanalyses is the assimilation of latent heating profiles derived from precipitation analyses (Lin et al. 1999). The precipitation dataset assimilated in NARR is a daily, 1/8° analysis obtained by gridding rain gauge observations from the URD using the orographic adjustment technique PRISM already discussed (Mesinger et al. 2006).

1.4 Methodology

1.4.1 Multi-resolution approach

To analyze the scale dependence of the above-described data, the multi-resolution (MR) approach is used. The MR method (see Mallat (1989) for details) has been used in several studies to analyze the temporal (Howell and Mahrt 1997; Vickers and Mahrt 2002) and spatial (Zepeda-Arce et al. 2000; Harris et al. 2001) variability of atmospheric variables. The MR method consists in the application of numerical filters in order to aggregate the original high-resolution time-varying precipitation fields into lower-resolution temporal and spatial scales. In both the temporal and spatial dimensions, the filtering is performed by aggregation of the original precipitation field into several lower resolution grids. A total of 5 spatial scales (~0.4°, 0.8°, 1.6°, 3.2° and 6.4°) and 8 temporal scales (ranging between 3 hours and 16 days) resolution datasets are considered. As it will be explained in detail later, the dependence of several precipitation statistics on spatial scales will be used to determine the relative importance of small scales and define various PAV quantities.

1.4.1.1 Spatial scale analysis

In this study, a slightly different version of the MR method of Mallat (1989) is developed by aggregating the original HRD precipitation fields on some common lower resolution grid meshes. The precipitation aggregation is performed over several resolution meshes occupying regions of 6.4° by 6.4° (i.e., about 550 km by 550 km at a latitude of 40°) as

a compromise between two opposing needs in relation to their size: first, that regions be large enough to estimate climate statistics at a range of spatial scales spanning the minimum resolved by current GCMs, and second, that they be small enough to represent fairly homogeneous regions across North America in order to analyze the dependence of results on different surface forcings. Figure 1.2 shows the seven regions selected for the analysis, together with the topography field as represented in the CRCM. In the following, regions are denoted by adding to LON the west longitude of their centre (e.g., the region centred on -118.0° of longitude is called LON118).

The finest scale of the MR analysis is done over grid meshes with 0.4° of grid spacing, which was chosen such as to be finer than the grid spacing of all NARCCAP RCMs; on this scale the precipitation field is identical to that simulated by the RCM, ensuring that the full information of each RCM is retained. The number of RCM grid

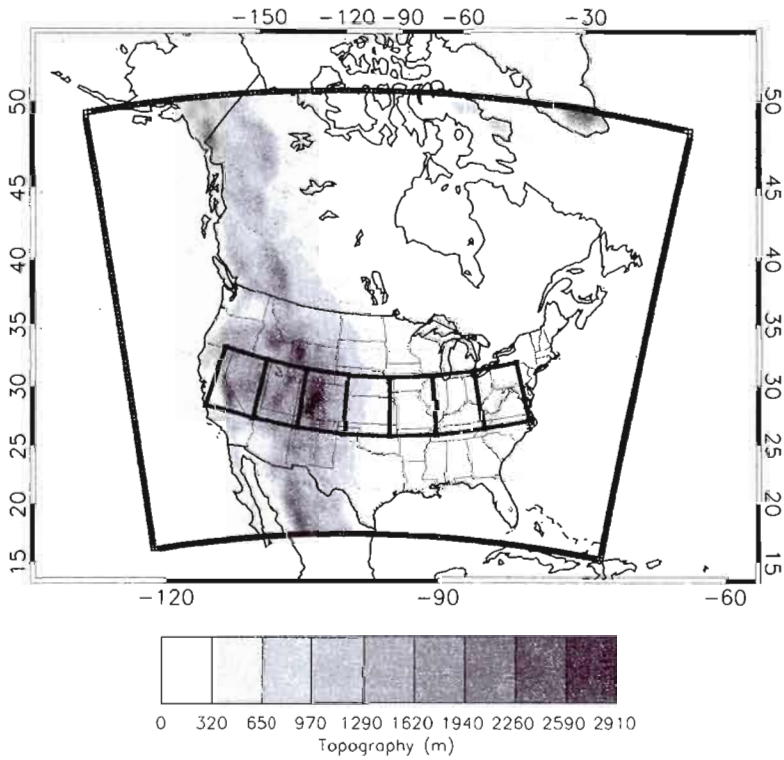

Figure 1.2 Computational domain and topographic field as represented in the CRCM together with the specification of the seven regions of interest. All regions have the same dimensions (i.e., 6.4° by 6.4°).

points contributing to the aggregation at each scale depends on each RCM due to their specific map projections and horizontal grid spacing. Table 3.2 shows the minimum and maximum number of grid points inside 6.4° by 6.4° regions (see Fig. 1.2) together with the mean grid spacing inside each region for each HRD.

NARR and CPC grid spacings are smaller than 0.4°. In those grid boxes with more than one NARR or CPC grid points, the 0.4° grid spacing value is obtained simply by computing the arithmetic area-average of the points every 3 hours. Hereafter, the finest scale will be denoted as 0.4°, but it should be clear that for models it does represent the data at the original grid spacing of each NARCCAP RCM (i.e., in the range 0.44°-0.51°). As an example of the spatial distribution of grid points inside a region, Fig. 1.3a presents the location of CRCM grid points (blue squares) together with the 0.4°-grid mesh (red crosses) over the 6.4° by 6.4° LON118 region.
The second scale next to the finest is obtained by aggregating the original precipitation field of each HRD over grid boxes defined by a grid mesh with a horizontal grid spacing of 0.8°. The upscaling at the 0.8° scale is made by simply computing, at each time interval, the average of all HRD-points inside each 0.8° grid box (i.e. by computing a simple arithmetic area-average value). As shown in Fig. 1.3b, grid boxes at the 0.8° scale contain a variable number of the original RCM grid points, that vary between 2 and 4 in the case of the CRCM.

In a similar way, other spatial scales are calculated by aggregating the original precipitation field over grid meshes characterizes by horizontal grid spacings of 1.6°, 3.2° and 6.4°, as illustrated in Fig. 1.3c, 1.3d and 1.3e, respectively. The 6.4° scale corresponds to the coarser spatial scale and it is obtained by averaging, at each time

Table 1.2 Minimum and maximum number of grid points and the corresponding effective grid spacing in the 6.4 by 6.4 regions of Fig. 1.2 for each high-resolution dataset.

	Numbrer of grid points		Effective grid spacing (°)	
	min	max	min	max
CRCM	195	208	0.46	0.44
ECPC	195	209	0.46	0.44
HRM3	165	169	0.50	0.49
MM5I	145	154	0.53	0.52
RCM3	159	167	0.51	0.50
WRFP	145	154	0.53	0.52

step, the precipitation rate values of all the RCM grid points inside the region (see Fig. 1.3e).

Giorgi (2002) used a similar filtering approach to study the spatial-scale dependence of interannual climate variability of temperature and precipitation over several regions around the Earth. Starting with a 0.5° grid spacing dataset, he computed a two-dimensional running spatial average at various spatial scales.

1.4.1.2 Temporal scale analysis

The temporal scale analysis is performed in a similar way as the spatial one. In this case, the finest temporal scale corresponds to the 3-hourly time series of archived precipitation for any given grid point. The second temporal scale, the 6-h scale, is obtained by simply computing the arithmetic average between two consecutive 3-hourly data and thus reducing in a factor of two the total number of data in the time series. Similarly, six other temporal scales are defined.

For each year between 1981 and 2000 (1998 for CPC gridded precipitation), we selected two subsets of 128 days in order to generate cold- and warm-season time series (a long season of 128 days was chosen in order to be able to represent the amount of 3-hourly data as a power of 2). Cold season is defined by the four months between November and February and warm season is defined by those months between April and June. For these periods, a total of 19 cold seasons and 20 warm seasons are obtained.

1.4.1.3 Spatiotemporal scale analysis

The spatial and temporal scale filtering are then applied simultaneously to each HRD in order to obtain a spatio-temporal multi-scale dataset composed of a total of 40 (5 spatial scales and 8 temporal scales) time-varying fields. For any given HRD, the multi-scale dataset is denoted as $Pr^{n,m}$ with index n, varying between 0 and 4, identifying the spatial scale and index m, varying between 0 and 7, denoting the temporal scales. As already mentioned, the 5 spatial scales are associated with grid spacings of 0.4°, 0.8°, 1.6°, 3.2° and 6.4°, and temporal scales vary from 3 h (m =0) to 384 h (m =7). Each dataset $Pr^{n,m}$ is illustrated in Fig. 1.1 according to their minimum temporal and spatial scale. Filled blue squares denote those datasets with spatial grid spacings smaller than ~3.2° (~275 km at 40° of latitude) that can only be represented by standard RCMs. Datasets denoted with non-filled blue squares correspond to those with spatial scales

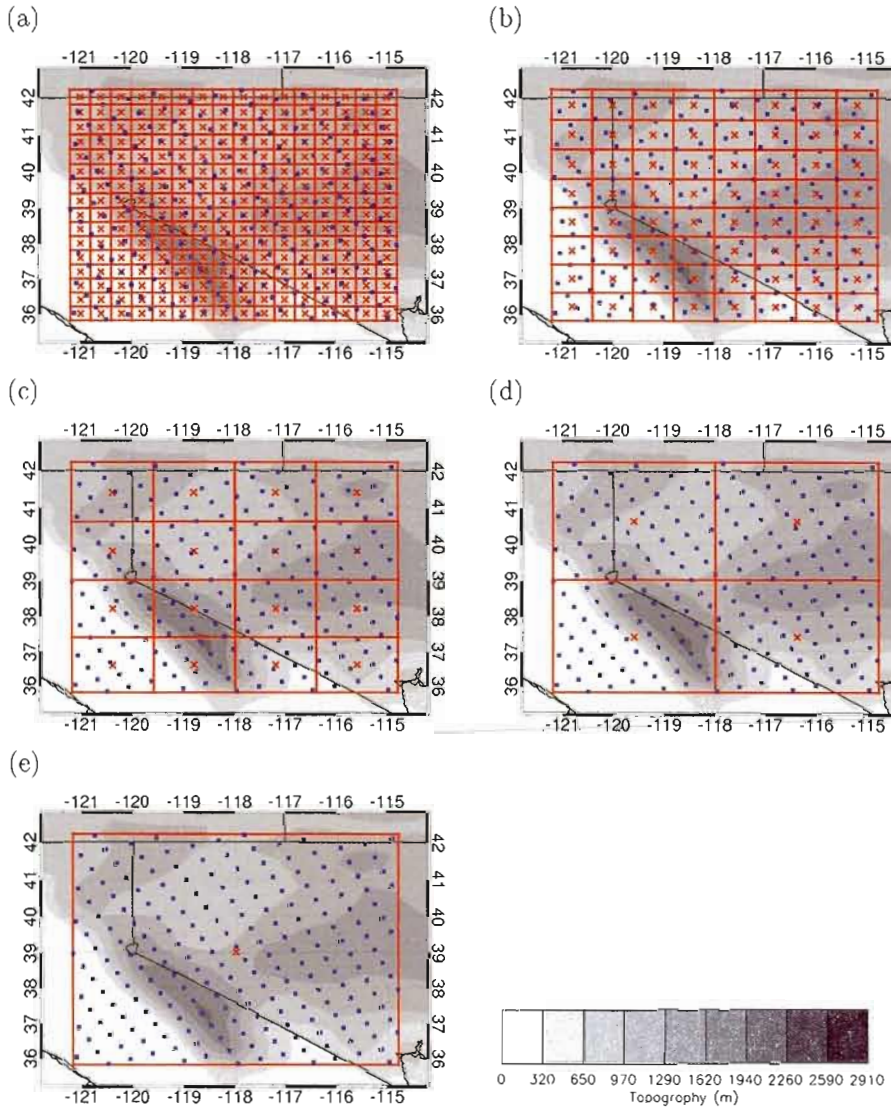

Figure 1.3 Location of the new grid points (red crosses) defined by upscaling the high resolution fields (blue dots) for spatial scales with grid spacings given by: (a) ~0.4° (original grid mesh), (b) 0.8°, (c) 1.6°, (d) 3.2° and (e) 6.4°. Data correspond to the CRCM model for the LON118 region. Blue dots represent the grid points of the CRCM model in its original grid (similar to red crosses for $\mathrm{Pr}^{0,m}$)

larger or equal than 3.2° that can be represented by both, RCMs and GCMs.

1.4.2 Multi-scale statistics

In order to compare results of the precipitation field at different resolutions, we will calculate a number of statistics over each region.

- Grid point statistics ($q_{95}^{n,m}$): for each time series $Pr^{n,m}$ (red crosses in Fig. 1.3) at spatial scale n and temporal scale m, the corresponding temporal histograms are calculated by partitioning the interval of possible wet events outcomes into subsets of 0.1 mm/day width, and then divided by the total number of outcomes to obtain the frequency in each bin. 95th percentiles are then computed for each grid point frequency distribution. Wet events are defined here as those events with a mean precipitation rate larger than 0.1 mm/day (as done in Lenderink et al. (2007)).

- Spatial-mean statistics ($q_{mean,95}^{n,m}$): for each spatial scale n, the spatial-mean 95th percentiles computed by putting in the same histogram (pooling) events from all grid points in a given region and then computing the 95th percentile (similar to method 3 of quantiles computations in Déqué and Somot (2008).

- Spatial-maximum statistics ($q_{max,95}^{n,m}$): in each region, the maximum value of the grid-point 95th percentile distribution at spatial scale n is taken.

In this way, $q_{mean,95}^{n,m}$ constitutes a regional measure by representing the spatial-mean statistics over any given 6.4° side region and $q_{max,95}^{n,m}$ a local measure at one grid point. Differences between the regional and local measures arise from the presence of spatial gradients in the temporal precipitation distributions. Several mechanisms can generate these gradients in instantaneous fields; when considering climatic statistics computed from 20-year data however, they are quite probably due to the existence of stationary forcings. It should be noted that the spatial-mean quantity is roughly equivalent to what would be obtained by applying a Fourier transform at a similar wavenumber.

In this paper results are presented only for the 95th percentile, but the analysis was conducted also for other quantities and some of these results will be summarized in the next section.

1.5 Results

1.5.1 Multiscale intensity-frequency distributions

The process of aggregating precipitation data in space (time) acts as a spatial (temporal) filter that tends to smooth out the extremes in the spatial (temporal) distribution of any given field (time series), thus narrowing the intensity-frequency distribution. As a result, systematic changes are introduced in the original high-resolution precipitation field (time series) as it is upscaled into lower resolution fields (time series):

- Local maximum values in the lower resolution dataset are always smaller than or equal to those in the original dataset. That is, higher-order percentiles (e.g., 95th percentile) tend to be smaller in the coarser resolution datasets than at higher resolution.
- The absolute number of dry events (those events with precipitation rate smaller than 0.1 mm/day) tends to decrease when the precipitation field is aggregated into lower resolution grid meshes.
- Low and moderate precipitation rates tend to be more frequent in lower resolution datasets, compensating the deficit in dry and heavier events.

The general changes suggested in this three points can be illustrated by showing the spatial-mean intensity distributions in the NARR data aggregated at several temporal and spatial resolution (see Fig. 1.4). Results correspond to the LON86 region but similar results are obtained in other regions (not shown). For 3-hourly data in cold (Fig. 1.4a) and warm (Fig. 1.4b) seasons, dry events represent on the order of 30-70% of the total events, with a larger value in the high horizontal resolution dataset (70.5% in cold and 66.9% in warm season) compared to the coarser one (46.5% in cold and 32.3% in warm season). Low and moderate precipitation events (those between 0.1 and 16 mm/day) are more frequent in the aggregated data at 6.4° grid spacing (42.8% in cold and 54.7% in warm season) compared to the 0.4° horizontal interval dataset (22.5% in cold and 20.5% in warm season). Finally, 3-hourly events with precipitation rates higher than 64 mm/day show a relative frequency more than an order of magnitude larger in the 0.4° grid spacing than in the 6.4° data (0.38 versus 0.005% in cold and 0.57 versus 0.03% in warm seasons); that is, heavier precipitation events are more frequent in high-resolution precipitation field (see Fig. 1.4a and 1.4b).

A similar behaviour is found when computing intensity-frequency distributions for several spatial resolution datasets for 16-day cumulated periods (Fig. 1.4c and 1.4d). In this case, the temporal aggregation tends to filter out the more extreme simulated precipitation (both the no-precipitation and heavier events), thus producing an increase in the relative frequency of low- to moderate-precipitation events for every spatial scale. As a result, differences in relative frequencies between different horizontal resolution datasets are strongly reduced, showing that time averaging can limit the effect of changing the spatial resolution of the data. Nevertheless, in both seasons, heavier precipitation events (those larger than 8 mm/day) are more frequent in the higher resolution dataset.

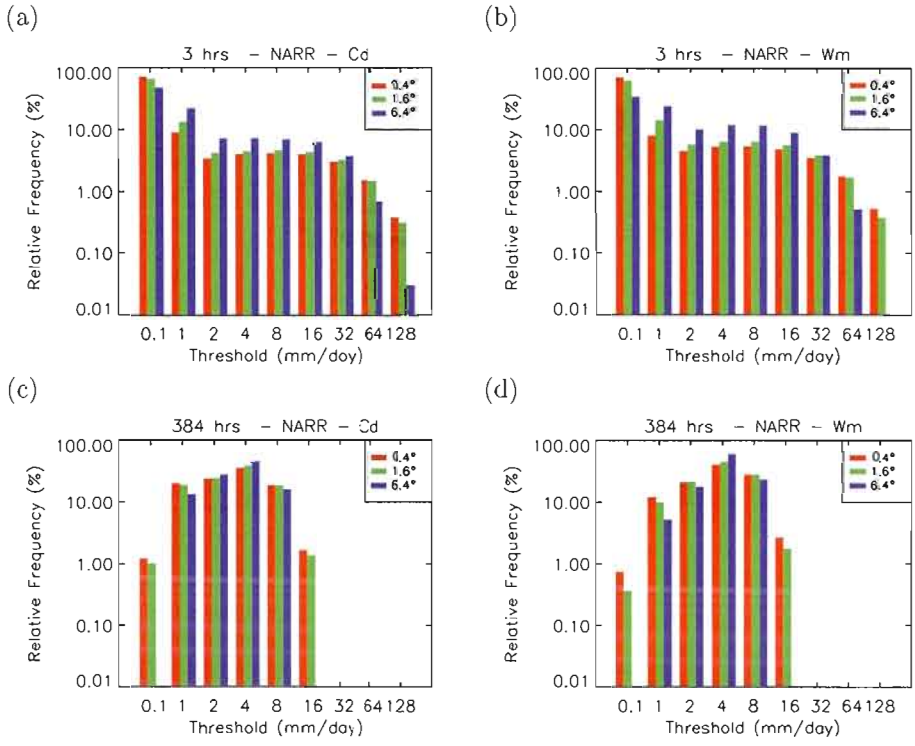

Figure 1.4 LON86 spatial-mean intensity distributions of precipitation rate as simulated by the NARR reanalysis for 3-hourly data in (a) cold and (b) warm seasons and for 16-days data in (c) cold and (d) warm seasons. Colors are associated with 0.4° (red), 1.6° (green) and 6.4° (blue) spatial scales. Only frequencies greater than 0.01% are shown.

The dissimilar sensitivity to changes in spatial resolution exhibited by different precipitation intensities has important implications in AV studies. It suggests that different statistics will show different potential for added value depending on which part of the distribution is sampled. That is, higher moments of the distribution (e.g., intensity and frequency of heavier precipitation rate events) show a much larger sensitivity to changes in resolution than central moments (e.g., low-moderate precipitation rate events). As already mentioned in section 1.4.2, we will use the 95th percentile of the wet-event distribution in order to assess the PAV for the several HRD.

1.5.2 Regional (Spatial-mean) potential added value results

Top panels in Fig. 1.5 show the spatial-mean 95th percentile ($q^{n,0}_{mean,95}$, see section 1.4.2 for computation details) of 3-hourly precipitation over the region LON86 as a function of spatial scales. Left and right panels show cold- and warm-season results, and the different curves represent percentiles as calculated from NARR and NARCCAP-RCM simulations. In both seasons and independently of the HRD considered, there is an increase of the $q^{n,0}_{mean,95}$ value as the spatial resolution increases. Quantitative changes, however, are significantly different when considering different HRDs. For example, in cold season, the WRFP model suggests an increase of 28 mm/day in $q^{n,0}_{mean,95}$ between the 6.4° scale (~25 mm/day) and the 0.4° spatial scale (~53 mm/day). The CRCM model shows a change of only 8 mm/day between the same spatial scales (~15 and ~23 mm/day, respectively). It is also clear from Fig. 1.5 that differences between model estimations tend to be larger as the horizontal scale of the data decreases; that is, the model uncertainty associated with the estimation of $q^{n,0}_{mean,95}$ is higher as the horizontal resolution of the data increases.

Fig. 1.5c and 1.5d show $q_{mean,95}$ for 16-days precipitation datasets. In this case, differences between the $q^{n,7}_{mean,95}$ value in high- and low-resolution datasets are greatly reduced and the spatial-scale dependence of the $q^{n,7}_{mean,95}$ is very low. Differences between the several dataset estimations of the spatial-mean 95th percentile are somewhat less important than in the 3-hourly case, and the change of $q^{n,7}_{mean,95}$ between 0.4° and 6.4° seems to be quite similar in all RCMs.

The difference between small and large spatial scale climatic statistics can be highlighted by defining the PAV measure as

$$PAV^m = q^{0,m}_{mean,95} - q^{3,m}_{mean,95}, \tag{1.1}$$

where $q^{0,m}_{mean,95}$ and $q^{3,m}_{mean,95}$ represent the spatial-mean 95th percentile at temporal scale m and spatial grid spacings of approximately 0.4° and 3.2° respectively (i.e., a jump in resolution of around 8 (64) in the linear (quadratic) horizontal dimension). The PAV^m quantity measures the difference between the representation of $q^m_{mean,95}$ at fine (i.e., RCMs) horizontal scale and its large-scale approximation at the temporal scale m. Assuming that the 3.2° spatial scale can be interpreted as a good proxy of the statistics estimated from a GCM at 3.2° grid spacing, then PAV^m can be used to estimate the potential added value of a RCM over a GCM as discussed in section 1.2.3.

A near zero value of the PAV quantity means that, for the quantity of interest (e.g., spatial-mean 95th percentile), the high-resolution estimation does not add extra information over the coarse resolution one. Analogously, $PAV \sim 0$ can be interpreted

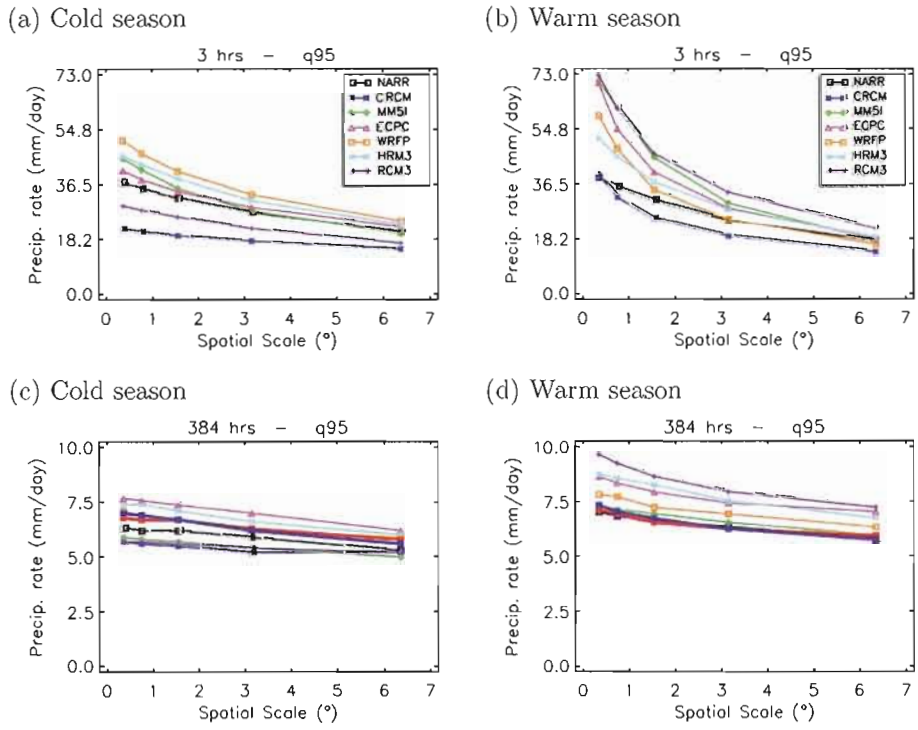

Figure 1.5 Spatial-mean 95th percentile as a function of spatial scales for 3-hourly precipitation in (a) cold and (b) warm seasons. Also shown is the 16-days spatial-mean 95th percentile in (c) cold and (d) warm seasons. Results correspond to the LON86 region. Symbols and colors denote the HRD used in each case. Red and blue thicker lines represents CPC and UWash results respectively (only available for 16-days results).

as if the application of spatial filters in order to approximate the high-resolution precipitation field at lower resolutions doesnt filter out any fine-scale variability. Sufficient conditions for $PAV = 0$ are given by a spatially uniform intensity-frequency distribution field or a field that only contains variability at scales larger than 3.2°.

It should be clear, as was discussed in the introduction, that a non-zero value for PAV does not necessarily mean that the RCM is adding value, because the small-scale variability may not necessarily be skilful. That is, $PAV \neq 0$ is a necessary, but not sufficient, condition for a high-resolution adding value to lower resolution fields.

A relative measure of spatial-mean PAV^m can also be obtained by defining

$$rPAV^m = \frac{PAV^m}{q^{0,m}_{mean,95}} = 1 - \frac{q^{3,m}_{mean,95}}{q^{0,m}_{mean,95}}, \tag{1.2}$$

so that $0 \leq rPAV^m \leq 1$. The $rPAV^m$ quantity evaluates the proportion of fine spatial scale 95th percentile ($q^{0,m}_{mean,95}$) that is not accounted by its large-scale part ($q^{3,m}_{mean,95}$). Thus $rPAV^m \sim 0$ suggests that no fine-scale information is needed to determine $q^{0,m}_{mean,95}$, and $rPAV^m \sim 1$ means that $q^{0,m}_{mean,95}$ is solely determined by the fine-scale information.

1.5.2.1 High temporal resolution data

The improvement in the representation of surface forcings such as topography, lakes and coastal regions due to the higher resolution of RCMs compared to GCMs is expected to strongly influence the added value. A simple but partial assessment of this dependence can be performed by evaluating the PAV in regions with significantly different surface conditions. We expect that the most important forcing is the topographic one, which is particularly relevant over western where relatively high values and large spatial gradients of the terrain height are found (see Fig. 1.2). It should be clear however that differences between regions are not limited to surface forcings but can also be related with other stationary forcings such as the planetary-scale waves (e.g., summertime subsidence in the West Coast) or the moisture sources (e.g., Gulf of Mexico low-level jet in the Great Plains).

Figure 1.6 shows the 3-hourly PAV (top panels) and rPAV (bottom panels) as a function of regions (from west to east) for the spatial-mean 95th percentile ($q^{n,0}_{mean,95}$). In cold season (see Fig. 1.6a), NARCCAP-RCMs show PAV values on the order of 12

mm/day with little variations between the regions, but showing some higher values in eastern regions (those regions to the east of LON98). Differences between RCM PAV estimations are on the order of ±5 mm/day (i.e., ~50%) with slightly larger values over eastern regions. PAV values as estimated from the NARR dataset (black line) are also on the order of 12 mm/day, showing a large resemblance with the NARCCAP ensemble-mean (grey line) latitudinal profile.

In warm season (Fig. 1.6b), most RCMs show significant differences between eastern and western regions, with maximum values in LON92 and LON86 regions, and minimum values to the west of LON105. The maximum near central regions is probably due to a relative decrease of the influence of convective activity toward eastern regions. PAV values are on the order of 10 mm/day in western regions and on the order of 25-30 mm/day in eastern regions. Differences between RCM estimations are approximately ±5 mm/day (i.e., ~50%) in western regions and ±15 mm/day (i.e., >50%) in eastern regions. In this season, the ECPC RCM shows much larger values of PAV than other RCMs, particularly in western regions with values 3 times larger than every other RCM, mainly due to much larger values of $q^0_{mean,95}$ for fine spatial scales (not shown). It is also evident that in this season the NARR tends to produce the lowest PAV values for all regions considered. In this case, NARR-low PAV values are related with a tendency to produce very low 95th percentile at fine spatial scales.

Figures 1.6c and 1.6d show the 3-hourly rPAV measure as a function of regions for cold and warm season, respectively. NARCCAP ensemble-mean cold-season values are on the order of 0.4, suggesting that around 40% of the fine scale $q^0_{mean,95}$ comes from fine-scale variability that is filtered when spatially averaged. In warm season, the NARCCAP ensemble-mean value is on the order of 0.6, showing that a larger part of the fine scale $q^0_{mean,95}$ comes from fine spatial scale variability. That is, in all regions, warm-season rPAV values are higher than cold-season values, showing that fine spatial scale variability of precipitation is relatively more important in warm season due to the finer scale of precipitation systems in summer (i.e., convection systems dominate) compared to winter (i.e., synoptic systems dominate). Again, in all regions and particularly in the warm season, NARR tends to produce the lowest rPAV values of all datasets with an average over regions of 0.3 and 0.4 in cold and warm seasons, respectively.

Interesting changes in the regional behaviour are noted when analyzing the rPAV measure. In both seasons, the ensemble-mean of rPAV shows higher values in western regions (0.45 in cold and 0.6 in warm seasons) compared to eastern region (0.35 in

cold and 0.5 in warm seasons). As already stated, western regions are characterized by more important surface forcings than eastern regions and so the larger rPAV values in western regions are probably induced by a fine-scale orographic component. In the warm season, there is also a decrease of rPAV from central to east regions maybe related with a relative decrease of the convective activity towards the Atlantic coast.

Differences between rPAV values as estimated from the several RCMs are somewhat smaller compared to the PAV quantity, suggesting that absolute values can be very different but the scaling properties of precipitation are similar for the several models.

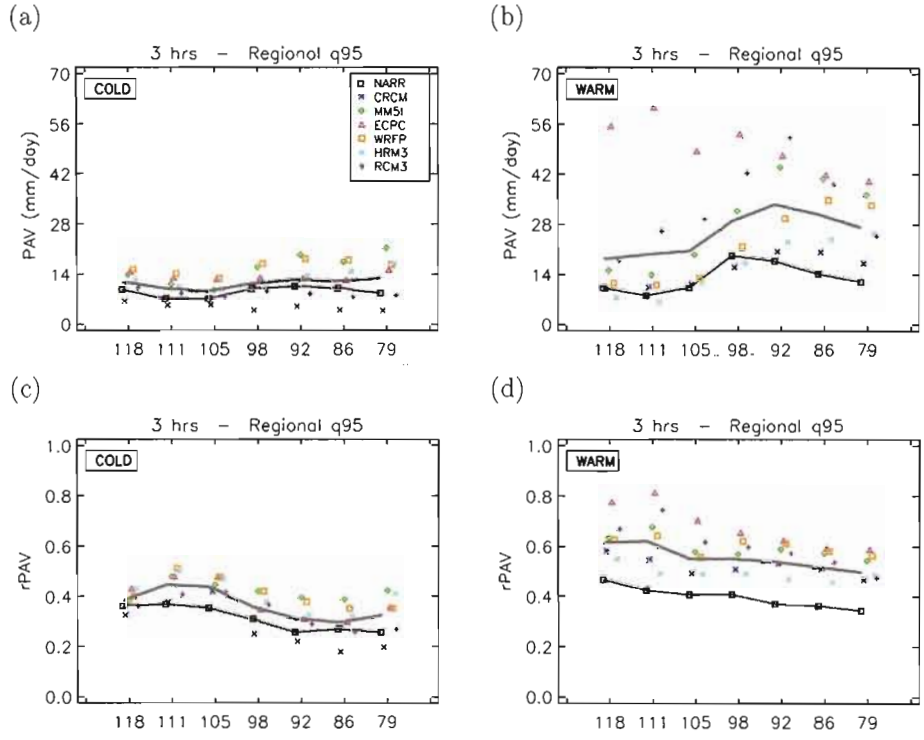

Figure 1.6 3-hourly regional PAV measure as a function of regions for the 95th percentile for (a) cold season and (b) warm season. Also shown is the relative PAV measure for (c) cold season and (d) warm season. Symbols denote individual NARCCAP-RCMs results and lines denote the NARCCAP-ensemble mean (grey) and NARR results (black).

1.5.2.2 Low temporal resolution data

Figure 1.7 shows PAV (top panels) and rPAV (bottom panels) for the spatial-mean 95th percentile for the 16-days temporal scale. In both seasons, differences between the 95th percentile at fine ($q^{0,7}_{mean,95}$) and large ($q^{3,7}_{mean,95}$) scales are much smaller than in the 3-hourly case, with PAV values generally smaller than 2 mm/day.

Cold-season results show that there is a very good agreement, particularly in eastern regions, between results produced by NARCCAP RCMs, NARR, CPC and UWash observations. In warm season and assuming that UWash observations represent the most reliable source of information, it seems that NARCCAP RCMs tend to produce a weak overestimation of the PAV quantity over western regions, with a large overestimation by the ECPC RCM. In eastern regions, NARCCAP RCM values are in good agreement with those from CPC and UWash, with NARR data tending to produce a slight underestimation compared to observed values. The underestimation of NARR is also noted when studying daily data (not shown), suggesting that the low values in the NARR over eastern regions at 3-hrs (Fig. 1.6b and 1.6d) are, at least partially, related with an underestimation of the potential AV of the NARR data.

More interesting is the behaviour of the rPAV measure (bottom panels in Fig. 1.7). As for the absolute PAV measure, rPAV decreases significantly compared to the 3-hourly values. In both seasons, the rPAV ensemble-mean value decreases by a factor of ~3-4 compared to the 3-hourly values (from 40 to 15% in cold season and from 60 to 15% in warm season). This decrease is due to the fact that the application of the temporal filter induces a different change in high and low spatial resolution 95th percentiles. As shown in Fig. 1.5, the relative change of the fine spatial resolution $q^{0}_{mean,95}$ between 3-hr and 16-day period (by a factor of 6 to 10) is much more important than the same change for the coarse-resolution $q^{3}_{mean,95}$ (by a factor of 3 only).

The 16-days NARCCAP ensemble mean rPAV measure still shows higher values in mountainous compared to non-mountainous regions, with values of 17% and 9%, respectively, for cold season, and 24% and 13%, respectively, for warm season. In the cold season, NARCCAP ensemble mean results are in very good agreement with those obtained using the observed datasets. In the warm season, however, CPC shows almost identical values of rPAV no matter the region considered, suggesting no clear influence of surface forcings in this season. In contrast, UWash mean values over mountainous and non-mountainous regions are of 20% and 14% respectively, indicating that there is

some impact of surface forcings in agreement with NARCCAP mean results. Whereas all datasets suggest similar values for the rPAV in non-mountainous regions, the differences between datasets arise in the representation of rPAV in mountainous regions. Given that the PRISM algorithm has exhibited a superior performance than other geostatistical methods in distributing point measurements of precipitation (see Daly et al. 1994), differences in mountainous regions may be interpreted as an underestimation of CPC rPAV compared to UWash data. The reasons of this underestimation are not well known but could be related with a misrepresentation of stations in these regions. The CPC station density is highest in the eastern two-thirds of the United States with lowest values over western regions (Higgins et al., 2008) where the complex topography would demand for higher densities.

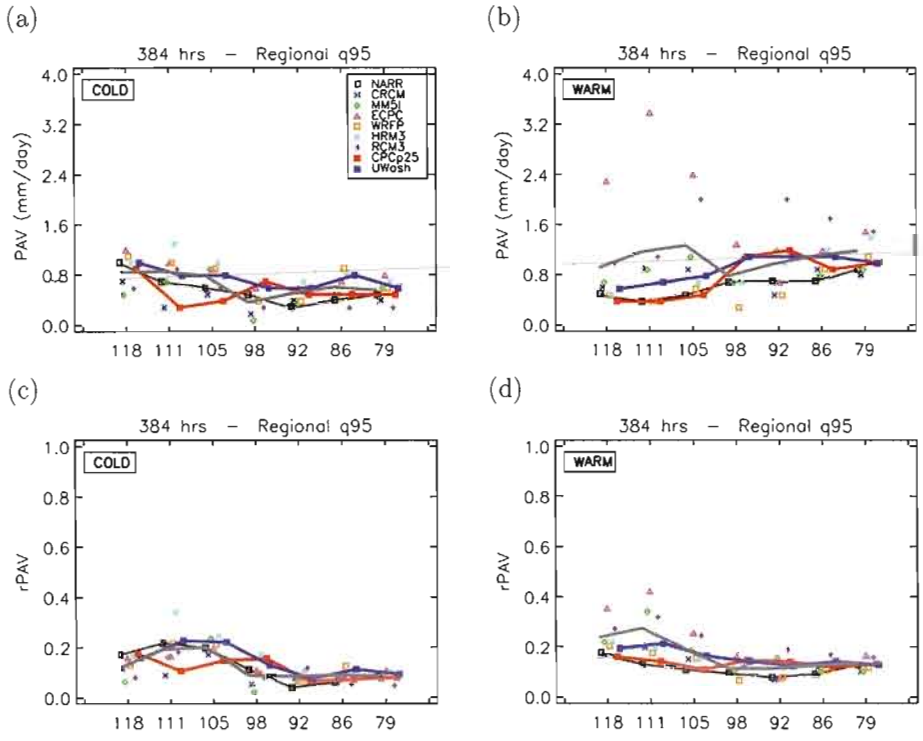

Figure 1.7 As in Fig. 1.6 but for the 16-days regional PAV and rPAV measures. Red and blue lines represent CPC and UWash results respectively.

1.5.3 Local (Spatial-maximum) potential added value results

So far, we have analyzed a regional contribution to the overall PAV by computing the spatial-mean percentiles ($q^{n,m}_{mean,95}$). In this section, we present results obtained by using a more local measure of the fine spatial scale variability by computing the PAV quantity with $q^{n,m}_{max,95}$ (see section 1.4.2). The use of the PAV measure computed from $q^{n,m}_{max,95}$ could be interpreted as an estimation of the maximum value that can be obtained from RCM simulations by considering individual grid-point (i.e., local) results over a given region. As was already stated, differences between $q^{n,m}_{mean,95}$ and $q^{n,m}_{max,95}$ arise mainly due to the presence of horizontal structures of stationary forcings and so they should be more important in those regions with complex topography.

1.5.3.1 High temporal resolution data

Top panels in Fig. 1.8 show the 3-hourly $q^{n,m}_{max,95}$ PAV for the different models as a function of regions for cold (Fig. 1.8a) and warm (Fig. 1.8b) seasons. In most of the regions, the PAV absolute values computed from $q^{n,m}_{max,95}$ are around twice as large as in the spatial-mean case ($q^{n,m}_{mean,95}$) (see top panels in Fig. 1.6), with the exception of the LON118 region that shows PAV values on the order of six times larger than in the mean case. In both seasons, differences between the several HRD estimations are somewhat larger than in the mean case, with absolute differences of the order of ± 25 mm/day.

Bottom panels in Fig. 1.8 show the spatial-maximum rPAV for cold (Fig. 1.8c) and warm (Fig. 1.8d) seasons. rPAV values are also higher in the spatial-maximum case than in the spatial-mean case (see bottom panels in Fig. 1.6), but differences are very dependent on the region and the season considered. In cold season and mountainous regions, the NARCCAP ensemble-mean rPAV value is $\sim$40% for the regional measure and $\sim$65% for the local measure. For the same season and flatter regions, NARCCAP mean rPAV values are $\sim$30% and $\sim$45% for the regional and local measures respectively. For the NARR dataset values are $\sim$30% and $\sim$45% for the regional and local measures respectively.

In the warm season, the NARCCAP mean rPAV values is $\sim$70% ($\sim$60%) in mountainous regions and $\sim$60% ($\sim$55%) in non-mountainous regions for the local (regional) measure. In this season, much smaller values on the rPAV measure are present in the NARR dataset. As it will be clear in the next section when including in the analysis CPC results, differences between NARCCAP and NARR arise because NARR tend

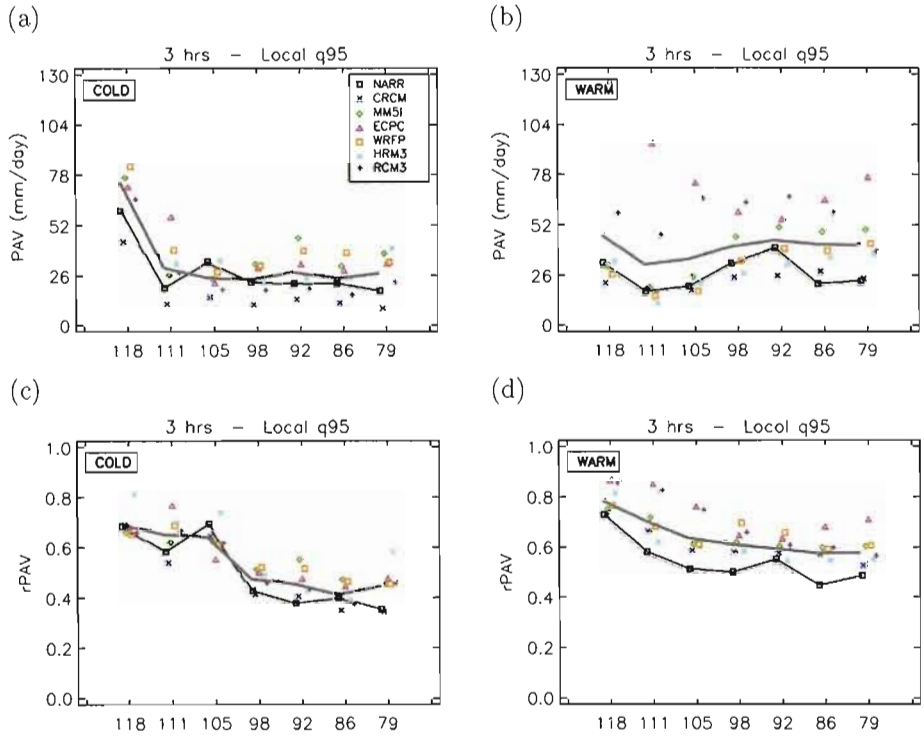

Figure 1.8 As in Fig. 1.6 but for the 3-hourly local PAV and rPAV measures.

to slightly underestimate rPAV values in both eastern and western regions, and the NARCCAP ensemble-mean tends to overestimate rPAV values, particularly in western regions.

1.5.3.2 Low temporal resolution data

Figure 1.9 shows PAV (top panels) and rPAV (bottom panels) for the spatial-maximum 95th percentile for the 16-day temporal scale. As in the spatial-mean case, PAV values are much smaller than in the 3-hourly case, generally smaller than 6 mm/day with the exception of western regions in cold season (see Fig. 1.9a).

Interestingly, in both seasons, $q_{max,95}^{n,m}$ rPAV results (Fig. 1.9c and 1.9d) show that the relative importance of small-scale features in western regions is quite well preserved after the temporal averaging, with a NARRCAP ensemble-mean rPAV value of ~55% (versus ~65% in 3-hourly data) in cold season and of ~60% (versus ~70% in 3-hourly

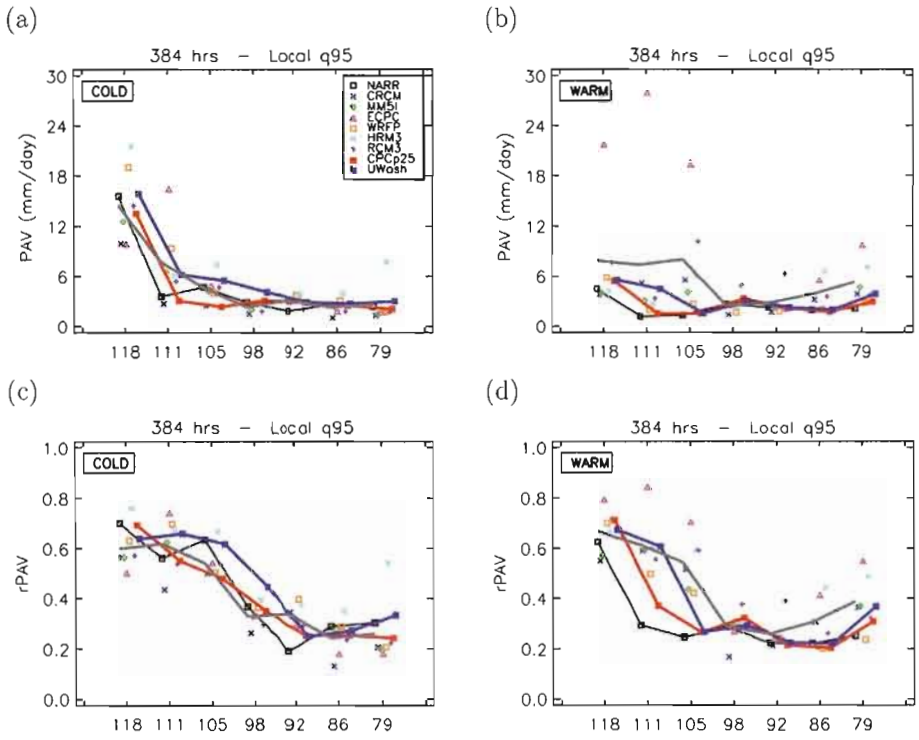

Figure 1.9 As in Fig. 1.6 but for the 16-days local PAV and rPAV measures. Red and blue lines represent CPC and UWash results respectively.

data) in warm season. The fact that rPAV is barely sensitive to temporal average shows that locally the surface forcing component of rPAV (i.e., stationary forcings) in mountainous regions plays an important role. In regions with lower influence of surface forcings, a larger decrease of rPAV is noted when comparing 3-hourly and 16-day spatial-maximum values, with rPAV values near ~25% and ~45% (~30% and ~60%) for 16-day and 3-hourly data respectively in cold (warm) season.

To what extent the results obtained for the 95th percentile can be extrapolated to other climate statistics? As mentioned, an analysis similar to this one was conducted for other climate statistics such as temporal mean, wet-events statistics and other percentiles. For example, the spatial mean of the temporal average is conserved for changes in the spatial resolution of the data and so the PAV associated with this quantity is nil. However, the spatial maximum of the temporal mean is not conserved (i.e., locally, the mean value can be different) and can be used to estimate the associated PAV. Results

(not shown) suggest almost identical results as for the 95th percentile, with slight decrease in rPAV values. That is, for local measures, the sensitivity of the temporal mean to changes in resolution tends to be similar to those found in high-order percentiles.

1.6 Discussion

The use of RCMs to dynamically downscale large-scale atmospheric fields in present and future climate conditions has gained popularity during the last 20 years. There is still a need, however, to objectively quantify the added value obtained by the RCM downscaling technique. For example, specific knowledge about where and with respect to which climate statistics RCMs can produce more skilful results than GCMs constitutes a very useful information for climate-scenarios users such as those performing impact and adaptation studies. Studies trying to validate the RCM downscaling technique are also essential to highlight the importance of developing RCMs and the use of its products instead of those coming from lower resolution GCMs in some particular applications.

This article concentrated on the characterization of a necessary condition that RCM-simulated climate statistics must satisfy in order to generate some AV: that the climate statistics of interest contain some fine spatial scale variability that is absent in coarser GCMs. This prerequisite condition and its dependence on several factors (seasons, regions, etc) was assessed in the context of a perfect-model framework, designated as potential added value framework, that includes:

1. The multi-resolution (MR) method is used to aggregate to several spatial and temporal scales the original high-resolution precipitation fields simulated by six RCMs (NARCCAP; Mearns et al. 2009) and as represented by a reanalysis (NARR; Mesinger et al. 2006) and two observation gridded datasets (CPC, Higgins et al. 2000; UWash, Maurer et al. 2002). The MR method is particularly suitable for the precipitation variable due to its non-periodicity (both in time and space), which allows performing a local analysis that cannot be done with, for example, Fourier-based procedures.

2. 95th percentiles are computed from each of the several datasets defined by the MR technique based on two different methods: one that estimates the spatial mean (regional) 95th percentile over a given region and a second that estimates the maximum (local) 95th percentile computed from individual grid points over a

given region.

3. Potential added value (PAV) measures are then defined as the difference between 95th percentiles estimated at large (GCM scale) and small (RCM scale) spatial scales for every high-resolution dataset.

The methodology appears to be robust to small changes in spatial scales and the location and size of regions. Several sensitivity tests were performed by slightly changing these three parameters and PAV values changes were on the order of 5-10%, rarely exceeding 15% in mountainous regions for longest temporal scales due to the lesser number of data. In any case, regional and seasonal dependence of PAV measures remains the same after the slight changes in parameters.

An overview of the results are summarized in Fig. 1.10 for the regional (Fig. 1.10a and 1.10b) and the local (Fig. 1.10c and 1.10d) rPAV measures. Results are shown for the NARCCAP RCM ensemble-mean and for NARR, CPC and UWash datasets when available. NARCCAP ensemble error bars are estimated by using the standard deviation computed from the ensemble of NARCCAP-RCM estimations. In general, results tend to confirm some statements generally outlined with respect to the advantages of using high-resolution RCMs. For the regional measure we obtain:

- PAV is much higher for short temporal scales due to the influence of transient forcings (e.g., convection) that tend to be filtered out by the time-averaging process. rPAV is 3-4 times larger in 3-hourly (see Fig. 1.10a) data than in 16-day mean data (see Fig. 1.10b).

- PAV is higher in warm compared to cold season due to the larger fraction of precipitation falling from small-scale systems (e.g., convection) in warm season (see Fig. 1.10a and 1.10b).

- Regions of complex topography (i.e., western regions) induce an extra component of rPAV, no matter the season or the temporal scale considered. Its relative importance is larger for long-term mean quantities and cold season due to the relatively minor importance of transient PAV sources (see Fig. 1.10a and 1.10b).

- Assuming that the UWash precipitation analysis constitutes the most reliable estimation of the real climate PAV, then the NARCCAP-RCMs ensemble-mean constitutes a very good approximation of the PAV measures with a slight overes-

timation of PAV in warm season and western regions. NARR tends to produce a slight underestimation of PAV values in warm season and in eastern regions.

When assessing the local measure some differences appear:

- No matter the region and season considered, there is an increase in rPAV values compared to the spatial mean rPAV estimations.
- The relative importance of the orographic component in the rPAV measure is larger than in the spatial mean case (see Fig. 1.10c and 1.10d), particularly for longer temporal scales.

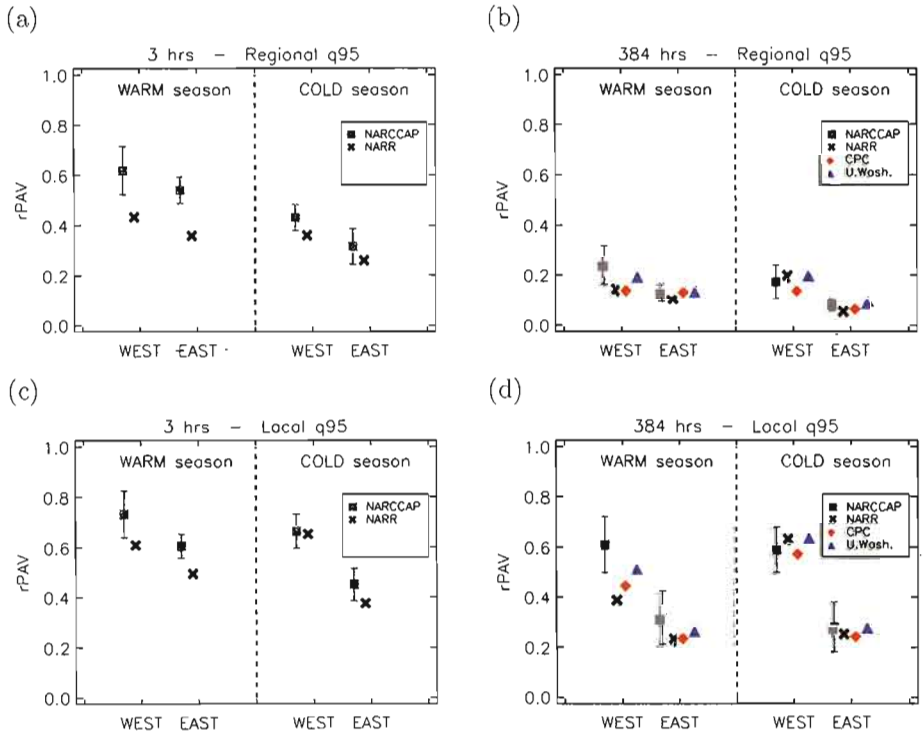

Figure 1.10 Ensemble-mean values for the rPAV measure computed from the regional 95th percentile for (a) 3-hourly and (b) 16-days data. Also shown is the local 95th percentile for (c) 3-hourly and (d) 16-days. Colors denote NARCCAP (grey squares), NARR (black crosses), CPC (red diamonds, when available) and UWash (blue triangles, when available) results. West and east designate the mean value obtained for regions to the west and east of the -98° of longitude respectively. Error bars are given by the standard deviation of the several NARCCAP-RCM estimations.

Results point out that the potential of RCMs to add some value can be very limited when considering time-averaged statistics for regional measures. For example, the spatial-mean rPAV for 16-day means data is on the order of 10-15% for non-mountainous regions in both warm and cold seasons. The estimated PAV was derived from the precipitation field, a variable that is particularly characterized by a flat power spectrum with a sizable variance in a wide range of spatial scales. PAV is expected to be less important for variables with a steeper power spectrum (e.g., geopotential height, temperature, sea level pressure), but this speculation remains to be confirmed and quantified.

Acknowledgements

This research was done as part of the PhD project of the first author and as a project within the Canadian Regional Climate Modelling and Diagnostics (CRCMD) Network, funded by the Canadian Foundation for Climate and Atmospheric Sciences (CFCAS) and Ouranos. The authors would like to thank Mourad Labassi, Abderrahim Khaled and Georges Huard for maintaining a user-friendly local computing facility, the helpful comments of two anonymous reviewers and to the North American Regional Climate Change Assessment Program (NARCCAP) for providing some of the data used in this paper. NARCCAP is funded by the National Science Foundation (NSF), the U.S. Department of Energy (DOE), the National Oceanic and Atmospheric Administration (NOAA) and the U.S. Environmental Protection Agency Office of Research and Development (EPA). We acknowledge the developers of the CPC US Unified Precipitation data, which we obtained from the NOAA/CIRES/ESRL PSD Climate Diagnostics Branch (Boulder, Colorado) from their Web site at http://www.cdc.noaa.gov/. NARR 3-hourly data were obtained from the Physical Sciences Division of NOAA (http://www.cdc.noaa.gov/cdc/data.narr.html). We acknowledge the Surface Water Modeling group at the University of Washington for making freely available the UWash precipitation product. Finally, thanks are extended to the Global Environmental and Climate Change Centre (GEC3), funded by the Fonds québécois de la recherche sur la nature et les technologies (FQRNT), for extra financial support.

CHAPTER II

POTENTIAL FOR ADDED VALUE IN RCM-SIMULATED SURFACE TEMPERATURE

This chapter is presented in the format of a scientific article that was submitted to the Climate Dynamics journal. The design of the research and its performance together with the analysis of data and the redaction of this article are entirely based on my work, with the co-authors involved in the supervision of all these tasks.

Di Luca, A., de Elía R. and Laprise, R.: "Potential for added value in RCM-simulated surface temperature". Submitted to Climate Dynamics.

Alejandro Di Luca - René Laprise
Centre ESCER (Étude et Simulation du Climat à l Échelle Régionale),
Département des Sciences de la Terre et de l'Atmosphère
Université du Québec à Montréal (UQAM)
B.P. 8888, Succ. Centre-ville
Montréal (Québec) Canada H3C 3P8

Ramón de Elía
Centre ESCER (Étude et Simulation du Climat à l Échelle Régionale),
Consortium Ouranos. 550 Sherbrooke West, 19^{th} floor. West Tower,
Montréal (Québec) Canada H3A 1B9

Abstract

Regional Climate Models (RCMs) have been developed in the last two decades in order to produce high-resolution climate information by downscaling Atmosphere-Ocean General Circulation Models (AOGCMs) simulations or analyses of observed data. A crucial evaluation of RCMs worth is given by the assessment of the value added compared to the driving data. This evaluation is usually very complex due to the manifold circumstances that can preclude a fair assessment. In order to circumvent these issues, here we limit ourselves to estimating the *potential* of RCMs to add value over coarse-resolution data. We do this by quantifying the importance of fine-scale RCM-resolved features in the near-surface temperature, but disregarding their skill. The Reynolds decomposition technique is used to separate the variance of the time-varying RCM-simulated temperature field according to the contribution of large and small spatial scales and of stationary and transient processes. The temperature variance is then approximated by the contribution of four terms, two of them associated with coarse-scales (e.g., corresponding to the scales that can be simulated by CGCMs) and two of them describing the *original* contribution of RCM simulations. Results show that the potential added value (PAV) emerges almost exclusively in regions characterised by important surface forcings either due to the presence of fine-scale topography or land-water contrasts. Moreover, some of the processes leading to small-scale variability appear to be related with relatively simple mechanisms such as the distinct physical properties of the Earth surface and the general variation of temperature with altitude in the Earth atmosphere. Finally, the article includes some results of the application of the PAV framework to the future temperature change signal due to anthropogenic greenhouse gasses. Here, contrary to previous studies centred on precipitation, findings suggest for surface temperature a relatively low potential of RCMs to add value over coarser resolution models, with the greatest potential located in coastline regions due to the differential warming occurring in land and water surfaces.

Keywords: regional climate model; temperature; surface forcings; potential added value; variance decomposition.

2.1 Introduction

Regional climate modelling consists of using time-dependent large-scale atmospheric fields and ocean surface boundary conditions to drive a high-resolution atmospheric model integrated over a limited-area domain (Giorgi et al. 2001). The models used for this purpose, usually called nested Regional Climate Models (RCMs), have been developed in order to simulate fine-scale climate processes and variability that cannot be resolved by lower resolution Atmosphere-Ocean General Circulation Models (AOGCMs) (Dickinson et al. 1989; Giorgi and Bates 1989). A major motivation in their development was, and still is, the need of detailed climate information at regional, and even local scales, in order to assess the possible impacts of climate changes in the next decades.

Most state-of-the-art RCMs include a land surface model representing mass, momentum and energy exchanges between the land surface and the atmosphere. Some of them are also coupled with other components of the climate system such as lakes, vegetation and ocean. Atmospheric variables (winds, temperature, pressure and water vapour) at the lateral boundaries and sea surface temperatures (SSTs) and sea ice (SI) concentrations at the surface boundaries are either derived from coarse-resolution AOGCMs or the analyses of observations (reanalyses). Actual horizontal grid spacing used to run multi-decadal RCM simulations varies between 10-50 km (e.g., Giorgi et al. 2009) thus implying a jump in resolution of 2 to 10 compared to AOGCMs. For a detailed discussion about technical issues related with the nesting RCM technique and its potential merits and limitations, readers may refer to one of the several review articles than have been published (Giorgi and Mearns 1991; Wang et al. 2004; Laprise et al. 2008; Rummukainen 2010).

A crucial element in the development of any numerical model trying to describe some aspect of the natural world is its evaluation. That is, in order to quantify how reliable a numerical model is and how confident we can be about its simulations and forecast, model results should be compared with observations in the real world (Randall et al. 2007). For instance, the evaluation of AOGCMs generally proceed by testing their ability to simulate the climate statistics of the recent past. A similar approach can, in principle, be used to test the behaviour of RCMs assuming that high-resolution reliable observations are available (see Prömmel et al. (2010) and references therein).

However, because RCMs are not self-contained tools for climate simulation (i.e., they need boundary conditions from other models or historical analyses), their evalua-

tion must also consider a comparison against the driving data. That is, as pointed out by Prömmel et al. (2010), the key question in RCMs evaluation is not simply whether the RCM-simulated climate compares well with the observed climate, but whether the RCM-simulated climate constitutes a *better* approximation of the observed climate, at least for some particular aspect, than the driving data, i.e., if the RCM produces some added value (AV) over the driving data.

Various articles have been published about the AV issue in the last years (see, for example, Prömmel et al. (2010), Di Luca et al. (2011a), Feser et al. (2011) and references therein). Several conclusions can be drawn from the existing literature about AV. First, that RCMs do not seem to add value to the driving data in a consistent and systematic way, but rather suggest that the generation of AV is conditional to a number of factors such as the variable and the climatic statistics of interest, the specific performance of an RCM and the driving data used in the comparison, the characteristics of the region, etc.

An example that illustrates this assertion can be taken from the study of Prömmel et al. (2010). They evaluated the added value in the 2-m temperature field as simulated by the REMO RCM compared to the driving European Centre for Medium-Range Weather Forecasts 40-years reanalysis (ERA40) by using a dense station dataset over the Greater Alpine Region (GAR, 0°-20°E and 40°-50°N). Temporal correlations between observed and ERA40 monthly-mean time series are generally slightly higher than between observations and REMO in most of the GAR with only the exception of the more complex topography subregions where REMO shows higher correlations. When looking at 2-m temperature root mean square error, results showed that REMO tends to slightly outperform ERA40 in regions of complex topography but showing little improvement or even degradation of results in flatter subregions surrounding the Alps, particularly during the summer season. Hence, the question is still open regarding in which particular cases (i.e., where, when, for which metric, etc.) an RCM will produce an improvement in the representation of the climate compared to the driving data.

A second point is that most of the articles concentrate on an individual pair of RCM results and driving data, thus precluding the generalisation of results. Particularly, AV results derived from a single pair of RCM-GCM could be strongly dependent on the climate models themselves, reflecting differences due to the models' performance instead of general conclusions about the advantages/disadvantages of the RCM technique.

As noted by Feser et al. (2011), most AV studies are based on the comparison

between RCMs output and their driving data. The AV arising from this kind of analysis can be considered as a minimum requirement to justify the additional computational effort of RCMs simulations. As pointed out by Laprise et al. (2002), a more complete evaluation of RCMs should be done also in terms of their improvements compared to other statistical and/or empirical downscaling method, generally more affordable and cheaper in terms of computational resources.

With the aim of contributing to the discussion about AV issues, Di Luca et al. (2011a) developed a framework nicknamed potential added value (PAV) based on the assumption that RCMs can add value in small scales if and only if they add variance at these fine scales. This methodology is well suited at clarifying the sources of added value in small scales, although the switch from AV to PAV is not without drawbacks. In particular, this framework was used to evaluate the potential of RCMs to add value in a variety of precipitation climate statistics using an ensemble of RCM simulations.

The objective of the present article is threefold: first, to describe a modified version of the PAV framework and a new set of statistics particularly useful for the study of the PAV in near-surface temperature; second, to apply this methodology in order to point out which seasons and regions of North America could benefit from dynamical downscaling of present climate; third, to briefly discuss the difference between added value in present climate and in the climate-change signal. We are aware that, while near-surface temperature is a key variable because it is widely used in climate studies and in climate change projections, it is not necessarily the best variable to assess the benefits of using high-resolution climate models. Indication about the PAV associated with temperature statistics, however, can be of great interest to those using it in climate and climate change studies.

The paper is structured as follows. The next section presents a brief description of the data used. Sect. 2.3 describes the general framework used to evaluate the PAV together with the variance decomposition used to separate large- and fine-scale contributions. Sect. 2.4 presents temperature results separated in three parts: the potential added value in present climate simulations, some discussion of the complexity of this AV, and the PAV in the temperature climate-change signal for future projections. Lastly, concluding remarks are given in Sect. 2.5.

2.2 Data

The RCM simulations used in this study were provided by the North American Regional Climate Change Assessment Program (NARCCAP; http://www.narccap.ucar.edu/; Mearns et al. 2009). In NARCCAP, six RCMs were run with a horizontal grid spacing of about 50 km over similar North American domains covering Canada, United States and most of Mexico. Acronyms, full names and a reference, and the modelling group of each RCM are presented, respectively, in the first three columns in Table 2.1.

The NARCCAP experiments include simulations of contemporary climate using lateral boundary conditions (LBCs) derived from the National Centers for Environmental Prediction (NCEP) Department of Energy (DOE) global reanalysis (Kanamitsu et al. 2002) for the 25-year period between 1980 and 2004. NARCCAP also comprises RCM simulations driven at the lateral and lower boundary conditions by AOGCM simulations for present (1971 - 2000) and future climate (2041 - 2070) using the A2 scenario (Mearns et al. 2009). Four AOGCMs are used to drive the RCMs: the Canadian Global Climate Model version 3 (CGCM3, Flato and Boer 2001), the NCAR Community Climate Model version 3 (CCSM3, Collins et al. 2006), the Geophysical Fluid Dynamics Laboratory Climate Model version 2.1 (GFDL, GFDL Global Atmospheric Model Development Team 2004]) and the United Kingdom Hadley Centre Coupled Climate Model version 3 (HadCM3, Gordon et al. 2000). The fourth column in Table 2.1 provides the LBCs used to drive each RCM. A total of 6 RCM-AOGCM pairs are used here to analyze the climate change signal, with two RCMs (CRCM and RCM3) driven by two AOGCMs and two RCMs (WRFG and HRM3) driven by only one AOGCM.

For each RCM simulation, several 3-hourly variables are available in their original map projection; but in this article we will concentrate only on 2-m temperature. Reanalysis driven RCM simulations use AMIP II sea surface temperature (SST) and sea ice (SI) concentration observations as lower boundary conditions (Kanamitsu et al. 2002). AOGCM driven RCM simulations use SST and SI from the AOCGM data. In both reanalysis- and AOGCM-driven simulations, SST and SI surface boundary conditions are updated every 6 hours by using a linear interpolation between consecutive monthly-mean values. Similarly, boundary conditions are interpolated from the low resolution to the ~50-km grid meshes by using a linear interpolation in the horizontal.

Table 2.1 Acronyms, full names (reference) and modelling group of RCMs involved in the NARCCAP project. Column 4 indicates the LBCs used to drive each RCM.

RCM	Full Name (Reference)	Modelling group	LBCs
CRCM	Canadian Regional Climate Model (version 4.2.0) (Caya and Laprise 1999)	Ouranos / UQAM	NCEP-DOE CGCM3 CCSM
ECP2	Experimental Climate Prediction Center Regional Spectral Model (Juang et al. 1997)	UC San Diego Scripps	NCEP-DOE
HRM3	Hadley Regional Model (version 3) (Jones et al. 2004)	Hadley Centre	NCEP-DOE HadCM3
MM5I	MM5 - PSU/NCAR mesoscale model (Grell and Stauffer 1993)	Iowa State University	NCEP CCSM
RCM3	Regional Climate Model (version 3) (Giorgi et al. 1993)	University of of California at Santa Cruz	NCEP-DOE GFDL CGCM3
WRFG	Weather Research and Forecasting model (Leung et al. 2005)	Pacific Northwest National Laboratory	NCEP-DOE CCSM

2.3 Methodology

2.3.1 Potential added value framework

The general conceptual framework used to study the PAV in the temperature field simulated by an ensemble of RCMs is described in Di Luca et al. (2011a); but in the present work some important methodological modifications are introduced. In that article, two types of AV were defined according to the spatial scales in which the AV would be produced. Small-scales AV (AV_{ss}) refers to those RCM improvements occurring in scales that are not explicitly resolved by the driving data. Large-scales AV (AV_{ls}) denotes improvements in those scales that are common to both RCMs and the lower resolution driving data.

Given that the main objective of RCMs is to add fine-scale features to the coarser AOGCMs, there is a general consensus in the RCM community (e.g., Feser

2006, Prömmel et al. 2010) that the primary added value of RCMs is related with AV_{ss}. Much less agreement exists about whether or not RCMs can generate AV at large scales. Although some authors (e.g., Mesinger et al. (2002) and Veljovic et al. (2010)) sustain a potential improvement of large-scale features through the use of RCMs, a large part of the RCM community (e.g., Castro et al. (2005) and Laprise et al. (2008)) seems to promote the use of large-scale nudging thus reducing large-scale differences between the RCM and the driving data.

As in Di Luca et al. (2011a), the experimental design used here to study the PAV is explicitly conceived to investigate AV_{ss}, that is, whether RCMs can add value in small scales. Since no attempt will be made here to identify AV_{ls}, the failure of a given RCM to potentially generate AV_{ss} should not be taken to imply that the RCM is incapable of producing some AV through AV_{ls}.

The PAV framework is based on the idea that a prerequisite condition for an RCM to produce AV_{ss} is that the RCM must be able to generate non-negligible variability in spatial scales finer than the smallest scale represented by the lower resolution driving data (i.e., fine scales). The contribution of fine-scale processes in the description of a given climate statistics can then be used to quantify the PAV of a given RCM simulation. The term *potential* in this definition accounts for the fact that the presence of small scales is not a sufficient condition to have AV_{ss} because RCM-simulated fine scales may not necessarily resemble the observed ones.

Instead of directly comparing RCM simulations and driving data statistics, a perfect-model approach is used here to determine the relative importance of fine-scale features. It is assumed that the statistics of the driving data can be approximated by aggregating the high-resolution (e.g., ~50-km grid spacing) field simulated by an RCM into a coarse grid mesh with an horizontal spacing similar to that used by the driving reanalysis or model. That is, we consider that a high-resolution field upscaled into a 300-km grid (i.e., a jump in resolution of around 6 in the linear horizontal dimension compared to RCMs) generates what we call a virtual GCM (VGCM) field whose statistics behave as those from a real GCM (i.e., as a model with 300-km grid spacing).

Differences between an RCM and its corresponding VGCM can be expressed using the Reynolds decomposition technique (Stull 1988). Let us consider an RCM-simulated time-varying field $T_{i,k}$, with index i identifying the spatial dimension and k the temporal dimension, within 300-km side regions containing about 36 RCM grid points. By applying Reynolds decomposition we can separate the quantity $T_{i,k}$ in its

spatial average and fluctuations around this average as follows,

$$T_{i,k} = \langle T_k \rangle + T^*{}_{i,k}, \tag{2.1}$$

where $\langle T_k \rangle$ is the 300-km spatial average temperature, at each time step, representing a low-resolution version of the RCM (i.e., the virtual GCM time series), and $T^*{}_{i,k}$ represents the time series departures of the 50-km grid spacing field from the 300-km average field. Figure 2.1a shows the location of MM5I RCM grid points in its original grid mesh (blue light squares) and the resulting VGCM grid point (black cross) in an individual region centred on -118.3° of longitude and 32.8° of latitude.

In a similar way as done with the spatial dimension of the $T_{i,k}$ field, Reynolds decomposition can be applied over the temporal dimension of both terms in Eq. (2.1) to obtain,

$$T_{i,k} = \overline{\langle T \rangle} + \langle T_k \rangle' + \overline{T_i{}^*} + T^{*\prime}{}_{i,k}, \tag{2.2}$$

with $\overline{\langle T \rangle}$ the spatio-temporal mean, $\langle T_k \rangle'$ the temporal fluctuation of the spatial mean, $\overline{T_i{}^*}$ the temporal mean of spatial deviations and $T^{*\prime}{}_{i,k}$ the spatio-temporal fluctuations of temperature. The Reynolds decomposition is performed in each individual VGCM grid box and so the spatial averaged is computed over 300-km side regions. Time-averaged values are computed using 20 (19) summer (winter) 3-hourly time series between 1981 and 2000. Winter season is defined as the three months between December and February

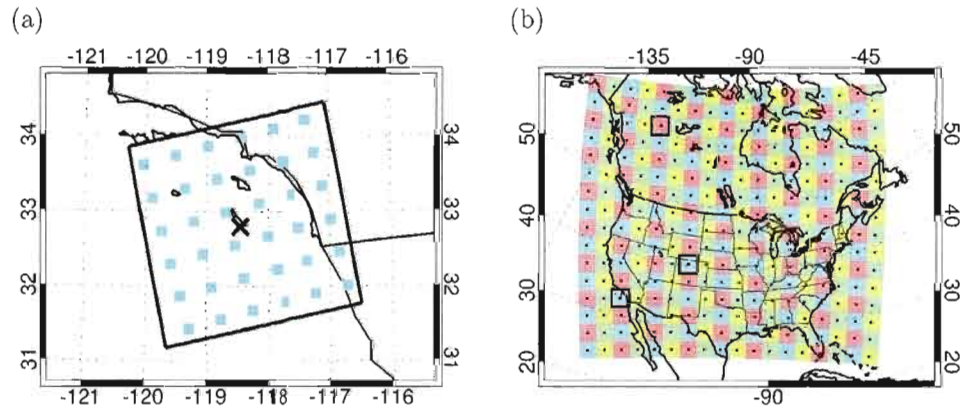

Figure 2.1 a) Individual 300-km side region centred on -118.3° of longitude and 32.8° of latitude and b) the 288 regions use in the analysis. The total domain of analysis is common to all 6 RCM domains and each sub region has the same dimensions (i.e., 300 km by 300 km).

and summer season is defined by the months between June and August.

2.3.2 Variance decomposition analysis and PAV quantities

By using properties of the variance operator and assuming that the temporal fluctuations of the spatial mean are independent of the spatio-temporal fluctutations (see Appendix 2.A for more details), the variance of Eq. (2.2) can be expressed as,

$$\begin{aligned}\sigma^2 = Var(T_{i,k}) &= Var(\langle T_k \rangle' + \overline{T_i^*} + {T_{i,k}}^{*\prime}) \\ &\approx Var(\langle T_k \rangle') + Var(\overline{T_i^*}) + Var({T_{i,k}}^{*\prime}) \\ &\approx \sigma^2_{tVGCM_k} + \sigma^2_{sRCM_i} + \sigma^2_{tRCM_{i,k}},\end{aligned} \tag{2.3}$$

with $\sigma^2_{tVGCM_k}$ denoting the temporal variance of the spatial-mean term, $\sigma^2_{sRCM_i}$ the spatial variance of the RCM time-averaged temperature in each VGCM grid box and $\sigma^2_{tRCM_{i,k}}$ the variance of the residual fluctuations. The approximation in Eq. (2.3) results from the assumption that the covariance term between $\langle T_k \rangle'$ and ${T^*}'_{i,k}$ is much smaller than the other contributions. In practice, when applied to temperature, the covariance term is at least one order of magnitude smaller than the sum of the RCM variance contributions (not shown).

The term $\sigma^2_{tVGCM_k}$ is assumed to represent what a low-resolution GCM can produce. The others two terms are the stationary ($\sigma^2_{sRCM_i}$) and transient ($\sigma^2_{tRCM_{i,k}}$) components of the RCM original contributions to the total variance. They represent the PAV of the RCM over the virtual GCM:

$$PAV = \sigma^2_{sRCM_i} + \sigma^2_{tRCM_{i,k}}. \tag{2.4}$$

A negligible value of the PAV quantity would suggest that the total variance is not affected by the high-resolution information but completely determined by its low resolution part. A normalized form of Eq. (2.4) can be defined in order to quantify the relative influence of RCM components in the total variance:

$$rPAV = \frac{\sigma^2_{sRCM_i} + \sigma^2_{tRCM_{i,k}}}{\sigma^2}, \tag{2.5}$$

with $rPAV$ varying between 0 and 1, thus allowing for a more proper comparison of PAV results across different regions and seasons. Again, $rPAV \sim 0$ would suggest that no RCM information is needed to determine the total variance in that region,

while $rPAV \sim 1$ would mean that all the variance comes solely from the fine-scale information simulated by the RCM with no influence from the VGCM term.

In order to evaluate the regional dependence of PAV quantities, the variance analysis is performed over 300-km side, non-overlaped, regions that are common to all RCM domains (see Fig. 2.1b). The VGCM grid mesh contains a total of 288 such grid boxes. The number of RCM grid points inside any given VGCM grid box depends on the specific map projection and the horizontal grid spacing of each RCM. For example, WRFG and MM5I have 36 grid points in every region at all latitudes because they use a 50-km Lambert conformal projection that conserves the distance between two consecutive grid points. ECP2 and CRCM models' regions contain a varying number of grid points with a minimum of 25 and a maximum of 66 in the northern and southern parts of the domain respectively.

In this paper results are showed only for the variance decomposition of the 3-hourly RCM time series, but the analysis was conducted also for daily and 16-day time series.

2.4 Results

2.4.1 PAV in current climate

Figure 2.2 shows the RCM ensemble-mean total variance of the temperature field in winter season together with the three terms derived using Reynolds decomposition as explained in Sect. 2.3.2. Ensemble-mean variance terms are obtained by simply computing the arithmetic average over each variance term in Eq. (2.3) as estimated from the individual RCMs. For example, in order to get the ensemble-mean of the $\sigma^2_{tVGCM_k}$ term, we computed $\sigma^2_{tVGCM_k}$ for each RCM simulation and then averaged over the six RCM variance estimations.

The ensemble-mean total variance term (see Fig. 2.2a) shows values between $\sim$2 K^2 ($\sim$1 K as standard deviation), in some subtropical oceanic regions, and $\sim$130 K^2 ($\sim$11 K) in continental and high-latitude regions with a domain average of 54 K^2. As is clear by comparing Fig. 2.2a and 2.2b, most of the temperature variance is generated by the temporal fluctuation of the spatial-mean term (i.e., the $tVGCM$ term). The $tVGCM$ term is influenced by a wide range of processes with time scales larger than 3 hours and up to decadal variability. Inspection of variance terms resulting from the

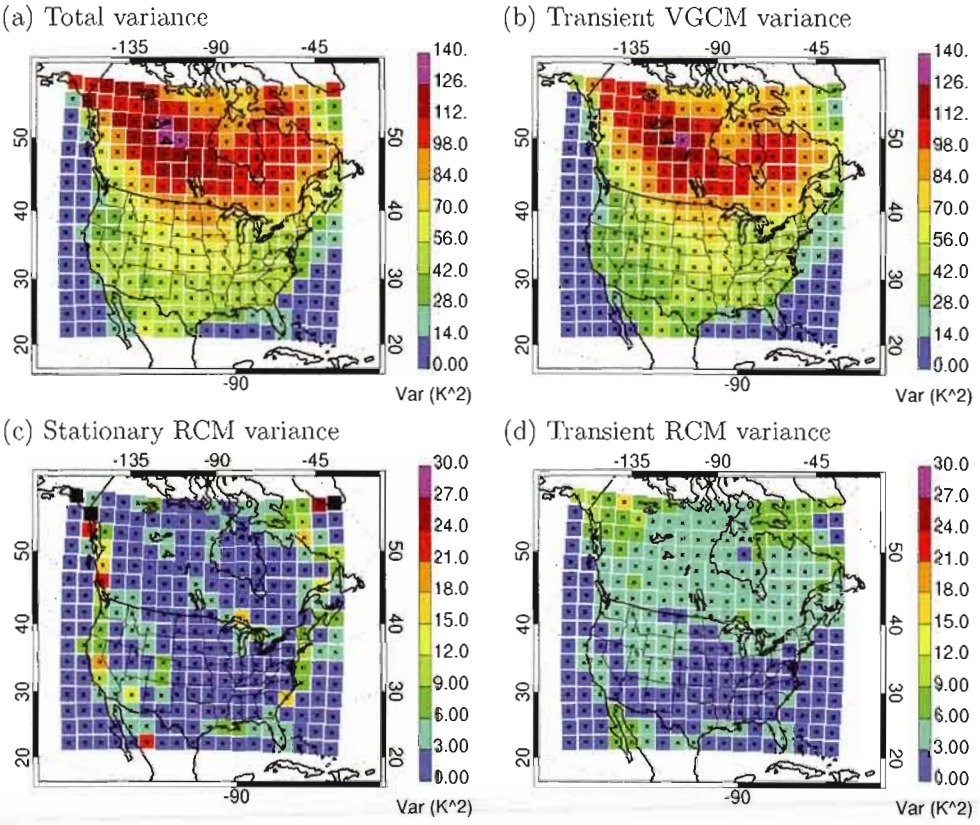

Figure 2.2 Ensemble-mean variance decomposition applied to the 3-hourly temperature field in winter season for (a) the total variance, (b) the virtual GCM variance, (c) the RCM stationary variance and (d) the RCM transient variance.

analysis of daily and 16-day time series (not shown) suggests that the general spatial pattern of variability seen in Fig. 2.2a and 2.2b is largely induced by intraseasonal and interannual variability, together with the influence of sub-daily (particularly in the south part of the domain) and synoptic (particularly in the north) variability.

It is also clear in Fig. 2.2a that 2-m temperature shows weak temporal variability over oceanic regions with values generally smaller than 10 K^2 due to the relatively weak temporal and spatial variability of SSTs, compounded by the fact that SSTs are updated only on a monthly basis in NARCCAP RCM simulations.

Figures 2.3a, 2.3b and 2.3c show an 8-day period of the $tVGCM_k$ time series in January of 1981 for three different regions located in the West Coast (centred on

-118.3° of longitude and 32.8° of latitude), the Rocky Mountains (centred on -106.1° of longitude and 40.3° of latitude) and in northern Canada (centred on -127.3° of longitude and 59.9° of latitude). All three regions are designated with black squares in Fig. 2.1b. Because most grid points in the West Coast region are water grid points, this region shows relatively weak temporal variability, mainly dominated by the land diurnal cycle (at least in the first 6 days). The other two regions show stronger day-to-day variability (they contain only land grid points), mainly related with the passage of synoptic-scale systems.

Figures 2.2c and 2.2d show the ensemble-mean temperature spatial variances of the temporal mean (i.e., $\sigma^2_{sRCM_k}$ stationary term) and the spatio-temporal fluctuation (i.e., $\sigma^2_{tRCM_{i,k}}$ transient term) terms in winter season (note that the colour scale is different from Fig. 2.2a and 2.2b). Both terms are of the same order of magnitude, with domain-average variances of about 4 K^2, but spatial patterns show significant differences.

The ensemble-mean spatial variance of the RCM stationary term tends to maximize in regions where the topographic and/or the land-water contrast forcings are important. The topographic forcing creates stationary temperature differences across grid points mainly due to the general variation of mean temperature with altitude. A more detailed example of the topographic source of stationary variance is given in Fig. 2.3e (see central United States black square in Fig. 2.1b). This figure shows the winter-season 20-year time-averaged temperature in MM5I grid points inside the Rocky Mountains' region characterised by significant fine-scale topography. The altitude effect induces mean horizontal temperature gradients of the order of 10 K / 250 km that result in relative large $\sigma^2_{sRCM_i}$ values of the order of 8 K^2.

Land-sea contrast also induces stationary temperature gradients simply because the time-averaged temperature in sea/lakes can be different from the mean temperature over land surfaces. Figure 2.3d shows the winter-season temporal-mean temperature in MM5I grid points for the region located in the West Coast (see southernmost black square in Fig. 2.1b). Relatively large values of $\sigma^2_{sRCM_i}$ appear in this region due to the differences between the warm temperatures in MM5I grid points located over the Pacific Ocean and those grid points in the colder land. This effect is even more pronounced in some regions located along the East Coast due to the stronger land-sea contrast induced by the warmer SSTs over the Gulf Stream (see Fig. 2.2c).

Figure 2.4 shows the fine-scale stationary variance term for each RCM in winter

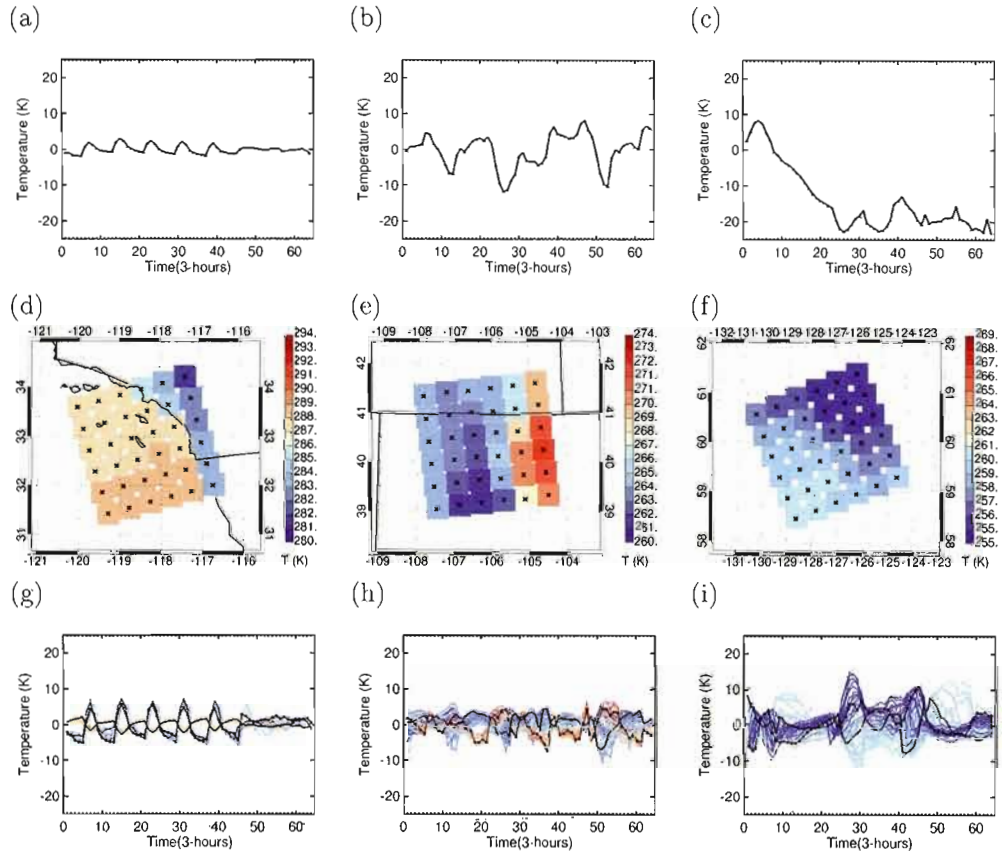

Figure 2.3 8-day period spatial-mean time series (VGCM term; top panels), 20-years time-averaged 2-m temperature (sRCM term; middle panels) and 8-day period fine-scale transient term (tRCM term; bottom panels) in winter season. Left panels correspond to a region located the in the West Coast of United States; centre panels correspond to a region with important topographic forcing, and right panels correspond to a flat region in northern Canada. Results correspond to the MM5I RCM and the several lines in bottom panels represent the 2-m temperature evolution in individual grid points with colours given by the colorbar scale in middle panels. All three regions are are shown in Fig. 2.1b.

season. The more important inter-model differences appear over the Great Lakes, the Hudson Bay and the Labrador Sea. The absence of continental contrast in the RCM3 stationary term (see Fig. 2.4e) simply results from its land-sea mask that does not contain any lake. In some regions (e.g., Great Lakes), differences across RCMs appear to be related with differences in the land-water fraction masks used by each RCM (see

Appendix 2.B for more details). In other regions (e.g., Labrador Sea), differences across RCMs seem to be related with more fundamental aspects such as the representation of latent and sensible heat fluxes in each RCM.

Over oceanic and relatively flat regions (in the central eastern part of United States and most of Canada), the variance of the fine-scale stationary term is very small, with values smaller than 1 K^2. The MM5I RCM time-averaged temperature field in the region located in northern Canada (see Fig. 2.3f) shows that, in flat continental regions, horizontal temperature gradients are weaker than in mountainous or coastal regions with a south-north gradient of about 5 K / 400 km due to the general increase of temperature to the Equator (note that the scale range is the same in Fig. 2.3d, 2.3e and 2.3f). Interestingly, values larger than 1 K^2 appear in some oceanic regions near the East Coast of US and Canada, a feature that arises in the ensemble-mean variance (see Fig. 2.2c) and in individual RCM simulations (see Fig. 2.4). This signature is related with the strong stationary SST gradients across the Gulf Stream in these latitudes since all RCMs share the same SSTs, with changes in the time-averaged temperature of about 10 K / 300 km in some of these regions.

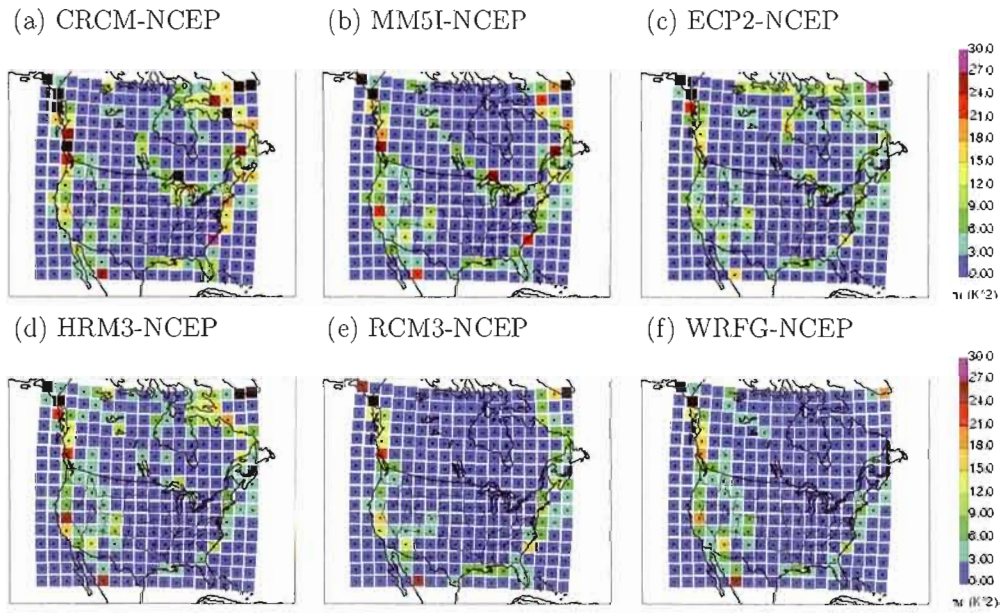

Figure 2.4 RCM stationary variance term computed from individual RCM simulations in winter season.

The ensemble-mean variance of the RCM transient term is shown in Fig. 2.2d and individual RCM transient terms are shown in Fig. 2.5. In general, several mechanisms can produce transient PAV. By its definition, there will be some transient PAV if there exists 50-km spatial differences in the temporal variability of the 2-m temperature. The comparison of the transient term variance derived using 3-hourly and daily time series shows that, particularly in the southern part of the domain, most transient variability comes from temporal scales shorter than 24 hours. The process that seems to dominate sub diurnal variability arises from the different diurnal cycle across RCM grid points in a given region. This effect tends to be larger in coastal regions where land grid points have a much intense diurnal cycle than water grid points explaining the relative maxima of transient PAV in the West Coast (e.g., Baja California coast), the south US coast and Great Lakes regions.

In order to better understand the diurnal cycle spatial variability and the sub-daily transient term, Fig. 2.3g-2.3i show the transient term $tRCM_{i,k}$ for an 8-day period (similar as that used in Fig. 2.3a-2.3c) in the same three regions as before. In the West Coast region (Fig. 2.3g), it is clear that the transient variability (at least in the first 6 days) is dominated by the different diurnal cycle in oceanic and land grid points. Differences between land (ocean) grid points and the spatial-mean term ($tVGCM_k$) appear as a positive (negative) anomaly during day-time and as a negative (positive) anomaly during night-time respectively. The diurnal cycle is, as expected, stronger over land than over ocean grid points.

Figure 2.3h shows that the topographic forcing induces little sub diurnal transient variability because, even if time-averaged temperatures are different across grid points, their diurnal cycle is very similar. In the northern Canada region (see Fig. 2.3i), the influence of the diurnal cycle is very small due to the weak solar forcing in high latitudes in this time of the year.

In winter season, the ensemble-mean fine-scale transient term (see Fig. 2.2d) systematically shows higher values in continental compared to oceanic regions. This continental transient component of PAV is a robust feature that appears in any single model experiment as shown in Fig. 2.5. The inspection of the fine-scale transient term computed using daily and 16-day time series (not shown) reveals that differences between oceanic and continental regions are present when looking at daily time series but do not appear when considering 16-days transient variability term, which seems to imply that the continental-oceanic feature is probably related to synoptic variability.

A process that can be important to explain continental-oceanic differences relates to middle-latitude synoptic systems and their associated surface fronts. The passage of a synoptic-scale perturbation over a given region (generally from west to east in middle latitudes) induces a spatial gradient of temperature that varies in time (as the system moves) and in space (relative position compared to the front). The spatial gradient induced by the perturbation is larger over continental compared to oceanic regions simply because of the important damping from the ocean.

The passage of synoptic-scale systems is also probably related to the general increase of the transient term to the northern part of the domain in winter season. This north-south gradient of the transient term is seen in the ensemble-mean term (see Fig. 2.2d) and in most of individual RCM terms, particularly in the north- western and eastern parts of the domain (see Fig. 2.5). Figures 2.3h and 2.3i illustrate the influence of synoptic variability in the transient term over continental regions. The range of transient variability is of the order of ~10 K in the Rocky Mountains region and of the order of ~20 K in the northern Canada region.

Figure 2.6 shows the RCM ensemble-mean total variance and its decomposition

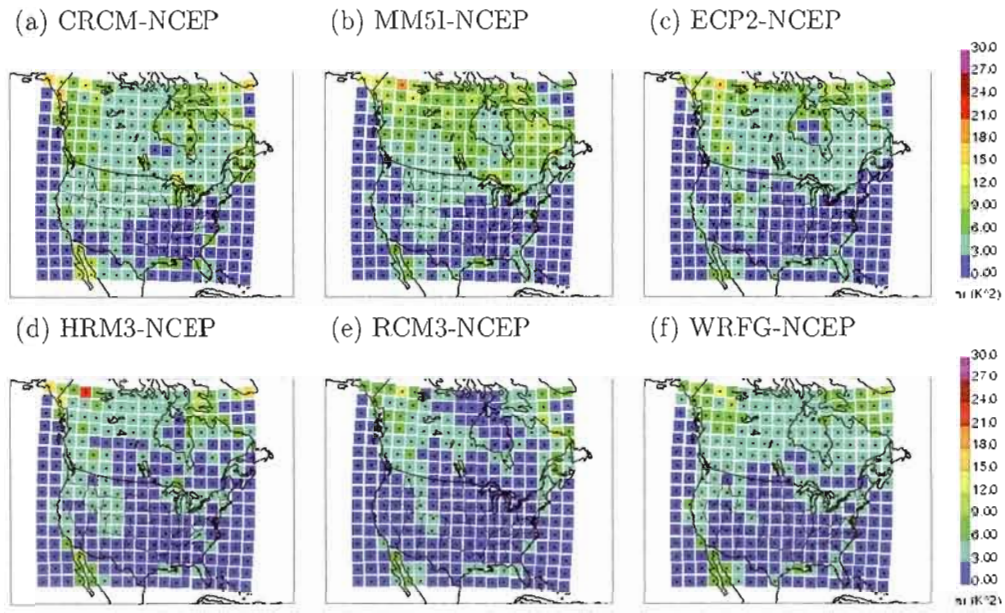

Figure 2.5 RCM transient variance term computed from individual RCM simulations in winter season.

terms as in Fig. 2.2 for the summer season. In this season, the ensemble-mean total variance (standard deviation) shows values varying from $\sim$1 K^2 in subtropical oceanic regions, to $\sim$75 K^2 ($\sim$9 K) in continental mid-latitude regions, with a domain-average value of 29 K^2. Again, most of the total variance is contained in the temporal fluctuation of the spatial-mean term. In this case, the virtual-GCM term shows maximum values in the central eastern part of the conterminous United States, at approximately 40° of latitude, as a result of a combination of intraseasonal and interannual variability, synoptic variability and the very large diurnal cycle in this region as a product of the large solar forcing and the relatively dry soils. A secondary maximum appears to the west of the Hudson Bay mainly due to interannual and synoptic variability. Figures 2.7a-2.7c show an 8-day period of the VGCM time series for the same regions as in Fig. 2.3. Comparing with winter season results, the most outstanding feature is that the diurnal cycle tends to dominate temporal variability everywhere, although modulated

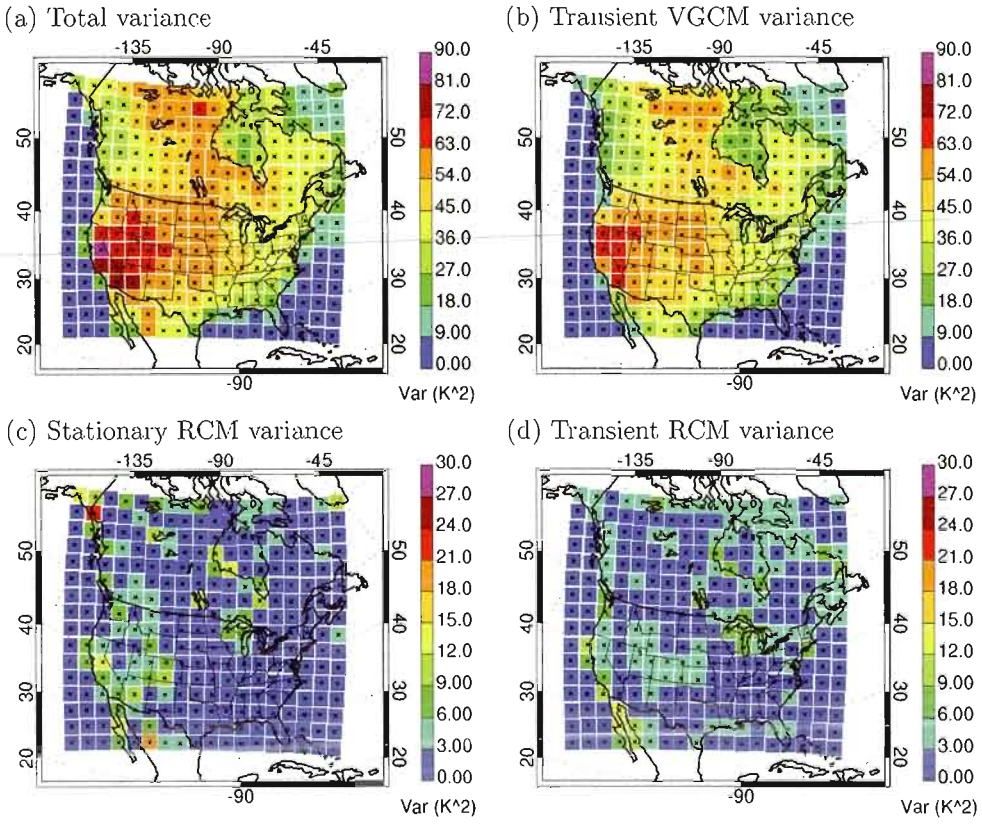

Figure 2.6 As in Fig. 2.2 but for summer season computations.

by longer time scale processes.

Figures 2.6c and 2.6d show respectively the ensemble-mean stationary and transient variance terms in summer season. As in winter season, the stationary and the transient terms show domain-average values of 2 and 3 K^2 respectively. The most important differences between the ensemble-mean stationary term in summer compared to winter season are the lower values in the North American East Coast and the higher values over the Hudson Bay coast: these two features appear in every RCM simulations (see Fig. 2.4 and 2.8).

As in winter season, the transient term shows higher values in continental compared to oceanic regions and maximum values occur in some regions where the land-water contrast forcing is important such as the West Coast and the Great Lakes regions.

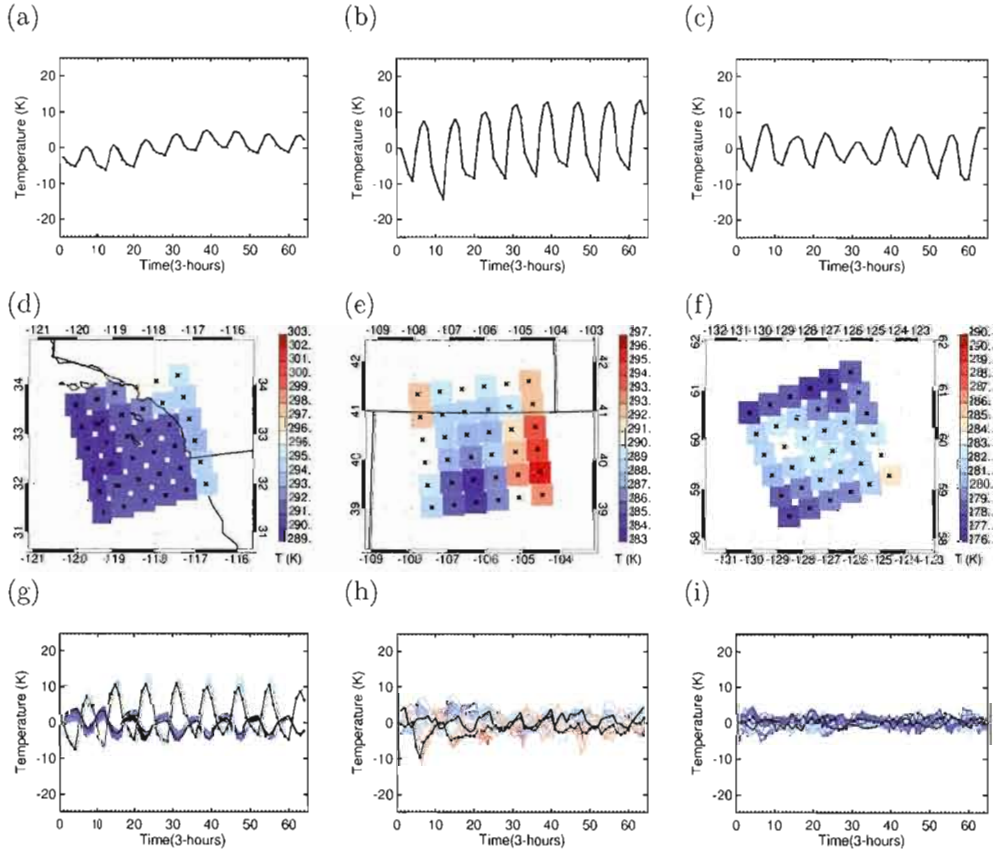

Figure 2.7 As in Fig. 2.3 but for summer season computations.

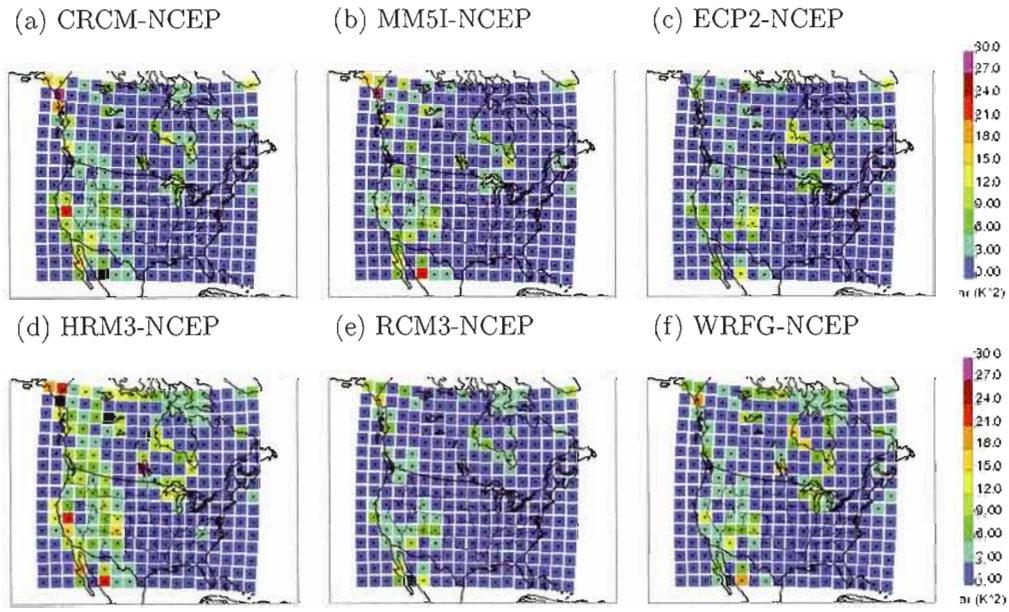

Figure 2.8 As in Fig. 2.4 but for summer season computations.

However, particularly on northern regions and in flat regions with little land-sea contrast, the fine-scale transient term is generally smaller than in winter season probably due to the weaker synoptic-scale variability (see Fig. 2.3h and Fig. 2.3i).

When looking at the ensemble-mean and individual RCM transient terms, important differences between winter and summer seasons appear in regions with significant influence of lakes. In particular, summer-season transient variances show higher values than winter-season ones probably due to the stronger contrast between water and land in this season compared to the contrast between ice and snow/permafrost in winter season. That is, in winter season, the land-water contrast forcing associated with the presence of lakes is partially hidden due to the presence of snow-ice layers in both land and water. The more important land-sea contrasts together with the much stronger diurnal cycle in summer season tend to increase transient term values.

2.4.2 Stationary and transient components of relative PAV

As defined in Sect. 2.3, the relative PAV measure ($rPAV$; see Eq. (2.5)) is given by the fraction of the total variance that is accounted by the sum of the stationary and

the transient RCM terms (i.e., the original, genuine contribution of the RCM field) to the total variance. Fig. 2.10 shows the RCM ensemble-mean $rPAV$ in winter (Fig. 2.10a) and summer (Fig. 2.10b) seasons. Qualitatively, results are quite different from those derived using the absolute variance terms. For example, some oceanic regions (e.g., south Pacific regions) show higher $rPAV$ values than flat continental regions even if PAV terms were higher in the later regions because the total variance in the denominator in Eq. (2.5) tends to be larger over land than over ocean. Similarly, some mountainous regions with relatively large stationary variance values show very little $rPAV$ due to the large total variance in these regions.

In both seasons, ensemble-mean $rPAV$ values are generally smaller than 15% and relative maxima are related with regions strongly influenced by land-sea contrast forcing. The RCM contributions to the total variance are higher in summer compared to winter season with a domain average of 16% and 5% respectively. At least in part, seasonal differences seem to be related to the general intensification of the diurnal cycle of the land-sea contrast forcing in summer season, particularly in mid-latitude and northern regions (e.g., Great Lake regions).

In winter season, relative maxima are found all along the North American West

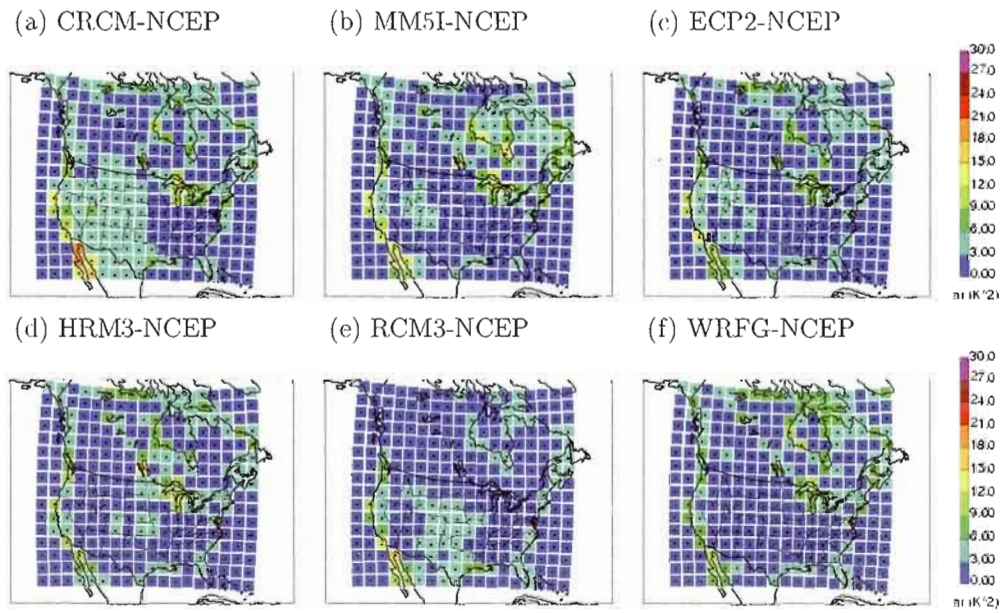

Figure 2.9 As in Fig. 2.5 but for summer season computations.

Coast and the south-east coast of the United States. In summer season, relative maxima are related mostly with coastline regions either near the sea or due to the presence of lakes.

Figures 2.10c and 2.10d show the fraction of $rPAV$ that is explained by the stationary and the transient terms computed as $2\sigma^2_{sRCM_i}/(\sigma^2_{sRCM_i} + \sigma^2_{tRCM_{i,k}}) - 1$. Positive (negative) values denote those regions where the stationary (transient) term tends to be dominant with values equal to 1 (-1) denoting that all the $rPAV$ comes from the stationary (transient) term. Black asterisks denote those regions where $rPAV$ is larger than 15%.

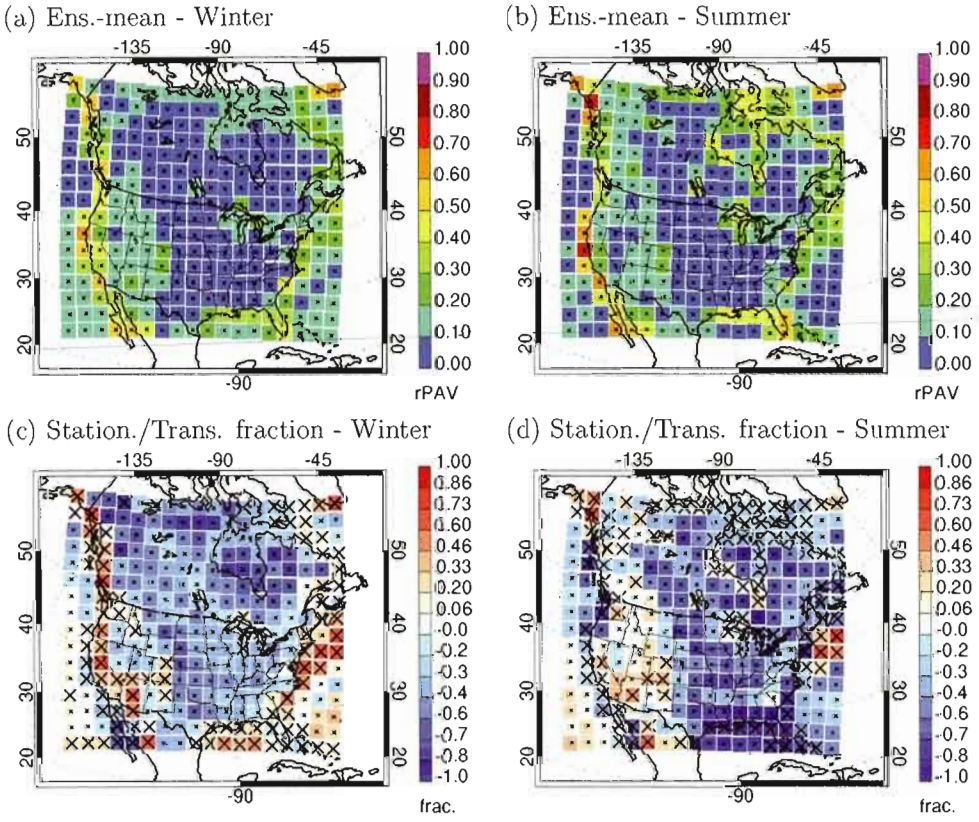

Figure 2.10 Ensemble-mean $rPAV$ in (a) winter and (b) summer seasons and the fraction of $rPAV$ coming from the stationary and transient terms in (c) winter and (d) summer seasons. Black asterisks in bottom panels denote those regions where the ensemble-mean $rPAV$ signal is larger 10%.

In both seasons, ensemble-mean $rPAV$ values larger than 15% are only found in regions where surface forcings are important, either due to complex topography or land-water contrasts. The number of regions with $rPAV$ larger than 15% is larger in summer (131 regions out of 288) than in winter (107 regions) season. Most of these regions appear in the northern part of the domain mainly due to the lower total variances in this season and the land-sea contrast intensification.

Winter season results show that regions with $rPAV \geq 15\%$ are dominated by the stationary term with only some exceptions in the West Coast and the Labrador Sea where the transient variance term tend to be more important. It is evident from Fig. 2.10c that $rPAV$ values in the Atlantic Ocean regions are induced by the permanent and relatively strong temperature gradients across the Gulf Stream and not as a result of a transient mechanism. Similar results are found in summer season with only a marked dominance of the transient term in the Gulf of Mexico.

$rPAV$ values derived from individual RCM simulations generally show similar results to the ensemble-mean $rPAV$ although differences can appear over the Canadian Archipelago, the Great Lakes and others lakes in Canada. A more detailed analysis of the uncertainties arising in the computation of $rPAV$ terms is presented in Appendix 2.B.

2.4.3 Simple and more complex $rPAV$ in mountainous regions

As discussed in the previous section, the PAV of high-resolution fields is mostly confined to those regions with significant influence of surface forcings. A fair question to ask is whether this PAV arises as a result of the influence of complex surface mechanisms (e.g., land-sea breezes or terrain-enhanced triggering of hydrodynamics instabilities) or results from simple, maybe linear, interactions between the fine-scale forcing and the variable of interest.

One such a simple mechanism that seems to be important to explain $rPAV$ in mountainous regions is related with the general relation between temperature and terrain elevation. The more detailed representation of terrain elevation gradients will create stationary temperature gradients even when no fine-scale atmospheric processes occur.

In order to test the influence of this last effect, the $rPAV$ measure has been computed from a synthetic high-resolution 2-m temperature field derived using a linear re-

lationship between the low-resolution VGCM temperature field and the high-resolution 50-km surface elevation field in the following way:

$$T_{RCM}^{orog} = T_{VGCM} + \Gamma \cdot h_{RCM}, \tag{2.6}$$

with T_{VGCM} the virtual GCM time series (in K), h_{RCM} the high-resolution topography (in km) of the RCM and $\Gamma = -6.5$ K/km the middle-latitude standard atmosphere (SA) lapse rate (see Dutton 1976 for a brief description). Equation (2.6) constitutes a crude way of taking into account the effects of changes in terrain-elevations when interpolating the temperature field into a higher resolution grid mesh. Several and important differences would appear between the actual 2-m temperature topographic lapse rate and the free air SA lapse-rate approximation, starting from the fact that the effects of the surface in the adjacent temperature (e.g., sensible and latent heat fluxes) are not taken into account in the SA lapse rate. As shown by Prömmel et al. (2010), the use of the constant SA lapse rate along the year may lead to biases not caused by the models themselves, particularly in winter months where the atmosphere can be much more stable with mean lapse rates of the order of $\Gamma = -3.0$ K/km.

In order to assess the similarity between the real stationary rPAV field and the artificial one, spatial correlations are computed using:

$$r = \frac{cov(rPAV_{stationary}, rPAV_{orog})}{\sigma(rPAV_{stationary})\sigma(rPAV_{orog})}, \tag{2.7}$$

with $rPAV_{stationary}$ the original stationary RCM $rPAV$, and $rPAV_{orog}$ the $rPAV$ derived using Eq. (2.6) as input temperature. The linear correlation is computed only for those regions with relatively complex topography but with no influence of the land-water contrast forcing. Complex terrain regions are defined by a standard deviation of the elevation field within the region larger than 250 m. For each RCM, the land-sea mask is defined by the fraction of land inside each grid box with values varying between 0 and 1. Regions with important influence of land-water contrast are then defined as those with a water fraction standard deviation larger than 0.2. The total number of regions considered in correlation calculations depends on the RCM due to the different representation of both surface fields and grid location and varies between 37 (ECP2 model) and 51 (CRCM model) across models.

Table 2.2 shows the 90% confidence interval of the linear correlations between $rPAV_{orog}$ and the stationary part of the rPAV term. Correlation confidence intervals

are estimated using a Monte Carlo approach by sampling 1000 times randomly with replacement over both spatial series. The 90% confidence interval is then computed by calculating the 5th and the 95th percentiles of the 1000-elements correlation distribution.

Table 2.2 90% bootstrap confidence interval for the spatial correlation coefficient between the $rPAV$ measure computed using RCM simulations and using the artificial temperature data. Only those regions characterized by complex topography (see the text for its denition) with no land-sea contrasts are included in the calculation.

	Winter season	Summer season
CRCM	[0.82; 0.96]	[0.72; 0.94]
MM5I	[0.87; 0.97]	[0.72; 0.94]
ECP2	[0.81; 0.93]	[0.35; 0.78]
RCM3	[0.88; 0.97]	[0.68; 0.92]
WRFG	[0.83; 0.96]	[0.71; 0.92]
HRM3	[0.81; 0.96]	[0.81; 0.92]
RCMs-MEAN	[0.84; 0.96]	[0.67; 0.90]

In both seasons and for every single RCM, correlations between the $rPAV_{orog}$ and the stationary $rPAV$ are very high with an RCM-mean 5th (95th) percentile value of 0.84 (0.96) and 0.67 (0.90) in winter and summer seasons respectively. This suggests that about 80% and 65% of the RCM $rPAV$ variance is linearly explained by the orographically-induced field in winter and summer seasons, respectively.

Inter-model differences are generally small, of the order of 10% of the mean correlations, and contained within the sampling errors as estimated from the 5th and 95th percentile differences, which are generally of the order of 15-20%, but can be as high as 40%.

2.5 PAV in the climate change signal (AOGCM driven simulations): preliminary results

So far, we have analyzed the potential of RCMs to add value over their associated virtual-GCMs in the simulation of temperature in present-climate conditions (i.e., driven by NCEP reanalyses). This information can be useful in a broad spectrum of RCM applications such as the reconstruction of recent-past climate on the regional scale (e.g., Mesinger et al. 2006; Kanamitsu and Kanamaru 2007), the downscaling of low-resolution global simulations in seasonal-prediction investigations (e.g., Rauscher et al. 2007; Seth

et al. 2007; De Sales and Xue 2011) and the study of processes and mechanisms in the regional scale (Pielke et al. 1999; Roebber and Gyakum 2003).

One of the main applications of RCMs in the last decade has been its use to downscale future-climate projections produced by coupled GCMs. In order to account for systematic biases in RCM projections, a popular approach used to estimate high-resolution future climate is through the "delta method" (e.g., see Rummukainen 2010). The delta method consist of modifying the observed high-resolution climate data with the RCM climate change (CC) signal to obtain an unbiased version of the future projection. This suggests that the RCM's added value in climate projections may not come directly from the simulation of future scenario periods but from the climate-change signal itself. While the problem of looking for PAV in the CC signal is intimately related with that of PAV in present climate, some differences appear.

The CC signal of the time-averaged temperature field is defined in the usual way by computing the difference between the time-mean field in present and future conditions. Using the same notation as in Sect. 2.3 we have:

$$CC_{RCM_i} \equiv CC_i = \overline{T_i}(future) - \overline{T_i}(present), \tag{2.8}$$

with CC_{RCM_i} the high-resolution CC signal over the ith 300-km side region. Following the ideas used for the present-climate PAV framework, we can aggregate CC_{RCM_i} over 300-km side regions in order to produce a low-resolution version of the CC signal that we denote by CC_{VGCM}.

A question that arises naturally in the context of the PAV framework is whether the high-resolution CC field contains fine-scale information that is absent in the low-resolution part. Given that some of the most important sources of climate change are large scale in nature (e.g., CO_2 concentration changes, water vapor feedback, etc), it is unclear whether the CC signal should contain a large high-resolution component. A simple way to quantify the relative importance of fine and large scales in the high-resolution CC signal can be done by defining:

$$rPAV^{CC} = \frac{\sigma(CC_{RCM_i})}{mean(CC_{RCM_i})} = \frac{\sigma(CC_{RCM_i})}{CC_{VGCM}}, \tag{2.9}$$

where $\sigma(CC_{RCM_i})$ denotes the spatial standard deviation of the high-resolution CC signal field (CC_{RCM_i}) and CC_{VGCM} the mean temperature change between future and present periods over the region of interest. With this definition $rPAV^{CC} \sim 0$ would

suggest that the high-resolution estimation does not add extra information over the coarse-resolution one and, $rPAV^{CC} \sim 1$ would suggest that the fine-scale contributions can be as large as the large-scale mean temperature change.

Again, it should be emphasised that the PAV measure as defined in Eq. (2.9) only accounts for the PAV small scales (PAV_{ss}), that is, the PAV arising from the simulation of fine-scale features that are absent in GCM fields. The ratio $rPAV^{CC}$ is mute about the potential of RCMs to add value in large scale variables (i.e., PAV_{ls}).

Figures 2.11a and 2.11b show the CC_{RCM_i} field for the CRCM-CGCM3 simulation in winter and summer seasons respectively. In both seasons, results show warmer conditions in the future with a stronger signal in continental compared to oceanic regions. In winter season, the spatial pattern of CC_{RCM_i} shows a general increase to the north and to the interior of the continent that attains almost 7 K in the centre of the Hudson Bay (2041-2065 minus 1971-1995). In summer season the spatial pattern of CC_{RCM_i} shows maximum values in continental-middle latitudes with changes as large as 4 K in central United States. Other RCM-AOGCM couples show similar spatial patterns of mean-temperature changes in winter season (not shown).

Figures 2.11c and 2.11d show the $rPAV^{CC}$ measure for the CRCM-CGCM3 simulation in winter and summer seasons, respectively. In both seasons, $rPAV^{CC}$ values are generally smaller than 10% with values somewhat higher in summer compared to winter season, particularly in coastline regions. The largest values in coastline regions result from the differential warming observed in land and water surfaces.

Figures 2.12 and 2.13 show the $rPAV^{CC}$ measure for the other individual RCM-AOGCM simulations (Fig. 2.12a-2.12e and 2.13a-2.13e) and for the ensemble-mean (Fig. 2.12f and 2.13f) results in winter and summer seasons respectively. Most models show similar results to the CRCM-CGCM3 simulation, with relatively small $rPAV^{CC}$ values everywhere, maxima in coastline regions and somewhat larger values in summer compared to winter season results. The WRFG-CCSM simulation shows very large $rPAV^{CC}$ values over lake regions in summer season (see Fig. 2.13) but this seems to be related with a different representation of lakes in present and future conditions.

Maybe the most interesting feature is related with the robustness of the $rPAV^{CC}$ results. Black asterisks in Fig. 2.12f and 2.13f denote regions in which $rPAV^{CC}$ satisfies two conditions: that the RCM ensemble-mean $rPAV^{CC}$ is larger than twice the inter-model standard deviation, and larger than 5%. That is, black asterisks identify

those regions in which a significant $rPAV^{CC}$ signal is robust across the different RCM simulations.

In winter season, robust regions (59 out of 288) appear all along the North American West Coast and in most coastline regions in the Hudson Bay. Similar results appear in summer season but robust regions (60 out of 288) appear in most coastal regions and also in some regions with important fine scale topography in the Rocky Mountains.

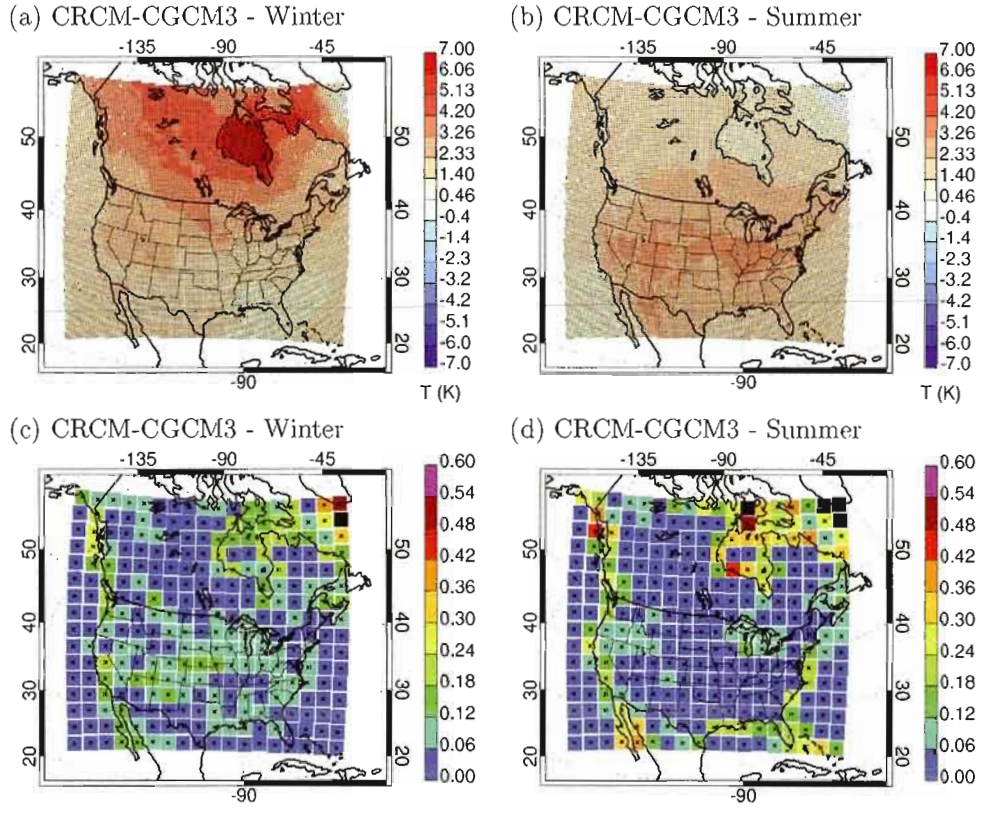

Figure 2.11 High-resolution climate change signal (top panels) and the $rPAV^{CC}$ measure (bottom panels) in winter (left panels) and summer (right panels) seasons. Results correspond to the CRCM-CGCM3 simulation. Only values smaller than 0.6 are shown in Fig. 2.11c and 2.11d.

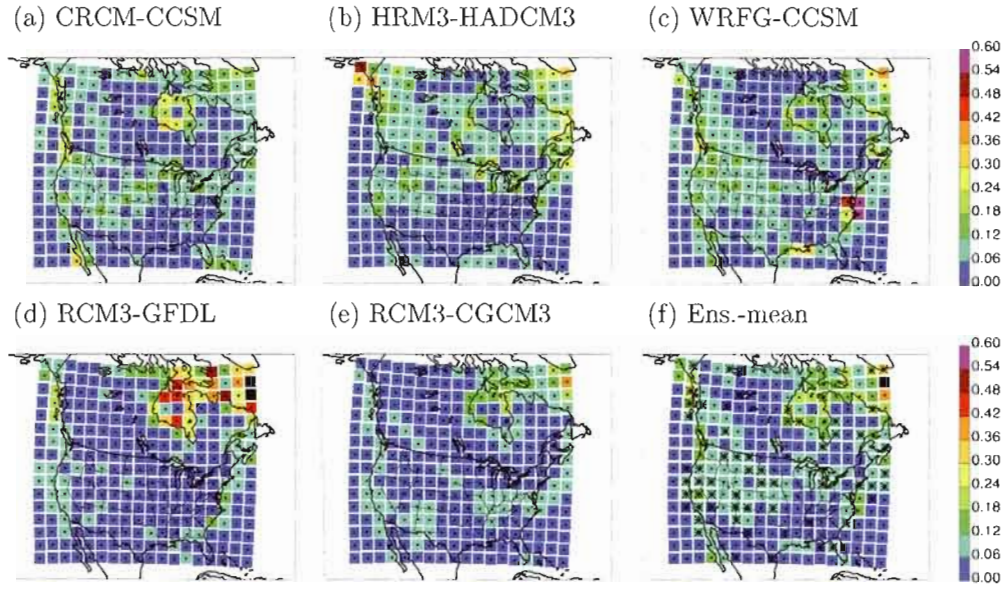

Figure 2.12 The $rPAV^{CC}$ measure in winter season as computed from individual RCM simulations (2.12a-e) and from the ensemble-mean field (2.12f).

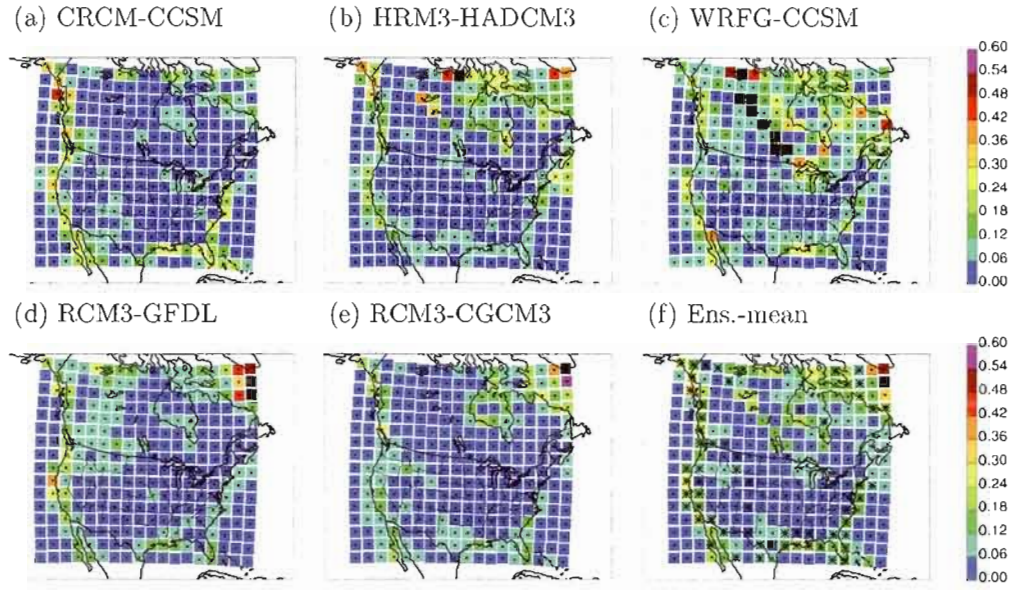

Figure 2.13 As in Fig. 2.12 but for summer season computations.

2.6 Discussion

The use of RCMs to dynamically downscale large-scale atmospheric fields in present and future climate conditions has gained popularity as a way to circumvent the spatial scale gap that exists between the climate information provided by AOGCMs and the input needed in impact and adaptation studies. There is still a need, however, to objectively quantify the gains arising from the use of RCMs as climate downscaling tools.

In this article we use the "potential added value" framework proposed in Di Luca et al. (2011a) with the aim of detecting the regions and seasons where RCMs show potential to improve the simulation of temperature statistics compared to the driving models. The methodological approach used in this paper can be summarised through three main steps:

1. 20-year 3-hourly time series of near-surface temperature fields simulated by 6 RCMs are decomposed using Reynolds averaging rules. The temperature field over 300 km by 300 km regions (i.e., approximately equivalent to GCM grid boxes and containing several RCM grid points) is separated in four terms: the spatio-temporal mean, a time series describing the temporal fluctuations of the spatial mean, a time-averaged field of the spatial-mean deviations and a residual time varying field containing the spatio-temporal fluctuations.

2. In each 300-km side regions, the variance of the high-resolution temperature field is then described by three terms that result from the Reynolds decomposition. The first is the temporal variance of the spatial-mean field that is assumed to represent the GCM contribution to the total variance. The other two terms depend on the spatial deviations and are related with the stationary (time mean) and transient RCM contributions to the total variance.

3. The PAV is then defined as sum of the fine-scale stationary and transient RCM variances. A normalised quantity ($rPAV$) is defined by computing the fraction of the total variance that is explained by RCM variances.

Our results indicate that, independently of the season considered, the high-resolution near-surface temperature variance is mostly explained by the virtual-GCM term, with a contribution from the RCM terms that is generally smaller than 15% but can attain 60-70% in some regions. The contribution from the fine-scale stationary and transient

terms is roughly of the same order of magnitude but they are induced by different mechanisms and therefore they show distinct spatial patterns of variability.

The fine-scale stationary spatial variance term is sensitive to time-averaged temperature gradients and is hence important in regions with significant small-scale surface forcings, either due to complex topography or land-sea contrast (i.e., with coastlines or lakes). The term can also arise due to the presence of strong stationary gradients from other sources such as the strong SSTs variation over the Gulf Stream.

The fine-scale transient variance term is associated with spatial differences in the temporal variability of 2-m temperature and seems to be dominated by two mechanisms. A first mechanism is related with the presence of land-sea contrast and describes the differential temporal variability of temperature in land and water grid points. A clear example of this mechanism is given by the different diurnal cycle over land and water grid points. The second mechanism is independent of the fine-scale surface forcings and describes the spatial variability induced by the passage of weather disturbances, mainly of synoptic scale. This last term appears to be more important in winter and over high-latitudes due to the stronger intensity and variability of synoptic-scale systems. In addition, due to the dominant thermal-inertia effect of ocean waters on 2-m temperature, this term is also stronger over the continent.

When computing the fraction of the total variance explained by RCM terms, we find that relatively large values of $rPAV$ are essentially confined to regions with important surface forcings mainly due to land-sea contrasts. In general, but particularly in coastline high-latitude regions, $rPAV$ tends to be larger in summer than in winter season due to an intensification of the land-sea contrast forcing related with ice/snow cover in winter season and a much stronger diurnal cycle in summer season.

In Section 2.5, the potential of RCMs to add value over lower resolution models in reproducing the climate-change (CC) signal is discussed. It is stressed that the existence of PAV in present climate does not imply that PAV will be present in the CC signal. Our results show that the fine-scale spatial variability in the high-resolution CC temperature over the 300-km side regions is generally one order of magnitude smaller than the mean CC signal itself. The analysis indicates that the largest potential for AV appears in coastline regions due to the differential warming in land and water surfaces. This effect tends to be more pronounced in summer than in winter season. It is seen that, in mountainous regions, the PAV founded in present climate is almost lost in the CC signal; this results mainly from the fact that, as shown in Sect. 2.4, the PAV in

mountainous regions is dominated by quasi-linear stationary processes that are very similar in present and future climate and hence tend to cancelled out when computing the CC signal.

In general, results point out that the potential of RCMs to add value in near-surface temperature is rather limited in oceanic and flat regions with little land-sea contrast. This result agrees with previous studies of Winterfeldt and Weisse (2009) and Winterfeldt et al. (2011) who showed similar results for the study of winds over oceanic and coastal regions. Furthermore, even for those regions showing relatively large $rPAV$ values, it remains to be seen whether this added value could not be obtained using simple, maybe even linear, relationships between the high-resolution surface forcing and the low-resolution variable of interest. An example of such a simple relation was shown in Sect. 2.4.3.

In agreement with results obtained by other authors (e.g., Sotillo et al. 2005; Feser et al. 2011; Di Luca et al. 2011a), our results suggest that efforts aiming to show the benefits of using RCMs over lower resolution GCMs should concentrate on moist processes or in climate statistics with significant fine-scale variability such as high-order statistics variables with large spectral power at high temporal frequencies. For example, as shown in Di Luca et al. (2011a), the PAV can be much larger when considering precipitation, higher order statistics (e.g., 95th percentile) and more local scale quantities.

Finally, two important caveats should be discussed regarding our results. First, as discussed in the methodology section, this work and the previous study by Di Luca et al. (2011a), concentrated on the added value on the small spatial scales, disregarding the possible impact of high-resolution simulations on larger scales. It was assumed that spatial average of RCM quantities within an area equivalent to the driving model grid-box is identical to the driving model grid-box value. This necessarily precludes any analysis of possible improvements at that scale. The second caveat relates to the fact that our methodology may be badly suited to detect potential added value of complex characteristics. For example, phenomena such as downslope winds near mountain ranges or lake-effect snowfall may need a methodology tailored to that particular objective.

Acknowledgements

This research was done as part of the PhD project of the first author and as a project

within the Canadian Regional Climate Modelling and Diagnostics (CRCMD) Network, funded by the Canadian Foundation for Climate and Atmospheric Sciences (CFCAS) and Ouranos. The authors would like to thank Mourad Labassi, Abderrahim Khaled and Georges Huard for maintaining a user-friendly local computing facility and to the North American Regional Climate Change Assessment Program (NARCCAP) for providing the data used in this paper. NARCCAP is funded by the National Science Foundation (NSF), the U.S. Department of Energy (DOE), the National Oceanic and Atmospheric Administration (NOAA) and the U.S. Environmental Protection Agency Office of Research and Development (EPA). Finally, thanks are extended to the Global Environmental and Climate Change Centre (GEC3), funded by the Fonds québécois de la recherche sur la nature et les technologies (FQRNT), for extra financial support.

Appendix 2.A: Variance decomposition

The high-resolution temperature field as simulated by any RCM can be decomposed in its spatial-mean and spatial-fluctuations as:

$$\begin{aligned} T_{i,k} &= \overline{T_{i,k}}^{i} + T^{*}{}_{i,k} \\ &= VGCM_k + RCM_{i,k}, \end{aligned} \tag{2.10}$$

where $\overline{(.)}$ denotes the arithmetic average over grid points (i) or time (k). $VGCM_k$ is the virtual GCM term given by the time series of the spatial mean and $RCM_{i,k}$ the RCM term representing the time series of the spatial deviations:

$$RCM_{i,k} = T_{i,k} - \overline{T_{i,k}}^{i}. \tag{2.11}$$

Similarly, each time varying term in Eq. (2.10) can be decomposed into a stationary and a transient part as:

$$\begin{aligned} VGCM_k = \overline{T_{i,k}}^{i} &= \overline{\left(\overline{T_{i,k}}^{i}\right)}^{k} + \left(\overline{T_{i,k}}^{i}\right)' \\ &= sVGCM + tVGCM_k, \end{aligned} \tag{2.12}$$

and

$$\begin{aligned} RCM_{i,k} = T_{i,k} - \overline{T_{i,k}}^{i} &= \overline{(T^{*}{}_{i,k})}^{k} + (T^{*}{}_{i,k})' \\ &= sRCM_i + tRCM_{i,k}, \end{aligned} \tag{2.13}$$

where

$$\begin{aligned} tVGCM_k &= \overline{T_{i,k}}^{i} - \overline{\left(\overline{T_{i,k}}^{i}\right)}^{k} \\ &= VGCM_k - \overline{VGCM_k}^{k} \end{aligned} \tag{2.14}$$

and

$$\begin{aligned} tRCM_{i,k} &= T_{i,k} - \overline{T_{i,k}}^{i} - \overline{T^{*}{}_{i,k}}^{k} \\ &= RCM_{i,k} - \overline{RCM_{i,k}}^{k}. \end{aligned} \tag{2.15}$$

From Eq. (2.10), (2.12) and (2.13) we obtain,

$$T_{i,k} = sVGCM + tVGCM_k + sRCM_i + tRCM_{i,k}. \tag{2.16}$$

The sample variance of Eq. (2.16) is given by,

$$\begin{aligned}
\sigma^2 &= \overline{\overline{(T_{i,k} - sVGCM)^2}^k}^i \\
&= \overline{\overline{(tVGCM_k + sRCM_i + tRCM_{i,k})^2}^k}^i \\
&= \overline{\overline{(tVGCM_k)^2}^k}^i + \overline{\overline{(sRCM_i)^2}^k}^i + \overline{\overline{(tRCM_{i,k})^2}^k}^i + 2(\overline{tVGCM_k}^k \overline{sRCM_i}^i) \\
&+ 2\overline{(tVGCM_k \overline{tRCM_{i,k}}^i)}^k + 2\overline{(sRCM_i \overline{tRCM_{i,k}})}^{ki}.
\end{aligned} \tag{2.17}$$

From Eq. (2.14) and (2.15) it follows that $\overline{tVGCM_k}^k = 0$ and $\overline{tRCM_{i,k}}^k = 0$. Hence, without any approximation, Eq. (2.16) can be writen as:

$$\sigma^2 = \sigma^2_{tVGCM_k} + \sigma^2_{sRCM_i} + \sigma^2_{tRCM_{i,k}} + 2\overline{(tVGCM_k \overline{tRCM_{i,k}}^i)}^k. \tag{2.18}$$

The PAV term can then be defined by the sum of those terms that include any contribution from the RCM. In practice, the covariance term $2\overline{(tVGCM_k \overline{tRCM_{i,k}}^i)}^k$ is at least 10 times smaller (not shown) than than the sum of other two contributions so it is neglected in the analysis.

The variance decomposition can be applied independently to each RCM dataset. That is, for each model m we obtain:

$$\sigma^2|_m = \sigma^2_{tVGCM_k}|_m + \sigma^2_{sRCM_i}|_m + \sigma^2_{tRCM_{i,k}}|_m. \tag{2.19}$$

The ensemble-mean for each variance term is then obtained by computing the arithmetic mean over all models. For the total variance the expression is given by:

$$\overline{\sigma^2|_m}^m = \frac{1}{M} \sum_m \sigma^2|_m, \tag{2.20}$$

and similar expressions for the other variance terms.

Appendix 2.B: Uncertainties in rPAV estimations

In order to examine how robust are the PAV results, we consider some of the uncertainties arising in the estimation of variances from the RCM simulated temperature time series. Two types of uncertainties are partially (roughly) assessed: uncertainty due to the natural variability of the climate system and the RCM structural uncertainty due to our incomplete knowledge of the climate system and the resulting differences in the representation of some processes in the several RCMs.

Inherent to the process of computing a climate statistics from a finite lengh time series (i.e., 20 years periods in our case) there is an uncertainty related with sampling variability. In order to get a quantitative measure of this uncertainty, variances in Eq. (2.3) have been estimated using a Monte Carlo approach. That is, each variance term is computed 500 times by sampling randomly with replacement over the original time varying field $T_{i,k}$. Traditional bootstrapping methods (Efron and Tibshirani 1993) rest on the assumption that the data of analysis are composed of independent samples, an hypothesis that is evidently not true in the case of the 3-hourly and 50-km temperature fields used to estimate variance terms. In order to account for the serial (or auto-) correlation in the temporal dimension, the temporal sampling is performed by randomly selecting a subset of the total data assuming that temperature values are independent every three days. This is equivalent to use a variance inflation factor as described in Wilks (2010). In the spatial dimension, the bootstrapping is performed assuming that adjacent grid points are independent, an hypothesis that we know is not adequate.

For each RCM, an estimation of the uncertainty can then be obtained by computing, for example, the standard deviation of the distribution of each variance term containing the 500 samples. The PAV sampling uncertainty can then be defined as the sum of the stationary and transient sampling standard deviations. In a similar way, the rPAV sampling uncertainty for each RCM can be obtained by computing the standard deviation of the rPAV Monte Carlo distribution. Figures 2.14a and 2.14b shows the ratio between the inter-model mean rPAV sampling standard deviation and RCM ensemble-mean rPAV for winter and summer seasons respectively. In both seasons, the sampling uncertainty pattern resemble the ensemble-mean rPAV pattern showing relatively uniform fields for the ratio between both. Inter-model mean values, but also individual model results (not shown), show domain-mean values of about $\sim$ 15% in both seasons, with values that can attain up to 50% in some regions. As clear from Fig. 2.14a and 2.14b, the largest values of the sampling ratio arise in those regions that have

the borders near the coast (i.e., with maybe only one grid point that differs from all the others).

A simple measure of the RCMs' uncertainty can be obtained by quantifying the spread between RCMs through the multi-model standard deviation. The unbiased formula of the standard deviation (von Storch and Zwiers 1999) is desirable because of the small number of simulations available for the analysis (in what follows, we use always the unbiased formula when computing the inter-model spread). Figures 2.14c and 2.14d show the ratio between the inter-model standard deviation and RCM ensemble-mean rPAV for winter and summer seasons respectively. Values of the ratio are larger than in the sampling uncertainty case particularly in some oceanic and coastline regions. In general, however, the standard deviation represents less than 20-30% of the signal showing that there is a relative large agreement between RCM simulations.

Assuming that robust features across RCMs are those for which the signal (i.e., the RCM ensemble-mean) is at least two times larger than the RCM spread, some regions can be pointed out to be non robust (not shown). In winter season, non-robust regions appear in the Atlantic Ocean in the southern part of the domain, in some high-latitude regions and near the Great Lakes. Uncertainties in some of these regions appear to be related with differences in the land-water fraction masks used by each RCM. Figure 2.14e shows the multi-model standard deviation of the land fraction standard deviation in each 300-km side region. The largest differences across RCMs arise near the Canadian Archipelago, the Great Lakes and others lakes in Canada, and in the Atlantic Ocean near Florida due to the presence of some islands.

The representation of lakes depends on each RCM and on the LBCs used to drive the RCM. Differences between RCMs arise because they do not share the fraction of water in every grid point (i.e., the land-water mask is model dependent). For example, the RCM3 model does not contain any lake and WRFG contains only the largest lakes.

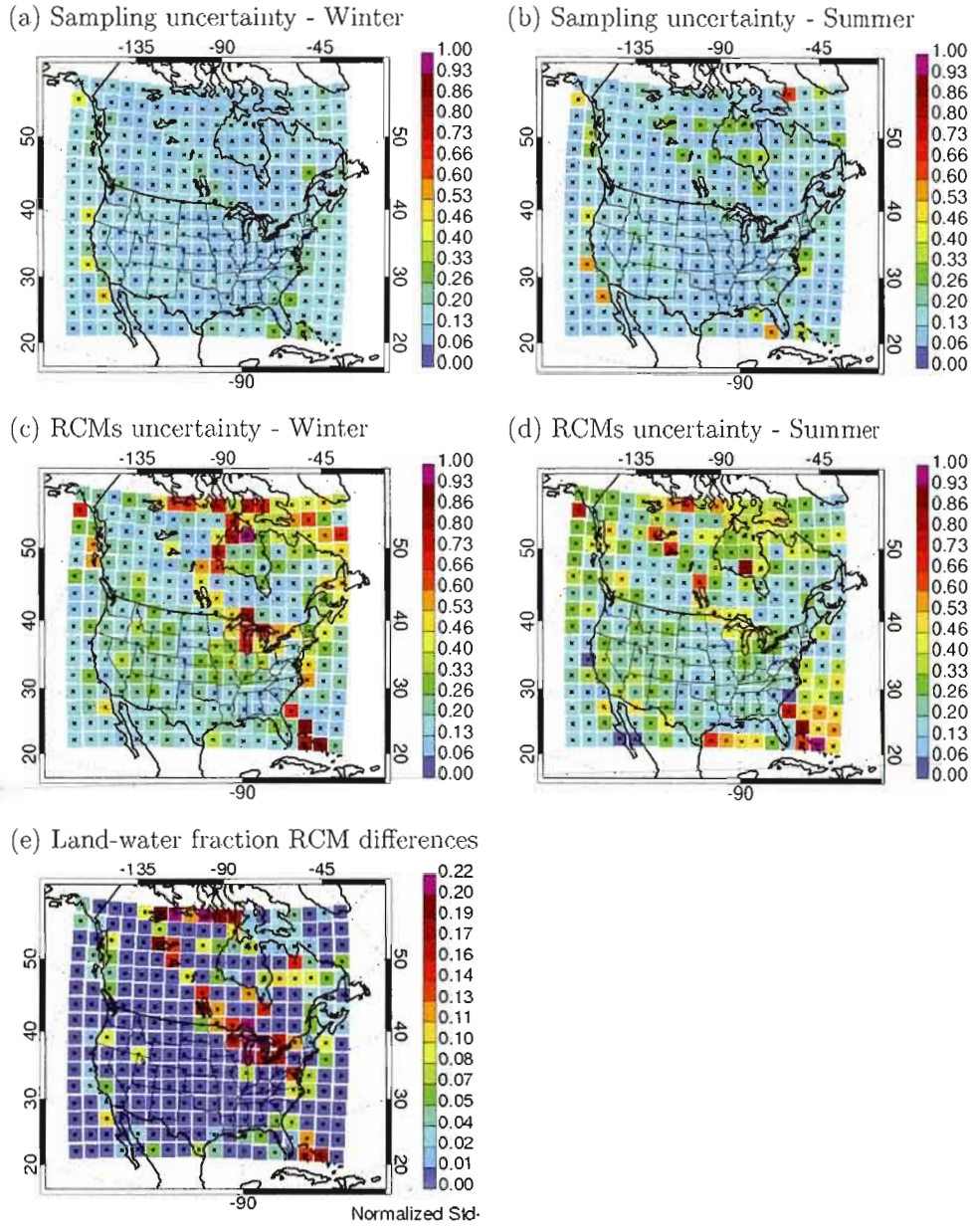

Figure 2.14 Inter-model mean sampling uncertainty in (a) winter and (b) summer seasons. RCMs uncertainty in (c) winter and (d) summer seasons. Figure 2.14(e) shows the inter-model standard-deviation of the standard deviation of the land-water fraction field.

CHAPTER III

POTENTIAL ADDED VALUE OF RCM'S DOWNSCALED CLIMATE CHANGE SIGNAL

This chapter is presented in the format of a scientific article that was submitted to the Climate Dynamics journal. The design of the research and its performance together with the analysis of data and the redaction of this article are entirely based on my work, with the co-authors involved in the supervision of all these tasks.

Di Luca, A., de Elía R. and Laprise, R.: "Potential added value of RCM's downscaled climate change signal". Submitted to Climate Dynamics.

Alejandro Di Luca - René Laprise
Centre ESCER (Étude et Simulation du Climat à l Échelle Régionale).
Département des Sciences de la Terre et de l'Atmosphère
Université du Québec à Montréal (UQAM)
B.P. 8888, Succ. Centre-ville
Montréal (Québec) Canada H3C 3P8

Ramón de Elía
Centre ESCER (Étude et Simulation du Climat à l Échelle Régionale).
Consortium Ouranos, 550 Sherbrooke West, 19^{th} floor. West Tower.
Montréal (Québec) Canada H3A 1B9

3.1 Introduction

In the context of a changing climate due to anthropogenic factors, it is generally argued that the planning for adaptation requires climate information accounting for specificities on scales at which human activities occur, for example about climatic characteristics within countries, provinces and even cities (Oreskes et al. 2010). This need of very fine-scale climatic information has important consequences for climate research and it has pushed climate modeling research centres to perform increasingly higher resolution climate simulations and to look for alternative techniques to produce fine-scale climatic information.

One such approach has been the development of nested, limited-area, regional climate models (RCMs). Basically, the RCM technique allows for an increase in resolution by concentrating the degrees of freedom, and hence the computational resources, over a limited region of the globe where the main interest of a user lies (Laprise et al. 2008). Technically, it consists of using time-dependent large-scale atmospheric fields and ocean surface boundary conditions to drive a high-resolution atmospheric model integrated over a limited-area domain (Giorgi et al. 2001). The atmospheric driving data are either derived from simulations of lower resolution coupled Atmosphere-Ocean General Circulation Models (AOGCMs) simulations or analyses of observations.

From the beginning of RCMs development, nearly 20 years ago, a large effort has ensued to assess their capability as climate downscaling tools by comparing RCM-simulated climate to observed data sets. Moreover, particularly in the last decade, important efforts were also devoted to assess the ability of RCMs to improve the simulated climate compared to their driving data in order to identify the value added by RCMs. The various added value (AV) studies (for a review of these studies the reader is referred to Feser et al. (2011) and references therein) have clearly shown that RCMs do not generate AV in an unambiguous way. Rather, the AV seems to be contingent upon a variety of factors such as the season and time scale, the variable and the climate statistics of interest, the region of analysis, etc.

To date, most studies have concentrated in the identification of AV using present climate simulations. However, when downscaling climate projections produced by AOGCMs, our interest is not necessarily directed towards the RCM climate simulation itself but sometimes towards the climate change signal computed from the difference between present and future RCM simulations. For example, in order to account for system-

atic biases in RCM projections, a popular approach used to estimate future climate is through the "delta method" (e.g., see Rummukainen 2010). The delta method consists of adding to the observed climate data the RCM-simulated climate change (CC) signal. This suggests that the RCM's added value in climate projections may not come directly from the simulation of future scenario periods but rather from the climate-change signal itself.

Implicit in the last argument is the idea that some changes in climate will occur in spatial scales smaller than those resolved by current AOGCMs. Several sources of fine-scale climate change can be conceived. For example, fine-scale climate forcings (e.g., land cover) can change in the future due to the influence of human activities (e.g., in agricultural activities). The non-linear interaction between a large-scale variable and fine-scale surface forcings can induce small-scale changes if the large-scale variable changes in the future. Feedback processes can also induce small-scale changes in meteorological variables due to the fine scale heterogeneity of surface physical properties.

It should be emphasised, however, that the arguments from which fine-scale features would appear in the climate change signal are not the same as those asserted for the climate itself. One example can help to understand the difference. A simple mechanism that can generate AV in mountainous regions in present climate simulations is related with the general relation between temperature and terrain elevation. The more detailed representation of terrain elevation gradients will create stationary temperature gradients even when no fine-scale atmospheric processes occur. But this mechanism may not generate AV in the CC signal because their effects may be cancelled out when computing the difference between future and climate statistics.

The objective of this article is twofold. First, to quantify the fine-scale part of the RCM-derived CC signal and to evaluate its relative importance compared to either the large-scale CC part or to present climate statistics. Second, to characterise the robustness of the fine-scale quantitative results in terms of the sampling uncertainty that results from interannual variability. The analysis concentrates on time-averaged seasonal temperature and precipitation climate change signals as reproduced by several RCM-AOGCM pairs in a domain that covers most of North America, thus encompassing a wide range of climate regimes.

The paper is organized as follows. The next section discusses in some detail the added value issue with special emphasis on two particular aspects: the difference between AV and potential AV (hereafter PAV) and; the difference between looking for

AV in the climate and in the CC signal. Section 3.3 presents a brief description of the data used. Section 3.4 describes the methodology used to analyze the importance of fine scale features and the metrics used to quantify the PAV and the sampling uncertainty. Temperature and precipitation results are presented in Sect. 3.5.1 and 3.5.2 respectively. Some discussion of the results and conclusions is given in Sect. 3.6.

3.2 Added Value issue

3.2.1 Present/Future Climate simulations

In order to illustrate the AV issue, let us consider a hypothetical AV study (a more general example is discussed in Appendix A). Let us suppose that we are trying to decide whether an RCM adds value over an AOGCM in the representation of some climate statistics X (e.g., time-averaged precipitation). Assuming that the metric chosen to assess model's performance is given by the squared error (SE), then the AV can be defined by

$$AV = (X_{GCM} - X_{OBS})^2 - (X_{RCM} - X_{OBS})^2 = SE_{GCM} - SE_{RCM}. \tag{3.1}$$

Defined in this way, the RCM generates some AV if its SE is smaller than the GCMs one, i.e., if AV is positive.

In order to gain more insight on the sources of AV, let us separate the field according to different spatial scales and express the value of X_{OBS} as follows:

$$X_{OBS} = X^{ls}_{OBS} + X^{ss}_{OBS}, \tag{3.2}$$

where the superscripts ls and ss designate, respectively, the *large scales* and *small scales* that are permitted or not by the GCM grid. Hence by definition $X^{ss}_{GCM} = 0$ and

$$X_{GCM} = X^{ls}_{GCM}. \tag{3.3}$$

Similarly the RCM-derived climate statistics (X_{RCM}) may be decomposed as

$$X_{RCM} = X^{ls}_{RCM} + X^{ss}_{RCM}. \tag{3.4}$$

Replacing Eq. (3.2), (3.3) and (3.4) in Eq. (3.5), rearranging and neglecting covariance

terms (see below and in Appendix A for details), we obtain:

$$AV \sim AV^{ss} + AV^{ls}, \tag{3.5}$$

where

$$\begin{aligned} AV^{ss} &= (X^{ss}_{OBS})^2 - SE^{ss}_{RCM} \\ &= (X^{ss}_{OBS})^2 - (X^{ss}_{RCM} - X^{ss}_{OBS})^2, \end{aligned} \tag{3.6}$$

and

$$AV^{ls} = SE^{ls}_{GCM} - SE^{ls}_{RCM}. \tag{3.7}$$

That is, the AV can be approximately decomposed into a small-scale term (AV^{ss}) and a large-scale term (AV^{ls}). We recall that these equations were arrived at neglecting two covariance terms: one corresponds to assuming that large-scale errors of GCM are uncorrelated with small-scale variance of observations, and the other that large-scale and small-scale errors of RCM are uncorrelated.

From Eq. (3.6) it is clear that three conditions must be satisfied for the RCM to generate small-scales added value ($AV^{ss} > 0$):

- the observed climate statistics X_{OBS} must contain non-negligible fine-scale information ($(X^{ss}_{OBS})^2 > 0$),
- the RCM-derived climate statistics X_{RCM} must contain non-negligible fine-scale information ($(X^{ss}_{RCM})^2 > 0$), and
- the fine-scale RCM information must have some skill, i.e. $(X^{ss}_{RCM} - X^{ss}_{OBS})^2 < (X^{ss}_{OBS})^2$.

This analysis suggests that a measure of the potential of RCMs to add value can be obtained by quantifying the maximum or available AV using observations:

$$MAV^{ss} = (X^{ss}_{OBS})^2. \tag{3.8}$$

The quantity MAV^{ss} is called *maximum added value* of the small scales and gives an estimation of the maximum value that an RCM or any downscaling technique can add. In those cases where observations are not available, the small-scale *potential added value*

of RCMs can be defined in terms of fine-scale RCM features:

$$PAV^{ss} = (X^{ss}_{RCM})^2. \tag{3.9}$$

It is important to note that if $(X^{ss}_{OBS})^2 \neq (X^{ss}_{RCM})^2$ then the quantity $(X^{ss}_{OBS})^2$ will under- or over- estimate MAV^{ss} by simulating too much or too little fine-scale variability. An under/over estimation of MAV^{ss} can be related with either positive or negative AV, depending on the values of SE^{ss}_{RCM} and $(X^{ss}_{OBS})^2$. The interests of computing PAV^{ss} is that allows to estimate the small-scale part of PAV in those cases where we do not have any knowledge about the observed climate statistics.

Figure 3.1 shows the dependence of AV^{ss} as a function of X^{ss}_{RCM} for three different values of X^{ss}_{OBS}. In the case where $X^{ss}_{OBS} = 0$ everywhere, an increase in fine-scale variance of X_{RCM} can only subtract value by making AV^{ss} negative. Where $X^{ss}_{OBS} \neq 0$, the fine-scale feature of X_{RCM} can add value over the GCM estimation wherever Eq. (3.6) is positive. The maximum AV^{ss} is found when $X^{ss}_{OBS} = X^{ss}_{RCM}$ and is given by $\overline{(X^{ss}_{RCM})^2}$. Furthermore, Fig. 3.1 shows that the term AV^{ss} can potentially increase as X^{ss}_{OBS} increase, justifying the idea of using an increase in fine-scale variance as a proxy of an increase in the PAV.

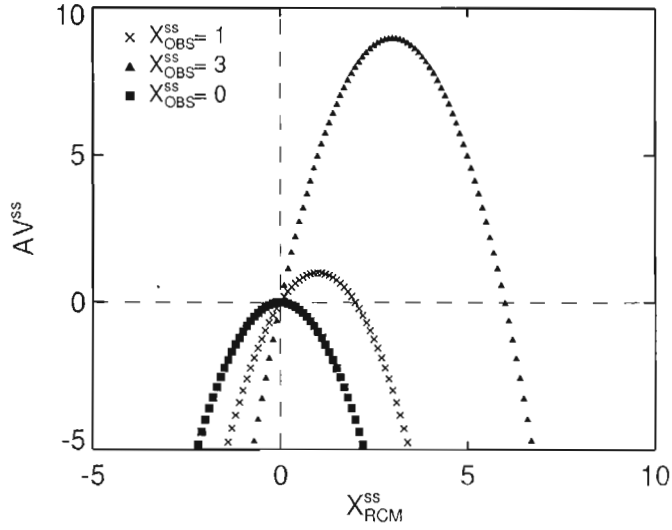

Figure 3.1 Small-scales added value (AV^{ss}) as a function of X^{ss}_{RCM} for three different values of X^{ss}_{OBS}.

The term AV^{ls} in Eq. (3.5) represents the AV generated by an RCM due to an improvement in the large-scale part of the climate statistics X. Given that the main objective of RCMs is to add fine-scale features to the coarser AOGCMs, there is a general consensus in the RCM community (e.g., Feser 2006; Prömmel et al. 2010) that the primary added value of RCMs is related with AV^{ss}. Much less agreement exists about whether or not RCMs can generate AV at large scales. Although some authors (e.g., Mesinger et al. 2002 and Veljovic et al. 2010) sustain the notion of a potential improvement of large-scale features through the use of RCMs, a large part of the RCM community (e.g., Castro et al. 2005; Laprise et al. 2008) seems to promote the use of large-scale nudging thus reducing large-scale differences between the RCM and the driving data.

The PAV^{ss} concept as described above was used to study the potential benefits of using high-resolution RCMs to simulate present climate precipitation (Di Luca et al. 2011a) and temperature (Di Luca et al. 2011b), and the PAV^{ss} dependence on several factors such as the season, the region and the climate statistics of analysis. In what follows, the application of the PAV framework to climate change studies will be considered.

3.2.2 Climate change signal

A variety of approaches can be used to show how a given climate statistics X will change in the future. A popular approach, generally designated as the "delta method" (e.g., see Rummukainen 2010), consists on computing the future climate statistics (X^{future}) by adding the climate change as estimated from climate model simulations ($CC_{simulated}$) to the past observed climate ($X_{OBS}^{present}$). That is, the delta method approximation can be expressed as:

$$X_{\delta}^{future} = X_{OBS}^{present} + CC_{simulated}, \tag{3.10}$$

where $CC_{simulated}$ is computed in the usual form as the difference between X in future and present climate ($X_{simulated}^{future} - X_{simulated}^{present}$) using either RCM ($CC_{RCM}$) or GCM ($CC_{GCM}$) simulations.

Another popular approach used to show changes in climate statistics X is through the use of the climate change signal ($CC_{simulated}$) itself, with no explicit consideration of present and future climate statistics. That is, in this case, we are not interested in

the future value of the climate statistics but only on how much X may change between present and future periods.

Following the development in Sect. 3.2, the CC signal added value (AV_{CC}) generated by a RCM simulation over a GCM can be defined using the delta method by:

$$\begin{aligned} AV_{CC} &= (X^{future}_{\delta,GCM} - X^{future}_{true})^2 - (X^{future}_{\delta,RCM} - X^{future}_{true})^2, \\ &= (CC_{GCM} - (X^{future}_{true} - X^{present}_{OBS}))^2 - (CC_{RCM} - (X^{future}_{true} - X^{present}_{OBS}))^2, \\ &= (CC_{GCM} - CC_{true})^2 - (CC_{RCM} - CC_{true})^2, \end{aligned} \tag{3.11}$$

where the subscript "true" denotes the still unknown climate statistics that will arise in future climate conditions. That is, the RCM generates some AV if its error in the CC signal estimation is smaller that the GCM one, i.e., if AV_{CC} is positive. It is important to note that, when using the delta method, the AV of RCM simulations in future climate statistics does not depend directly on the future climate statistics ($X^{future}_{simulated}$) but on the CC signal ($CC_{simulated}$).

Replacing the total CC signal in Eq. (3.11) according to the contribution of large (CC^{ls}) and small (CC^{ss}) scales we have,

$$AV_{CC} \sim AV^{ls}_{CC} + AV^{ss}_{CC}, \tag{3.12}$$

with

$$\begin{aligned} AV^{ss} &= (CC^{ss}_{true})^2 - (SE^{ss}_{CC,RCM})^2 \\ &= (CC^{ss}_{true})^2 - (CC^{ss}_{RCM} - CC^{ss}_{true})^2, \end{aligned} \tag{3.13}$$

and

$$AV^{ls} = (SE^{ls}_{CC,GCM})^2 - (SE^{ls}_{CC,RCM})^2. \tag{3.14}$$

Again, the approximation in Eq. (3.12) results from neglecting two covariance terms. As with the present climate case, three necessary conditions for the RCM to add value in the fine-scale CC signal can be identified:

- the true CC signal (CC_{true}) must contain non-negligible fine-scale information ($(CC^{ss}_{true})^2 > 0$),
- the RCM-derived CC signal (CC_{RCM}) must contain non-negligible fine-scale information ($(CC^{ss}_{RCM})^2 > 0$), and

- the RCM-derived CC signal must have some skill, i.e. $(CC^{ss}_{true})^2 > (CC^{ss}_{RCM} - CC^{ss}_{true})^2$.

Given that we do not have any knowledge about the true CC signal, the first condition cannot be explicitly addressed. However, the CC signal PAV can be defined in terms of the other two conditions in the following way:

$$PAV^{ss}_{CC_1} = (CC^{ss}_{RCM})^2, \tag{3.15}$$

and

$$PAV^{ss}_{CC_2} = (CC^{ss}_{RCM})^2 - (\Delta^{ss}_{RCM})^2, \tag{3.16}$$

where Δ^{ss}_{RCM} constitutes a measure of the uncertainty in the estimation of CC^{ss}_{RCM} and is used as a proxy of the error $(SE^{ss}_{CC,RCM})^2$. Defined in this way, relatively large values of both $PAV^{ss}_{CC_1}$ and $PAV^{ss}_{CC_2}$ are related with a large and robust estimation of the fine-scale component of the CC signal.

Finally, for the large-scale part, the PAV can be simply defined as:

$$PAV^{ls}_{CC} = (CC^{ls}_{RCM} - CC^{ls}_{GCM})^2. \tag{3.17}$$

Several arguments can be presented to expect a large-scale component of the PAV_{CC} quantity. For example, Gao et al. (2011) argue that because GCMs do not adequately simulate higher elevations where temperature changes have less effect on snow cover (where temperatures are still cold enough to retain snow), the large-scale temperature change can be differently simulated in a RCM compared to a GCM. In this article we will concentrate in the study of PAV^{ss}_{CC} with no explicit consideration of its large-scale counterpart, PAV^{ls}_{CC}.

3.3 NARCCAP data

The RCM simulations used in this study were provided by the North American Regional Climate Change Assessment Program (NARCCAP; http://www.narccap.ucar.edu/; Mearns et al. 2009). In NARCCAP, RCMs were run with a horizontal grid spacing of about 50 km over similar North American domains covering Canada, United States and most of Mexico. Acronyms, full names and a reference, and the modelling group of the RCMs used in this study are presented, respectively, in the first three columns in Table 3.1.

Table 3.1 Acronyms, full names and modelling group of RCMs involved in the NARCCAP project. Column 4 indicates the LBCs used to drive each RCM.

RCM	Full Name	Modelling group	LBCs
CRCM	Canadian Regional Climate Model (version 4.2.0) (Caya and Laprise 1999)	Ouranos / UQAM	CGCM3 CCSM
RCM3	Regional Climate Model (version 3) (Giorgi et al. 1993)	UC Santa Cruz	CGCM3 GFDL
HRM3	Hadley Regional Model (version 3) (Jones et al. 2004)	Hadley Centre	HadCM3

Five RCM-AOGCM pairs are used in this study to analyze the climate change signal, with two RCMs (CRCM and RCM3) driven by two AOGCMs and one RCMs (HRM3) driven by only one AOGCM. Four AOGCMs are used to drive the RCMs: the Canadian Global Climate Model version 3 (CGCM3, Flato and Boer 2001), the NCAR Community Climate Model version 3 (CCSM3, Collins et al. 2006), the Geophysical Fluid Dynamics Laboratory Climate Model version 2.1 (GFDL, GFDL Global Atmospheric Model Development Team 2004]) and the United Kingdom Hadley Centre Coupled Climate Model version 3 (HadCM3, Gordon et al. 2000). The fourth column in Table 3.1 provides the LBCs used to drive each RCM. A total of ten RCM simulations are considered, five of them simulating a present period (1971 - 1995) and the other five simulating the future climate (2041 - 2065) using the A2 scenario (Mearns et al. 2009).

For each RCM simulation, several 3-hourly variables are available in their original map projection; but in this article we will concentrate only on the instantaneous 2-m temperature and on the 3-hourly average total precipitation. Sea surface temperatures (SST) and sea ice (SI) surface boundary conditions comes from AOGCM data and are updated every 6 hours by using a linear interpolation between consecutive monthly-mean values. Similarly, boundary conditions are interpolated from the low resolution to the ~50-km grid meshes by using a linear interpolation in the horizontal.

All NARCCAP RCMs include some more or less sophisticated representation of land surface and the upper soil levels. The representation of lakes depends on each RCM and on the LBCs used to drive the RCM. RCMs do not share the fraction of water in every grid point (i.e., the land-water mask is model dependent) although most RCMs,

with the only exception of the RCM3, represents the Great Lakes, Winnipeg Lake and other relatively large lakes in the west northern part of Canada. In all cases, as with oceanic regions, surface temperatures in lakes are prescribed using the driving AOGCM data.

3.4 Methodology

The methodology use to study the importance of fine scales in the determination of the climate change signal is based in a perfect model approach designated as the *potential added value* framework. A main advantage of this framework is that allows to estimate PAV^{ss}_{CC} quantities independently of the relative performance between the RCM and the driving AOGCM without necessity of having high-resolution observations. A brief description of the framework is given here but a more detailed discussion can be found in Di Luca et al. (2011a) and Di Luca et al. (2011b).

3.4.1 Potential added value measures

Let us consider a two-dimensional field representing the projected change of a given climate statistics X computed using ~50 km grid-spacing RCM simulations that we denote by CC_{RCM}. A domain of analysis, common to all RCMs, is selected and divided in non-overlapping boxes of 300 km by 300 km leading to a low-resolution grid mesh containing a total of 288 grid boxes (see Fig. 3.2). Using this grid mesh, we can define a lower resolution version of CC_{RCM}, that we denote by the virtual GCM version of the climate change signal (CC_{VGCM}), by aggregating the CC_{RCM} over each 300-km side grid boxes. For any RCM-AOGCM simulation, the upscaling is simply performed by computing the arithmetic average of the statistics X over all the RCM grid points inside the region of interest.

As discussed in Sect. 3.2.2, a question that arises naturally in the context of the PAV framework is whether the high-resolution CC_{RCM} contains fine-scale information that is absent in the low-resolution part (CC_{VGCM}). Given that some of the most important factors of anthropogenic climate change are large scale in nature (e.g., greenhouse gases concentration changes), it is unclear whether the CC signal would contain a significant high-resolution component. A simple way to quantify the importance of fine scales in the high-resolution CC signal can be done by defining:

$$PAV^{ss}_{CC} = \sigma^2(CC_{RCM}), \tag{3.18}$$

where $\sigma^2(CC_{RCM})$ denotes the spatial variance of the high-resolution CC signal field over a given 300-km side region. Similarly, we can define a relative PAV quantity that evaluates the proportion of the CC signal that is accounted only by the fine-scale part by writing

$$rPAV^{ss}_{CC} = \frac{\sigma^2(CC_{RCM})}{CC^2_{VGCM}}, \tag{3.19}$$

where CC^2_{VGCM} is the square of the spatial-mean climate change signal in each region. Defined in this way, $rPAV^{ss}_{CC}$ varies between 0 and $+\infty$; $rPAV^{ss}_{CC} \sim 0$ would indicate that the high-resolution estimation does not add extra information over the coarse-resolution one. For a given region, $rPAV^{ss}_{CC} \sim 1$ indicates that the change in the fine-scale temperature is as large as the large-scale part change.

For the time-averaged temperature, CC_{VGCM} is always greater than zero in continental North America and Eq. (3.19) is well defined. When considering time-averaged precipitation, CC_{VGCM} can be near zero and so an alternative $rPAV$ quantity should

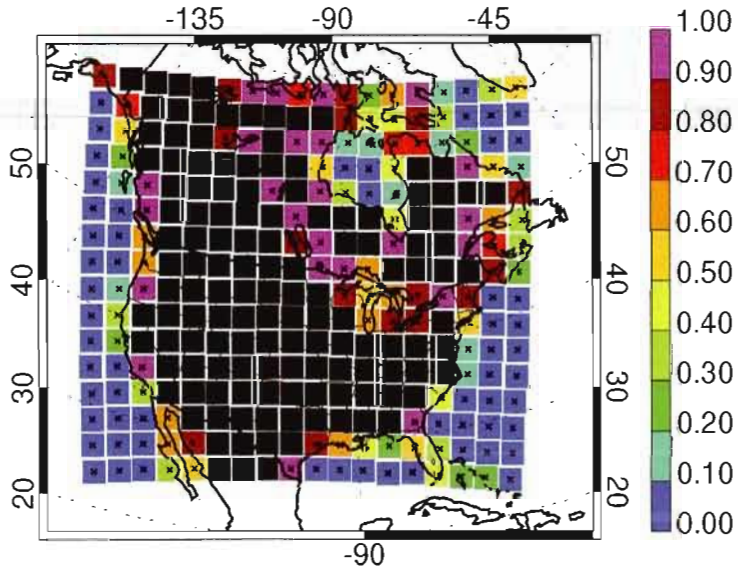

Figure 3.2 Spatial-mean CRCM model land fraction over the 288 regions use in the analysis. The total domain of analysis is common to all 6 RCM domains and each sub region has the same dimensions (i.e., 300 km by 300 km). Black (blue) colors denote those regions entirely covered with land (water).

be considered to avoid that $rPAV$ be indefinite. This can be done, for example, by normalising the PAV_{CC}^{ss} with the square of the mean precipitation of the region:

$$rPAV_{CC}^{ss} = \frac{\sigma^2(CC_{RCM})}{(pr_{VGCM}^{present})^2}, \tag{3.20}$$

where $pr_{VGCM}^{present}$ represents the spatial-mean precipitation over each 300-km side region in present climate. Again, with this definition, $rPAV_{CC}^{ss}$ varies between 0 and $+\infty$; $rPAV_{CC}^{ss} \sim 0$ indicating that the high-resolution estimation does not add extra information over the coarse-resolution one. For a given region, $rPAV_{CC}^{ss} \sim 1$ indicates that the change in the fine-scale precipitation is as large as the spatial-mean precipitation itself.

It should be emphasised that the quantities PAV_{CC}^{ss} and $rPAV_{CC}^{ss}$ defined in Eq. (3.18), (3.20) and (3.19) only account for the potential added value of the small scales (PAV_{CC}^{ss}), that is, the PAV arising from the simulation of fine-scale features in the statistics X that are absent in GCM fields. The two quantities are mute about the potential of RCMs to add value in the large scale or in the covariance terms.

3.4.2 Interannual variability of PAV measures

Inherent to the process of computing climate statistics from a finite length time series (i.e., 25 years periods in our case) there is an uncertainty related to sampling. The existence of sampling uncertainty implies that two adjacent grid points can show somewhat different present and future statistics (e.g., time-averaged values), leading to differences in the CC signal and its derived spatial variance, even if physical mechanisms that determine the climate in both grid points are essentially the same. Ideally, in any grid point and for any given RCM-AOGCM simulation, the sampling uncertainty can be quantified using several RCM simulations performed employing different boundary conditions arising from running the AOGCM with slightly different initial conditions (i.e., using several members of the driving AOGCM). In NARCCAP, modelling efforts has been put on the number of RCM-AOGCM pairs and there is only one realisation of each pair available for analysis thus preventing the internal variability sampling study.

In order to circumvent this practical limitation, the sampling uncertainty will be quantified by estimating the fine-scale CC signal in each 300-km side region using a Monte Carlo approach. First, for each RCM-AOGCM simulation, the high-resolution climate change signal CC_{RCM} is computed 100 times by sampling randomly with re-

placement over the 25-year seasonal averages of present ($X_{RCM}^{present}$) and future (X_{RCM}^{future}) simulations, thus obtaining a distribution for CC_{RCM} that we denote by CC_{RCM}^{i}.

Second, for each sample of CC_{RCM}^{i}, we compute the spatial variance obtaining a 100 sample distribution of variances in each region, denoted by $\sigma_i^2(CC_{RCM})$, that can be used to estimate the mean spatial variance and some measure of the spread around the mean. Defined in this way, the sampling uncertainty gives a measure of the interannual variability in each region.

A similar method to estimate sampling uncertainty was used by Déqué et al. (2011). Using a Monte Carlo procedure and a 10 members sampling they found a very good agreement between the sampling uncertainty computed using various runs only differing on initial conditions and the Monte Carlo approximation for time-averaged precipitation. For time-averaged temperature, they found a good agreement in summer season but they found that the Monte Carlo approximation underestimates by nearly 30% the "true" spread in winter. Although these results are encouraging, a more detailed study should be undertaken to confirm that the Monte Carlo estimation constitutes a good approximation.

The existence of sampling uncertainty has implications when attempting to evaluate the necessary conditions for AV that were discussed in Sect. 3.2.2 (see Eq. (3.15) and (3.16)). First, when trying to identify regions containing non-negligible fine-scale variance (i.e., $PAV_{CC}^{ss} = (CC_{RCM}^{ss})^2 > 0$), the sampling uncertainty implies that we cannot use a zero threshold but some non-zero threshold that measures the level of noise inside each region. That is, a "variance noise" threshold must be used in order to determine whether the fine-scale variance is induced by physical mechanisms or only arising from sampling uncertainty. We will refer to the use of such threshold as "physically significant" condition.

The *physically significant condition* is defined here in a simple way by arbitrarily choosing a minimum value, the same for all regions, for PAV_{CC}^{ss} to be statistically different from zero. In order to take into account the sampling uncertainty in the variance computations and the possibility of getting a value below the threshold by chance, the criterion imposes that 95% of the Monte Carlo-generated variances must be larger than the threshold:

$$q_5(\sigma_i^2(CC_{RCM})) > threshold. \tag{3.21}$$

For the absolute quantity (PAV^{ss}_{CC}), relatively small values are chosen for both temperature ($(0.1K)^2$ threshold) and precipitation ($(0.04mm/day)^2$ threshold). Assuming that CC_{RCM} values are normally distributed inside each region, this implies that 95% (99%) of the CC_{RCM} differences between two grid points are smaller than 0.2 K (0.3 K) for temperature and smaller than 0.08 mm/day (0.12 mm/day) for precipitation. Similarly, for relative PAV quantities ($rPAV^{ss}_{CC}$), regions will be considered as physically significant when $rPAV^{ss}_{CC}$ values are larger than 0.05^2 and 0.02^2 for temperature and precipitation respectively.

The second implication introduced by the existence of sampling uncertainty is related with the condition $(CC^{ss}_{true})^2 > SE^{ss}_{CC,RCM}$ (see Eq. (3.16)) that suggests that a large error in the estimation of $(CC^{ss}_{RCM})^2$ can prevent the RCM from adding value. The sampling uncertainty can be used as a proxy of the unknown error $SE^{ss}_{CC,RCM}$ to quantify the potential skill of the fine-scale spatial variance estimation.

In order to define a condition quantifying the skill of the several RCM simulations, let us suppose that the mean value of $\sigma^2_i(CC_{RCM})$ is a good estimation of the spatial variance of the true climate-change signal (i.e., $\overline{\sigma^2(CC_{RCM})} \sim \sigma^2(CC_{true})$). In this case, for any sample $\sigma^2_i(CC_{RCM})$, there will be some AV in the fine-scale climate-change signal if and only if $\sigma^2_i(CC_{RCM}) < 2 \cdot \overline{\sigma^2(CC_{RCM})}$ (see Eq. (3.13)). In order to guarantee some form of skill in the estimation of a PAV^{ss}_{CC} we will consider as skillful those regions that verify:

$$q_{95}(\sigma^2_i(CC_{RCM})) > 2 \cdot \overline{\sigma^2(CC_{RCM})}. \tag{3.22}$$

with q_{95} the 95th percentile of the $\sigma^2_i(CC_{RCM})$ distribution.

Several uncertainty sources can influence PAV quantities; see Foley (2010) for a detailed discussion. The uncertainty related with the use of different RCM and GCMs will not be directly addressed here, although PAV quantities derived from individual pairs of RCM-AOGCM simulations will be shown. Also, NARCCAP future climate simulations are available only based on the A2 scenario (see IPCC 2007), thus preventing any scenario uncertainty analysis. While this can be a main source of uncertainty when looking at the end of the 21st century climate, it is probably less important when looking at the first half of the century.

It should be noted that quantitative results related to the "physically significant" and the "skill" conditions depend on the arbitrary choice of the threshold and the

sampling uncertainty measure, respectively. The use of other thresholds and sampling uncertainty measures would lead to different quantitative results. However the results are qualitatively similar.

3.5 Results

3.5.1 Temperature

Figures 3.3 and 3.4 show the time-averaged projected temperature change (2041-2065 minus 1971-1995) for individual RCM simulations in winter and summer seasons respectively. In both seasons, results show warmer conditions in the future with generally a stronger warming in continental compared to oceanic regions. In winter season, the spatial pattern of CC_{RCM} shows a general increase to the north and to the interior of the continent that reaches almost 7 K in the centre of the Hudson Bay for all RCM simulations with the only exception of the RCM3-GFDL simulation. This pattern of warming is related with the positive feedback induced by the reduction of the period of snow sea-ice cover and the associated increase in absorbed solar radiation (see for example IPCC 2007).

Warming is smaller in summer than in winter in northern regions and generally larger in central and southern regions. The spatial pattern of CC_{RCM} shows maximum values in continental-middle latitudes with changes as large as 4 K in central United States in most RCM simulations. This pattern of warming is mainly explained by the positive feedback induced by the decreased of latent heat fluxes and the increase in sensible fluxes due to negative anomalies in surface soil moisture in most central-western regions (Seneviratne et al. 2010).

Figures 3.5 and 3.6 show the square root of the PAV^{ss}_{CC} measure (see Eq. (3.18)) for the RCM-AOGCM simulations and for the ensemble-mean results in winter and summer seasons, respectively. As stressed in Sect. 3.3, oceanic boundary conditions in NARCCAP simulations are obtained by interpolating SST and SI fields coming from the driving AOGCM simulations. This means that stationary fine-scale patterns in the ocean fields, if they exist, are artificial and do not reflect any physical processes. For this reason, we decided to mask oceanic regions in the PAV analysis. Oceanic regions are defined as those containing 100% water-fraction and the total number depends on the RCM considered, varying between 50 in the CRCM to 58 in the HRM3 model.

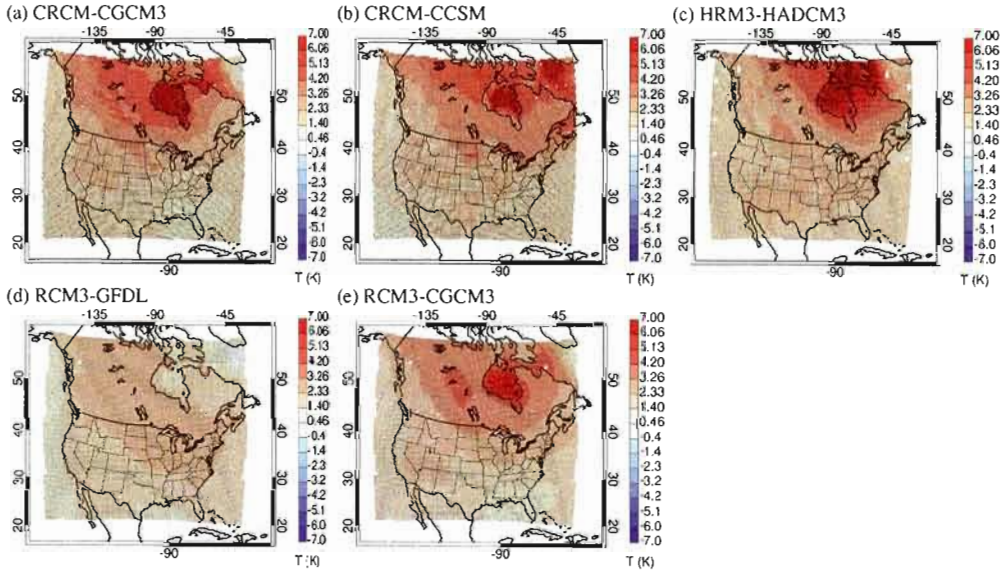

Figure 3.3 Climate change signal for the time-averaged temperature in winter season for individual RCM-AOGCM simulations.

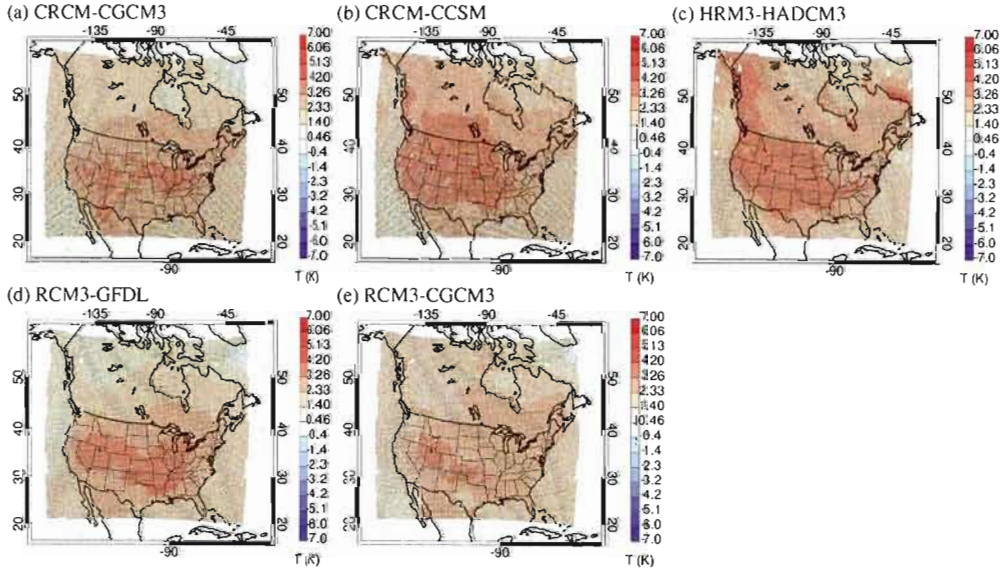

Figure 3.4 Same as Fig. 3.3 but for summer season results.

In winter season (Fig. 3.5), the largest $\sqrt{PAV_{CC}^{ss}}$ values (~1.2 K) appear in northern-coastal regions mainly along the Hudson Bay and the Canadian Archipelago coasts with relatively large values also along the Pacific Coast (~0.5 K) and in central western United States. Different mechanisms appear to produce the relatively large values in coastline regions depending on whether or not sea ice is present during the winter. For example, most RCM-AOGCM simulations show large values of PAV_{CC}^{ss} over the northern part of the Pacific Coast, associated with larger warming over land compared to water (see Fig. 3.3), probably explained by the snow-albedo feedback that is present in land but absent in water surfaces. On the contrary, large values of PAV_{CC}^{ss} in the Hudson Bay and the Canadian Archipelago coasts are generally related with a more pronounced warming over oceanic regions, maybe due to a stronger albedo feedback in sea ice compared to land surfaces. A mechanism that can be important in regions along the Rocky Mountains is related with the snow-albedo feedback resulting from the differential snow cover change in varying altitude regions.

A large number of regions show that at least 5% of winter $\sqrt{PAV_{CC}^{ss}}$ sample values are smaller than the 0.1 K threshold established for physical significance (white mask in Fig. 3.5 and 3.6). The number of these regions depends on the simulation and varies between 74 in the HRM3-HADCM3 and 170 in the RCM3-GFDL simulations, with all simulations showing "zero" values in the south-eastern part of the continent.

Figure 3.5f shows the square root of the average of PAV_{CC}^{ss} across the five individual simulations ($\sqrt{\langle PAV_{CC}^{ss} \rangle}$) in winter season. A total of 154 out of 230 non-oceanic regions appear to be physically significant and these regions are mostly located along a coast (Canadian Archipelago, Hudson Bay, Pacific and Atlantic Oceans) and in the central-western part of the continent.

In summer season (Fig. 3.6), the largest $\sqrt{PAV_{CC}^{ss}}$ values (~0.6 K) appear also in coastal regions along the Hudson Bay, but in this case relatively large values extend to the south, along the Pacific and the Atlantic coasts and over the Great Lakes and other smaller lakes in Canada, at least in those simulations containing lakes (CRCM and HRM3). In this season, the relatively large PAV_{CC}^{ss} values in coastal regions seem to be forced mainly by a larger warming over land compared to oceanic regions (see Fig. 3.4) probably due to the slower response of the ocean because of its larger heat capacity. The number of regions that verify the "physically significant" criterion (see Eq. (3.21)) varies between 105 in the HRM3-HADCM3 and 158 in the RCM3-GFDL simulations, thus showing similar values although less variability than the winter case.

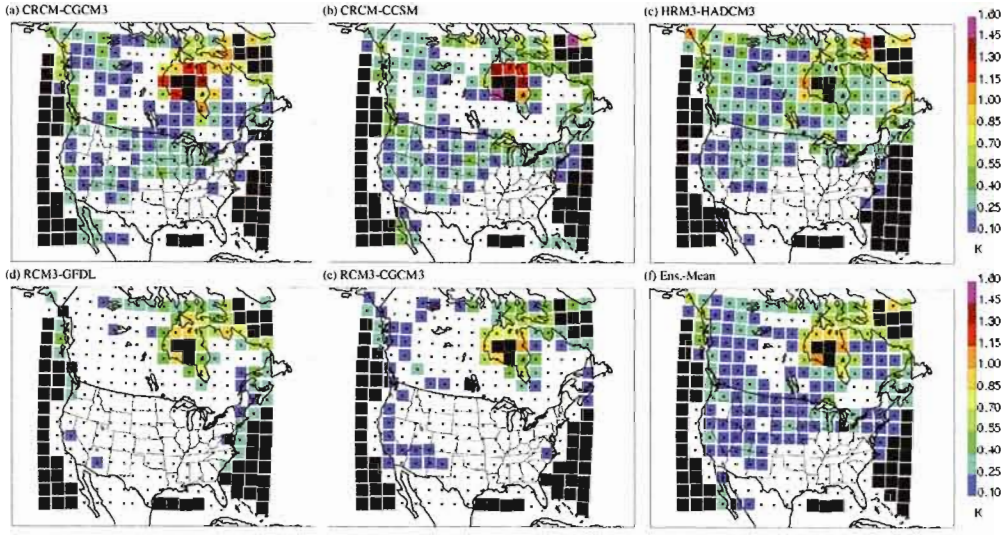

Figure 3.5 Temperature potential added value (see Eq. (3.18)) in winter season for individual RCM-AOGCM simulations and for the ensemble mean. White regions designate those regions that do not satisfy the "non-zero" criteria. Crosses (x) designate those regions that do not satisfy the "skill" criteria. Oceanic regions are in black.

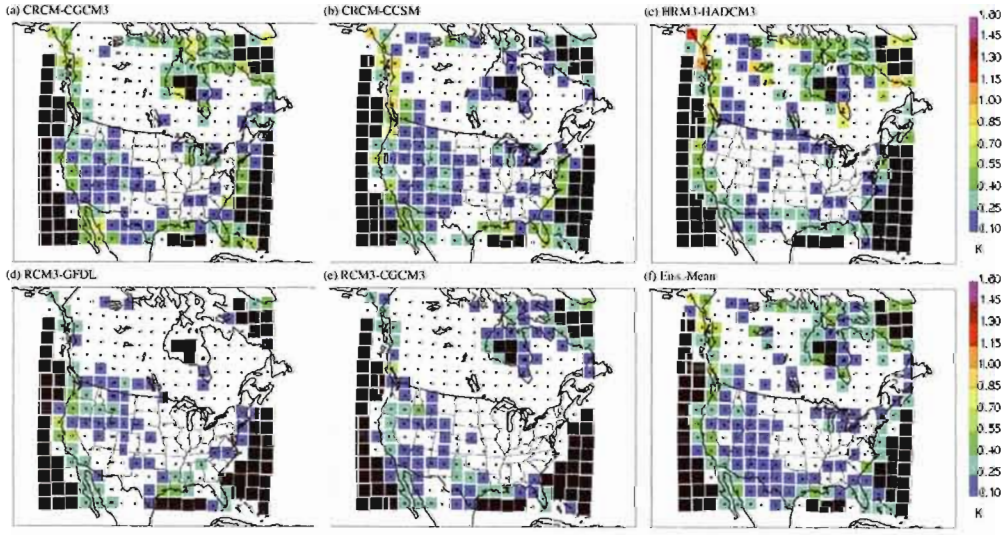

Figure 3.6 Same as Fig. 3.5 but for summer season results.

Figure 3.7 shows the square root of the ensemble-mean temperature relative PAV measure (computed using Eq. (3.19)) in winter and summer seasons, respectively. $\sqrt{\langle rPAV_{CC}^{ss}\rangle}$ values are always smaller than 0.6, suggesting that fine-scale mean-temperature changes are generally smaller than the large scale ones. The domain-averaged $\sqrt{\langle rPAV_{CC}^{ss}\rangle}$ in winter (summer) is 0.086 (0.093) with a maximum value of 0.31 (0.58). That is, averaged over continental North America, the contribution of the fine scales to the total climate change signal is of the order of 10% although it can attain 60% in specific regions.

In both seasons, as with the absolute PAV_{CC}^{ss} measure, the largest ensemble-mean $rPAV_{CC}^{ss}$ values appear along coastal regions due to the differential heating observed in land and ocean surfaces. In winter (summer), there is a total of 101 (93) out of 230 non-oceanic regions where at least 5% of $\sqrt{\langle rPAV_{CC}^{ss}\rangle}$ sample values are smaller than the threshold imposed for physical significance. Other than in coastal regions, relatively large winter $\langle rPAV_{CC}^{ss}\rangle$ values appear over west-central United States (probably associated with fine-scale topography) and over the Great Lakes. The general spatial pattern of $\sqrt{\langle rPAV_{CC}^{ss}\rangle}$ closely resembles the $\sqrt{\langle PAV_{CC}^{ss}\rangle}$ field suggesting that fine-scale variances of the CC signal tend to follow the mean CC.

Interestingly, according to the skill condition (see Eq. (3.22)), the estimation of $\langle PAV_{CC}^{ss}\rangle$ and $\langle rPAV_{CC}^{ss}\rangle$ quantities appear to be very robust in all regions for both summer and winter seasons.

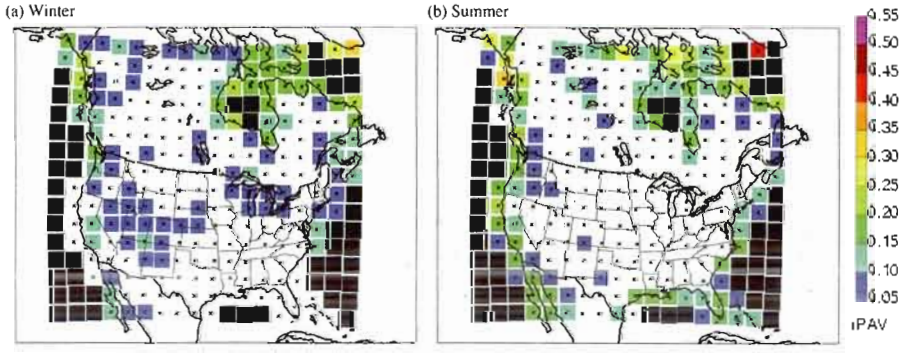

Figure 3.7 Same as Fig. 3.5 but for the $rPAV_{CC}^{ss}$ quantity.

Table 3.2 Number of non-oceanic regions that do not satisfy the physical (see Eq. (3.21)) or the skill (see Eq. (3.22)) conditions for the ensemble-mean PAV and rPAV measures in winter and summer seasons. *Robust* regions designate those that satisfy simultaneously both conditions.

		Temperature		Precipitation	
		Summer	Winter	Summer	Winter
PAV	(1) $q_5 <$ threshold	90	76	70	123
	(2) $q_{95} > 2 \cdot \overline{\sigma^2}$	0	2	9	11
	Robust	140	154	160	107
rPAV	(1) $q_5 <$ threshold	134	126	130	122
	(2) $q_{95} > 2 \cdot \overline{\sigma^2}$	0	0	41	24
	Robust	96	104	91	108

3.5.2 Precipitation

A similar analysis to the one presented above is also performed for the precipitation variable. Figures 3.8 and 3.9 show the time-averaged precipitation change (2041-2065 minus 1971-1995) for individual RCM-AOGCM simulations (CC_{RCM}) in winter and summer seasons, respectively. The high-resolution CC signal is normalised by the present climate mean precipitation in order to account for the important mean-precipitation gradients across the North American continent.

In winter, most simulations tend to produce an increase in precipitation over most of the continent mainly as a result of the increase of atmospheric moisture due to the temperature dependence of the water vapour saturation pressure together with a displacement of the westerlies to the north (see IPCC 2007). Increments are generally smaller than 30-40%, with maximum values generally located over the Hudson Bay. In absolute terms (not shown), the maximum increase in precipitation amounts appear along the northern part of the Pacific Coast, with values of the order of 3 mm/day. Most RCM-AOGCM simulations tend to show a decrease of precipitation in the south-western part of the domain, a feature that seems to be related with an enhanced subsidence in this region due to an intensification of the subtropical anticyclone in this season (IPCC 2007).

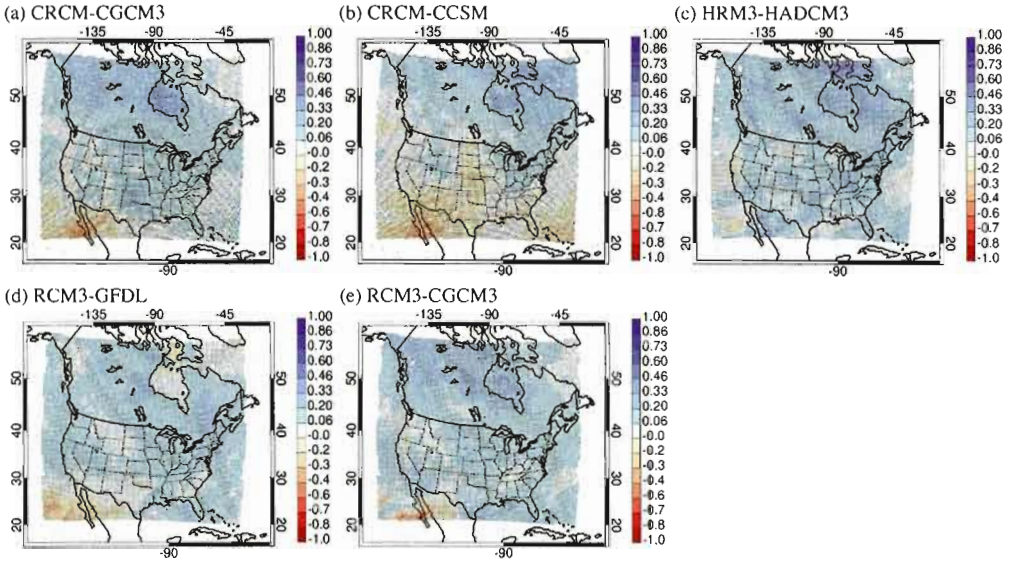

Figure 3.8 Climate change signal for the time-averaged precipitation in winter season for individual RCM-AOGCM simulations.

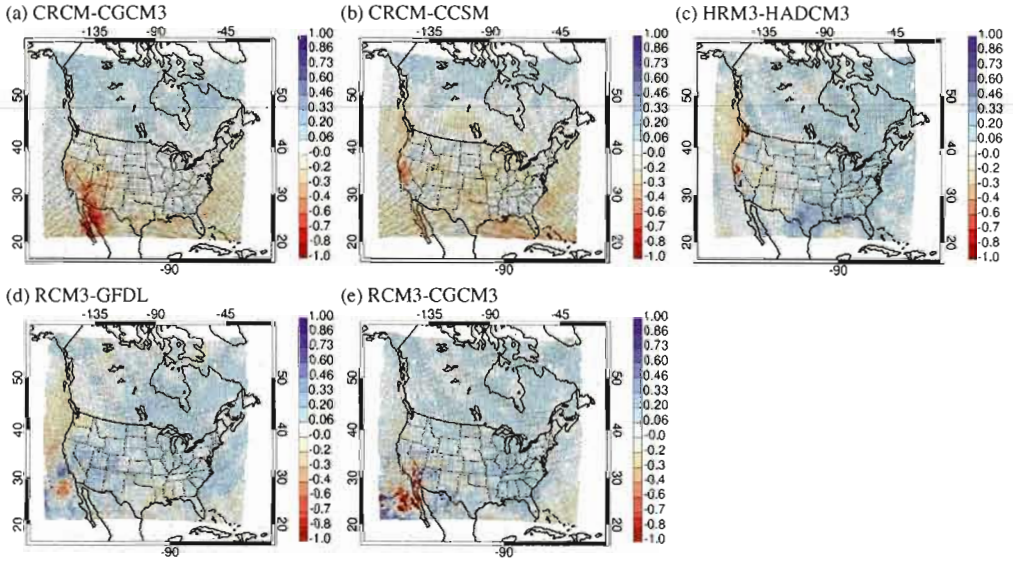

Figure 3.9 Same as Fig. 3.8 but for summer season results.

In summer, in agreement with results found in IPCC (2007), the precipitation CC signal is strongly dependent on the RCM-AOGCM simulation and, in some simulations,

the increase in precipitation is only limited to the northern part of the domain. Some simulations suggest a decrease of about 30% in mean-precipitation in the northern part of the Pacific Coast.

Figures 3.10 and 3.11 show the square root of the precipitation PAV_{CC}^{ss} measure for individual RCM-AOGCM simulations and for the ensemble-mean results in winter and summer seasons, respectively. In winter season (Fig. 3.10), the largest $\sqrt{PAV_{CC}^{ss}}$ values are found along the Pacific coast, mainly in the northern part, with values attaining 1.15 mm/day. In some individual simulations, the $\sqrt{PAV_{CC}^{ss}}$ winter season field shows a secondary maximum in the south-eastern part of the domain, with values of about 0.4 mm/day. In regions located in central United States and most of Canada, the 5th percentile of the $\sqrt{PAV_{CC}^{ss}}$ distribution is generally smaller than the 0.04 mm/day threshold, suggesting that most of these regions are physically non-significant.

In summer, no clear pattern of PAV_{CC}^{ss} can be identified and, in most regions, mean $\sqrt{PAV_{CC}^{ss}}$ values are generally smaller than 0.3 mm/day. In this season, the PAV precipitation analysis in individual RCM-AOGCM simulations shows that a minimum of 107 and a maximum of 213 appear as physically non significant according to the criterion defined in Eq. (3.21).

Figure 3.12 shows the square root of the relative PAV precipitation measure (see Eq. (3.20)) for the ensemble-mean results in winter and summer seasons, respectively. In both seasons, it is clear that the fine-scale component of the CC signal is much smaller than the present time-averaged precipitation. Domain-average $\sqrt{\langle rPAV_{CC}^{ss} \rangle}$ values are about 0.045 and 0.048 in winter and summer seasons respectively, suggesting that fine scales induce a precipitation change of about 5% compared to the present time-averaged precipitation.

In winter season (Fig. 3.12a), the largest changes in mean precipitation ($\sim 10\%$) seem to arise related with the presence of fine-scale topographic features along the Rocky Mountains and with a small-scale process taking place in the northern part of the domain.

In summer season (Fig. 3.12b), the largest $\sqrt{\langle rPAV_{CC}^{ss} \rangle}$ values appear in the south-western part of the continent with values attaining 0.3 in some regions. Interestingly, most of these regions seem to be non-robust to the sampling uncertainty criterion indicating that in these regions negative added value could be the net result due the generation of too much or too little fine-scale features.

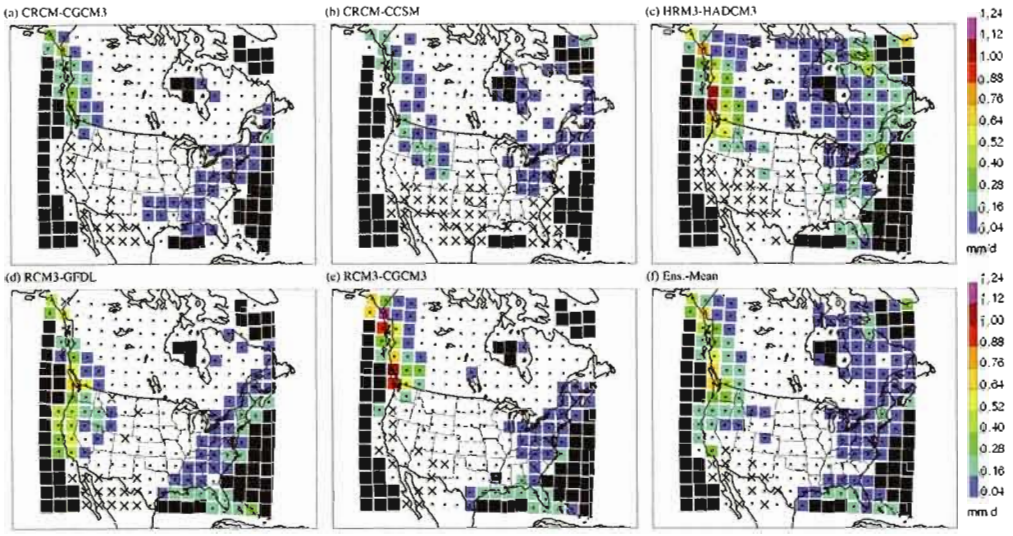

Figure 3.10 Precipitation relative potential added value in winter season for individual RCM-AOGCM simulations and for the ensemble-mean. White regions designate those regions that do not satisfy the "non-zero" criteria. Crosses (x) designate those regions that do not satisfy the "skill" criteria. Oceanic regions are in black.

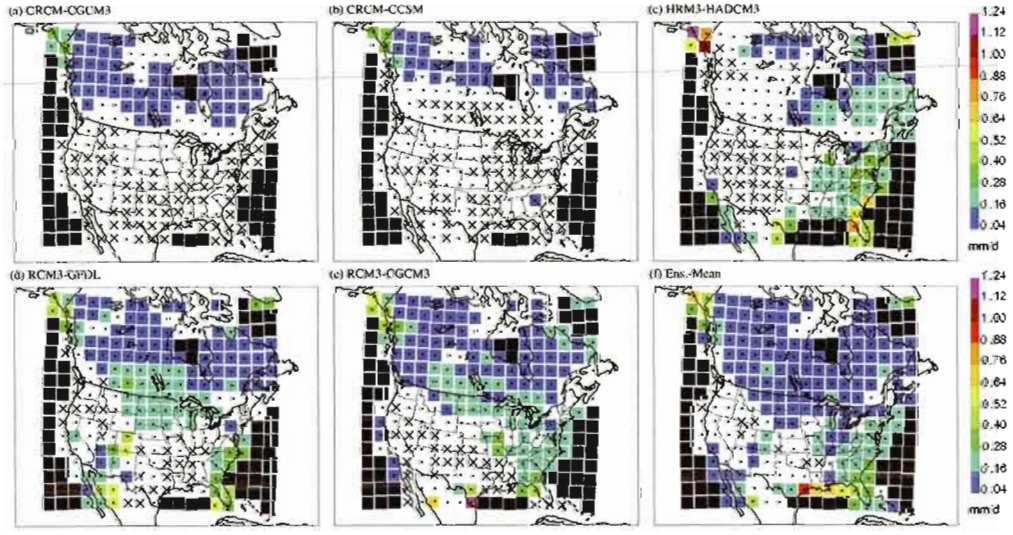

Figure 3.11 Same as Fig. 3.10 but for summer season results.

According to the skill condition, the estimations of PAV_{CC}^{ss} and $rPAV_{CC}^{ss}$ for precipitation are much more uncertain than for the temperature case. For the PAV_{CC}^{ss}

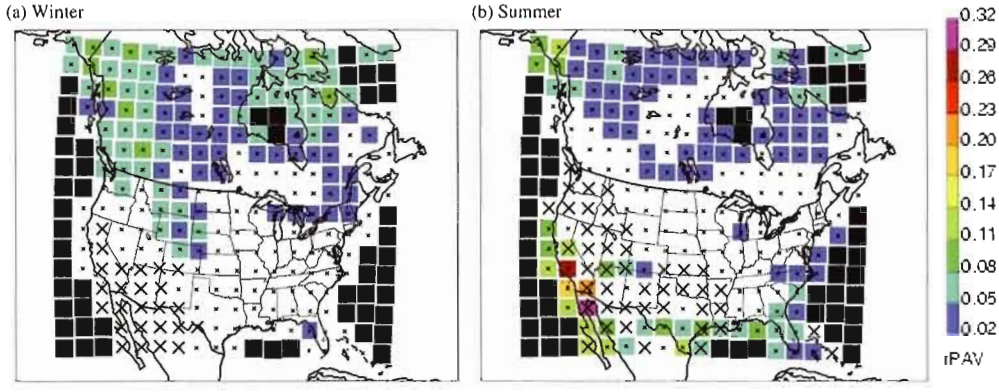

Figure 3.12 Same as Fig. 3.10 but for the $rPAV^{ss}_{CC}$ quantity.

quantity, a total of 9 (11) regions appear to show that the 95th percentile of the sampling distribution is larger than two times the mean value in summer (winter) season. Table 3.2 shows that the number of regions increases to 41 (24) in the same seasons for the $rPAV^{ss}_{CC}$. The lasts two results suggest that, for precipitation, the sampling uncertainty induce by interannual variability can be relatively large not only to determine fine-scale variances $\sigma^2(CC_{RCM})$ but also the time-average precipitation CC^2_{VGCM}.

3.6 Conclusion

The need of future climate information at local and regional scales together with objective evidence supporting the improvement of climate simulations arising from the use of higher resolution models have pushed the climate modelling community to perform increasingly higher resolution simulations and to develop alternative approaches to obtain the fine-scale climatic information.

In this article, various nested RCM simulations have been used to try to identify regions across North America for which the higher resolution afforded by RCMs can potentially be important to determine the future climate change. It is first noted that the issue of looking for added value in future climate is equivalent to searching for AV in the climate change signal instead of in the climate itself, at least when considering the "delta method" to approximate future climate statistics. Further, the absence of knowledge about the "true" climate change means that only necessary (but not sufficient) conditions for AV can be studied leading to the concept of potential added value.

This concept has already been discussed for present climate applications in Di Luca et al. (2011a) and Di Luca et al. (2011b).

Two conditions were identified for an RCM to produce added value over lower resolution GCMs in the fine-scale component of the climate change signal. First, the RCM-derived climate change signal must contain some non-negligible fine-scale information. Second, the uncertainty related with the estimation of this fine-scale information should be small enough to suggest some skill in future climate projections. That is, since non-negligible fine-scale information can either add value to or deteriorate the representation of the climate change signal compared to its large-scale part, large spread in the potential added value indicates a high chance to deteriorate the large-scale CC signal.

The importance of fine scales in the climate change signal is studied using the *potential added value framework* as presented in Di Luca et al. (2011a). For each NARCCAP RCM simulation, large-scale CC values are computed by aggregating the high-resolution CC signal over a lower resolution 300-km grid spacing mesh (denoted as virtual GCM grid) that tries to emulate the grid of a real low resolution GCM. Using a common North American domain for all NARCCAP RCM simulations, a total of 288 non-overlapping virtual GCM grid boxes are defined. An absolute potential added value measure is then defined by estimating the fine-scale variability of the CC signal inside each 300 km side region and a relative quantity is similarly derived by calculating the fraction of the total CC signal accounted for by the small-scale component.

For the temperature variable, the largest potential for added value appears in coastal regions mainly related with differential warming in land and oceanic surfaces. In northern regions along the Hudson Bay and the Canadian Archipelago this seems to be related with a differential snow-sea-ice albedo feedback. Along the Pacific and Atlantic coasts, the relatively large PAV seems to be more related with the differential warming due to the dissimilar thermodynamical properties (e.g., heat capacity) of water and land surfaces. Fine-scale features can account for nearly 60% of the total CC signal in some coastal regions although for most regions the fine scale contributions to the total CC signal are of only $\sim$5%.

For the precipitation variable, fine scales contribute to a change of generally less than 15% of the time-averaged precipitation in present climate with a continental North American average of $\sim$5% in both summer and winter seasons. In winter, the largest PAV appears in mountainous regions and in the north part of the continent. In the first case, fine-scale features may be related with the interaction between large-scale

precipitation changes in mid-latitudes (see IPCC (2007)) and the fine-scale topography of the Rocky Mountains.

An important aspect to take into account when estimating the future change of a given climate statistics is related with its uncertainties. As expected, and in agreement with Giorgi (2002), we found that the sampling uncertainty due to interannual variability tends to increase as the spatial scale of the data used to compute climate statistics decreases (not shown).

The analysis also shows that the uncertainty due to interannual variability associated with fine-scale features in the CC signal seems to be much larger in precipitation than in temperature. This has as a consequence that while the RCMs may add fine-scale features to precipitation fields at all time scales, some of this gain may be lost due to the relatively short time periods usually analyzed (i.e., 25 years periods in our case). This result may be of importance for impact and adaptation studies and for this reason deserves further exploration.

Probably the most important limitation of this study is related with the choice of time-averaged quantities in the PAV analysis without explicit consideration of higher order statistics. The larger sensitivity of higher moments to changes in resolution is expected to lead to a larger potential for added value and an increase in the fine-scale signal. It is not clear, however, how the uncertainty associated with these high-order statistics and the derived signal to noise ratio will evolve.

A second important caveat is that the analysis of the "skill" of the RCM-derived PAV quantities was performed only in terms of the sampling uncertainty, with no consideration of others sources of uncertainties such as structural model uncertainties. As a consequence, the number of skilful regions obtained in this study probably corresponds to an upper limit compared to a more complete analysis including other uncertainty sources.

Acknowledgements

This research was done as part of the PhD project of the first author and as a project within the Canadian Regional Climate Modelling and Diagnostics (CRCMD) Network, funded by the Canadian Foundation for Climate and Atmospheric Sciences (CFCAS) and Ouranos. The authors would like to thank Mourad Labassi, Abderrahim Khaled and Georges Huard for maintaining a user-friendly local computing facility, and to the North

American Regional Climate Change Assessment Program (NARCCAP) for providing some of the data used in this paper. NARCCAP is funded by the National Science Foundation (NSF), the U.S. Department of Energy (DOE), the National Oceanic and Atmospheric Administration (NOAA) and the U.S. Enviroumental Protection Agency Office of Research and Development (EPA). Finally, thanks are extended to the Global Environmental and Climate Change Centre (GEC3), funded by the Fonds québécois de la recherche sur la nature et les technologies (FQRNT), for extra financial support.

Appendix 3.A: Added value as a spatial scale issue

This section contains an extension of the analysis presented in the Introduction. Here we will develop a more detailed expression for the AV as a function of spatial scales (see Eq. (3.1)).

Let us assume that we can compute a two-dimensional climate statistics X at very high-resolution based on observations and let us also assume that a perfect spatial decomposition method is available that allows to separate the field according to several spatial scales as follows:

$$X_{OBS} = X^{ls}_{OBS} + X^{ss}_{OBS} + X^{vss}_{OBS}. \tag{3.23}$$

Super-index ls designates the large scales that can be resolved by the GCM, ss denotes the small scales that can be resolved by the RCM and are absent in the GCM, and vss designates the very small scales that cannot be resolved by either the RCM and the GCM.

Before applying the spatial decomposition method to the RCM- and GCM-simulated X, both X_{RCM} and X_{GCM} fields are projected into some very high-resolution grid mesh on which an analysis of observations is available. For simplicity, the projection consists of assigning the value of the RCM and GCM fields on each grid points of the observed high-resolution mesh that fall inside the corresponding RCM and GCM grid box. For this particular projection we have $X^{vss}_{RCM} = X^{ss}_{GCM} = X^{vss}_{GCM} = 0$ and

$$X_{RCM} = X^{ls}_{RCM} + X^{ss}_{RCM}, \tag{3.24}$$

and

$$X_{GCM} = X^{ls}_{GCM}. \tag{3.25}$$

The added value can be simply defined as the difference between the GCM and the RCM errors

$$\begin{aligned} AV &= \overline{(X_{GCM} - X_{OBS})^2} - \overline{(X_{RCM} - X_{OBS})^2} \\ &= MSE_{GCM} - MSE_{RCM}, \end{aligned} \tag{3.26}$$

with $\overline{(\delta)^2} = \frac{1}{N}\sum_{i=0}^{N-1} \delta_i^2$ denoting the average of the square differences between observed

and simulated climate statistics X over all grid points i. Defined in this way, an RCM generates some added value if AV is larger than 0, i.e., if the RCM constitutes a better approximation of the observed field compared to the GCM. Using Eq. (3.23), (3.24) and (3.25) the RCM and GCM mean square errors can be expressed as:

$$\begin{aligned} MSE_{RCM} =& \overline{(X_{RCM} - X_{OBS})^2} \\ =& \overline{(X^{ls}_{RCM} + X^{ss}_{RCM} - (X^{ls}_{OBS} + X^{ss}_{OBS} + X^{vss}_{OBS}))^2} \\ =& \overline{(\epsilon^{ls}_{RCM} + \epsilon^{ss}_{RCM} - X^{vss}_{OBS})^2} \\ =& MSE^{ls}_{RCM} + MSE^{ss}_{RCM} + \overline{(X^{vss}_{OBS})^2} + 2 \cdot \overline{\epsilon^{ls}_{RCM}\epsilon^{ss}_{RCM}} \\ & - 2 \cdot \overline{\epsilon^{ls}_{RCM}X^{vss}_{OBS}} - 2 \cdot \overline{\epsilon^{ss}_{RCM}X^{vss}_{OBS}}, \end{aligned} \tag{3.27}$$

and

$$\begin{aligned} MSE_{GCM} =& \overline{(X_{GCM} - X_{OBS})^2} \\ =& \overline{(X^{ls}_{GCM} - (X^{ls}_{OBS} + X^{ss}_{OBS} + X^{vss}_{OBS}))^2} \\ =& \overline{(\epsilon^{ls}_{GCM} - X^{ss}_{OBS} - X^{vss}_{OBS})^2} \\ =& MSE^{ls}_{GCM} + \overline{(X^{ss}_{OBS})^2} + \overline{(X^{vss}_{OBS})^2} - 2 \cdot \overline{\epsilon^{ls}_{GCM}X^{ss}_{OBS}} \\ & - 2 \cdot \overline{\epsilon^{ls}_{GCM}X^{vss}_{OBS}} + 2 \cdot \overline{X^{ss}_{OBS}X^{vss}_{OBS}}. \end{aligned} \tag{3.28}$$

By replacing Eq. (3.27) and (3.28) in Eq. (3.26) we obtain:

$$AV = AV^{ss} + AV^{ls} + AV^{cov} \tag{3.29}$$

where

$$AV^{ss} = \overline{(X^{ss}_{OBS})^2} - MSE^{ss}_{RCM}, \tag{3.30}$$

$$AV^{ls} = MSE^{ls}_{GCM} - MSE^{ls}_{RCM}, \tag{3.31}$$

and

$$AV^{cov} = 2 \cdot \overline{X^{ss}_{OBS}X^{vss}_{OBS}} - 2 \cdot \overline{\epsilon^{ls}_{RCM}\epsilon^{ss}_{RCM}} + 2 \cdot \overline{\epsilon^{ls}_{RCM}X^{vss}_{OBS}} + 2 \cdot \overline{\epsilon^{ss}_{RCM}X^{vss}_{OBS}}. \tag{3.32}$$

Hence the total AV can be decomposed in a small-scale (AV^{ss}), a large-scale (AV^{ls}) and a covariance (AV^{cov}) part. The term AV^{ss} was already described in the introduction but its relation with X^{ss}_{RCM} is further discussed here. Fig. 3.1 shows the dependence of AV^{ss} as a function of X^{ss}_{RCM} for three different values of X^{ss}_{OBS}. In the case where $X^{ss}_{OBS} = 0$ everywhere, an increase in fine-scale variance of X_{RCM} can only subtract

value by making AV^{ss} negative. Where $X^{ss}_{OBS} \neq 0$, the fine-scale feature of X_{RCM} can add value over the GCM estimation wherever Eq. (3.30) is positive. The maximum AV^{ss} is found when $X^{ss}_{OBS} = X^{ss}_{RCM}$ and is given by $\overline{(X^{ss}_{RCM})^2}$. Furthermore, Fig. 3.1 shows that the term AV^{ss} can potentially increase as X^{ss}_{OBS} increase.

Terms AV^{ls} and AV^{cov} are out of the scope of our analysis. includes the covariances between observed fine- and micro- scales ($2 \cdot \overline{X^{ss}_{OBS} X^{uss}_{OBS}}$), between large- and fine- scale RCM errors ($2 \cdot \overline{\epsilon^{ls}_{RCM} \epsilon^{ss}_{RCM}}$) and between GCM and RCM error terms and observed variables.

CONCLUSION

Nearly 20 years after the first application of limited-area models as climate downscaling tools, nested Regional Climate Models (RCM) have been shown to be technically feasible and to be able to generate small-scale features with the appropriate amplitudes, leading to more realistic patterns of meteorological variables compared to the coarser resolution driving data. From the beginning of RCMs development, a large effort has ensued to assess their capability as climate downscaling tools by evaluating the RCM-simulated climate compared to high-resolution observed data sets. Moreover, particularly in the last decade, important efforts were also devoted to assess the ability of RCMs to improve the simulated climate compared to their driving data in order to identify the value added (AV) by RCMs.

The effort behind the search of AV has not shown univocal gains, suggesting that there is still a need to objectively quantify the RCM's added value. In particular, a clearer identification of variables and climate statistics for which RCM simulations can produce more skilful results would be very useful in the context of a changing climate for which plans for adaptation need information at local and regional scales (Oreskes et al. 2010). Furthermore, a better understanding of the AV issue can help to increase our confidence in downscaling techniques products, thus maybe supporting their use instead of those derived from lower resolution GCMs as mostly done, for example, in the "Regional Climate Projections" chapter of the IPCC Fourth Assessment Report (IPCC 2007).

In the following sections we will give a more detailed description of some of the original contributions of this thesis together with some of the limitations of the methodology and possible research lines to explore in the future.

Potential added value

In this thesis we investigated the potential of RCMs to add value over coarser resolution GCM data. The analysis of PAV can be interpreted as the study of prerequisite conditions that can lead to RCM's added value. The PAV concept is relatively recent (Rauscher et al. 2007; Bielli and Laprise 2007; Separovic et al. 2008; Bresson and Laprise

2009), although it has been implicitly used in a number of articles. For example, Castro et al. (2005) computed the power spectra of some atmospheric variables derived from an RCM simulation and from a reanalysis data set. They found that the RCM provides additional information in small scales, particularly in those regions with strong surface boundary forcing, by showing larger values of fine-scale spectral power in the RCM compared to the NCEP reanalysis. This fine-scale added variability, which they designated as AV, is what we call PAV from the fact that adding variability does not guarantee that there is some effective added value.

Two main contributions are made in this thesis to the PAV issue: first, we provide an objective definition of what we mean by PAV, by establishing a distinction between added value (e.g., added skill) and potential added value (e.g., added variability); and second, as explained in the Introduction and in Appendix A, we separate the PAV in various terms according to whether or not processes can be resolved by the coarser driving data.

We concentrated the analysis in the PAV arising from the direct influence of fine-spatial scales and we presented a framework that is explicitly designated to its study. The PAV framework is based on the study of two necessary conditions. The first condition requires that the climate statistics computed using high-resolution observations must contain non-negligible fine-scale information, i.e. $PAV^{ss}_{OBS} = (X^{ss}_{OBS})^2 > 0$. This condition constitutes an intrinsic feature of the climate system, independent from climate model simulations, and can be viewed as a general requirement for high-resolution climate modelling to be meaningful. Further, as already stated in the Introduction, PAV^{ss}_{OBS} gives a measure of the maximum value that a RCM can add.

The second condition requires that the climate statistics computed using high-resolution RCM simulations must contain non-negligible fine-scale information ($PAV^{ss}_{RCM} = (X^{ss}_{RCM})^2 > 0$). Even if the PAV^{ss}_{RCM} measure can give an erroneous estimation of the real PAV, it is still an interesting and useful quantity because allows to estimate PAV in those cases where high-resolution observations of the variable of interest are not available.

The PAV framework presented in this thesis allows to study both conditions in an independent way, allowing to estimate the relative influence of fine-scale features in a given climate statistics. When evaluating PAV^{ss}_{RCM}, the framework is based on two hypotheses: first, that large-scale climate statistics derived from a coarse-resolution model are similar to those derived from the aggregation of high-resolution results into

a coarse-resolution grid mesh. This hypothesis, partially assessed in Di Luca (2009) and discussed in Sect. 1.2.3, needs to be further explored by comparing the large-scale representation of a variety of variables using an ensemble of RCM and GCM simulations.

The second hypothesis is to consider that the relative importance of fine and large scales is well reproduced in RCMs compared to observations. As shown in Section 1.5, this seems to be a reasonable hypothesis for a complex variable such as precipitation, although some differences between PAV^{ss}_{RCM} and PAV^{ss}_{OBS} appear particularly in warm season and mountainous regions. No attempts were made to test this hypothesis for the temperature variable, but we are confident that RCMs reproduce relatively well the real PAV or, at least, their regional and seasonal variations. Ultimately, however, this speculation should also be confirmed and quantified.

PAV in present climate

The PAV framework was applied to the precipitation and temperature variables derived from an ensemble of RCM simulations and, in the precipitation case, using also high-resolution reanalysis and gridded observed data sets. Concluding remarks for precipitation and temperature were presented in Sections 1.6 and 2.6, respectively, and here we will only highlight some differences between PAV results in both variables.

A main difference between temperature and precipitation is related with the magnitude of the PAV. The use of different methodologies to assess PAV in both variables prevents to perform a direct comparison between them. In order to quantitatively compare PAV results for both variables, the variance decomposition method as used in Chapter 2 for the temperature variable was applied to the time-varying precipitation field. Results (not shown) suggest that the relative influence of RCM contributions to the total variance is much larger in precipitation than in temperature. For example, for 3-hourly time varying fields, the ensemble-mean domain average rPAV in cold (warm) season is ~5% (~16%) for temperature and ~23% (~40%) for precipitation.

Another fundamental difference between temperature and precipitation is related to the different mechanisms that produce PAV. The main source of PAV in near-surface temperature is associated with the presence of surface forcings, mainly through the influence of land-sea contrast but also due to fine-scale topographic features. For example, the different heat capacity of water and land surfaces can lead to differences in surface temperature seasonal values (i.e., stationary PAV) and also in sub-diurnal, diurnal and

synoptic variability (i.e., transient PAV).

In the case of precipitation, the dominant source of PAV is related with high-temporal resolution fine-scale atmospheric processes (e.g., hydrodynamics instabilities) that tend to develop almost independently of surface forcings. This is confirmed by the fact that the largest $rPAV$ precipitation values appear in warm season and low latitudes (not shown) for high-temporal resolution data (e.g., 3-hourly). Regions of complex topography induce an extra-component of $rPAV$ independently of season or temporal scale considered. Its relative importance is larger for long-term mean quantities and cold season due to the relatively minor importance of transient PAV sources.

Results point out that the potential of RCMs to add value can be limited when considering climate statistics computed using time-averaged values for both variables. For example, a large number of regions show $rPAV$ values smaller than 10-15% for both precipitation and temperature when considering 16-day averaged periods time series in both warm and cold seasons.

A main limitation associated with our methodology is that it does not allow identifying the processes and phenomena that are actually responsible for the fine-scale variability. Particularly, simply by looking at the relative importance of fine-scale variability, one cannot assert about the complexity of the processes leading to the PAV (e.g., linear vs. non-linear). For example, the distinct response of water and land surfaces to the diurnal variation of solar radiation can lead to much larger PAV values than those resulting from land-sea breeze effects, but the representation of the latter effect is much more challenging than the former. This can have an impact when comparing the PAV generated by a RCM and other simpler downscaling techniques (DTs).

Further, some phenomena can induce modest fine-scale variability according to our PAV measures but could have important societal and/or economical impacts. This suggests that PAV studies, at least those using similar methodologies as here, should be complemented with other analyses aimed at understanding the sources of variability by including an evaluation at the process level.

PAV in the climate-change signal

The PAV concept is particularly interesting when considering the problem of ascertain whether increasing model resolution improves climate projections. For future climate

simulations, there is no way to decide about the existence of added value in RCM simulations and we can only estimate the PAV.

As discussed in Section 2.5, the problem of looking for the potential of RCMs to add value in future climate simulations is not directly related with the future climate itself but with the climate-change (CC) signal (i.e., the difference between future and present climate statistics). The difference of considering PAV of climate statistics or climate-change statistics may appear subtle but can have important implications. For example, a large part of the added value in the temperature variable coming from stationary forcings such as fine-scale topography and coastlines can be mostly filtered out when computing the difference between future and present climate.

In Section 2.5, we briefly studied the PAV in future mean-temperature change by computing the ratio between the spatial standard deviation of the fine-scale CC signal and the large-scale climate-change signal. The analysis shows that the fine-scale variability of the CC signal is generally very small compared to its large-scale component, suggesting that little AV can be expected for the time-averaged temperature. The largest values of $rPAV$ appear near coastline regions related with the differential future warming in land and water surfaces.

A more comprehensive study should be undertaken in order to better understand the CC PAV. The use of higher order climate statistics (e.g., 95th percentiles) but mainly the use of other variables (e.g., precipitation) is expected to show more CC PAV. Maybe more important, no attempt was done here to assess the robustness of CC fine-scale features. As pointed out by Giorgi (2002), the interannual variability of some atmospheric variables (e.g., precipitation) shows a very strong sensitivity to changes in spatial scales. In particular, interannual variability tends to increase at more refined spatial scales leading to a deterioration of the signal to noise ratio. That is, the CC PAV study should include a discussion about the relative importance of fine scales in the CC signal but also an estimation of the natural variability of the system and the influence on fine-scale climate predictability.

Extended added value framework

The definition of necessary conditions for $AV > 0$ can be used to developed a series of evaluation steps in order to decide on the existence and sources of added value in RCM simulations. This, in turn, should help to decide on the relevance of using RCMs,

direct GCMs output or maybe other simpler and computationally cheaper downscaling techniques (e.g., geo-statistical post-processing), depending on the problem at hand.

Figure 4.1 shows a flow chart describing a possible AV^{ss} testbed resulting from the inclusion of a PAV framework type. To illustrate the chart, let us consider the case where high-resolution observations are available (left panel in Fig. 4.1). The first step when considering AV^{ss} consists in verifying whether the climate statistics of interest derived from observations contains non-negligible fine-scale information (i.e., if $PAV^{ss}_{OBS} > 0$). In the case that $PAV^{ss}_{OBS} = 0$, neither a RCM nor any other DT can add value at small scales over the GCM, so we should either check for PAV^{ls} or simply use the GCM output. If $PAV^{ss}_{OBS} > 0$ then we should ask if the RCM-derived statistics contain some fine-scale information (i.e., if $PAV^{ss}_{RCM} > 0$). Again, if the answer is no, then we should inquire about the existence of PAV^{ls} or use the GCM estimation of the climate statistics. If there exists some PAV^{ss}_{RCM}, the next step is to check whether there is also some AV^{ss}. Finally, in the case that there is some AV^{ss}, we should compare the RCM's AV^{ss} with results obtained using other cheaper DTs such as statistical and/or empirical downscaling techniques. Only when cheaper DTs cannot account for the AV^{ss} we should prioritise the use of costly RCM simulations.

In the case where high-resolution observations are not available, the quantity PAV^{ss}_{OBS} cannot be computed and we can only estimate the maximum AV using PAV^{ss}_{RCM} (right panel in Fig. 4.1). If $PAV^{ss}_{RCM} = 0$ then the RCM cannot add value to the coarser GCM. In the case that $PAV^{ss}_{RCM} > 0$ we can ask whether or not this PAV can be generated using other simple DTs by comparing PAV^{ss}_{RCM} with PAV^{ss}_{DT} as done in Section 2.4.3.

Note that this flow chart can be equally used to evaluate the AV generated by other techniques used to produce high-resolution results, such as high-resolution AGCM in time-slice mode or statistical/empirical DTs. Also, a similar set of steps may be design to evaluate the AV coming from the large-scale component of the climate statistics of interest (AV^{ls}).

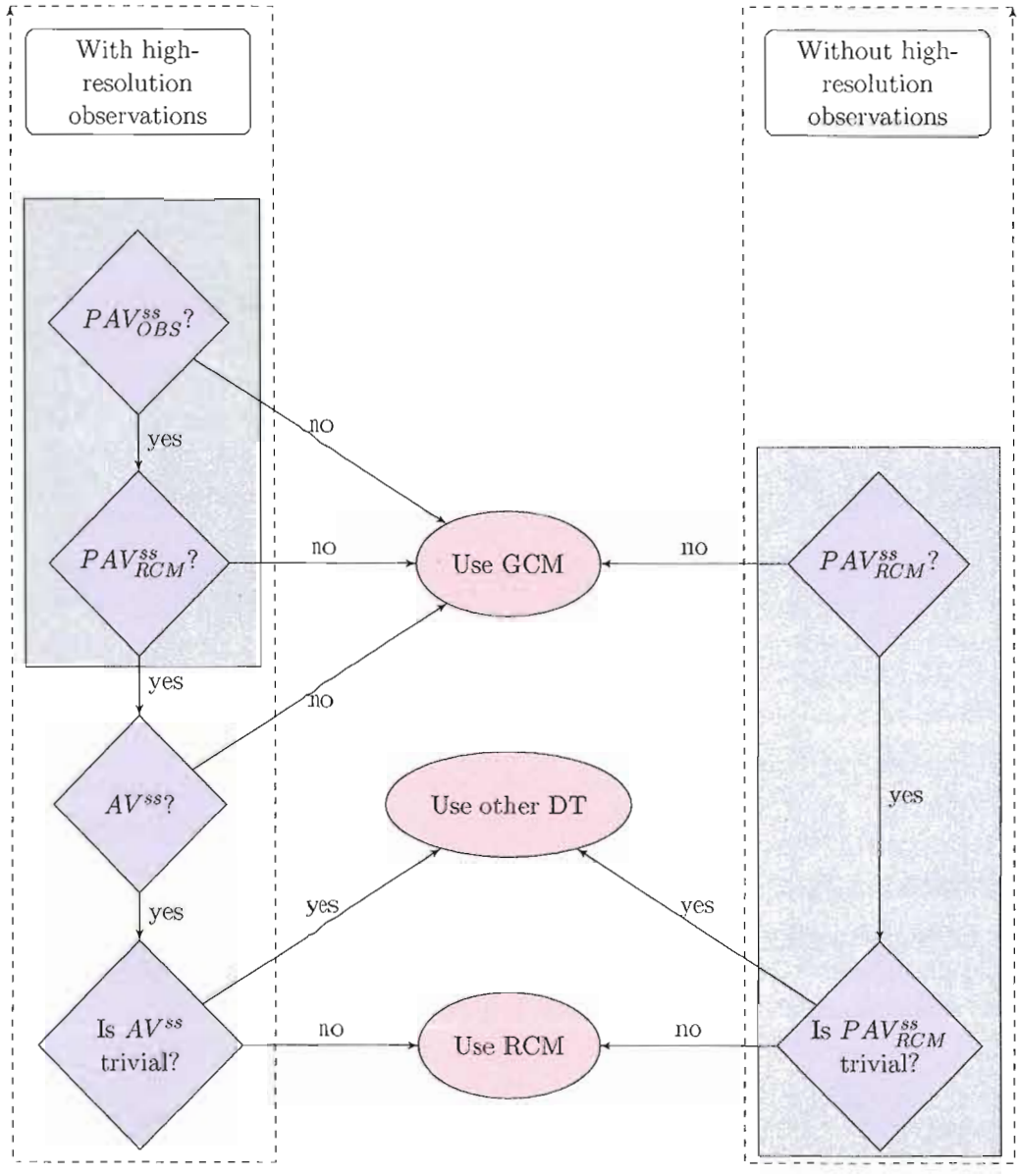

Figure 4.1 Flow chart describing several steps in order to decide about the generation of small scales added value in RCM simulations. Grey shaded areas include steps partially covered in this thesis.

REFERENCES

Bärring, L. and Laprise, R., editors (2005). *High-resolution climate modelling: Assessment, added value and applications*. High-resolution Climate Modelling: Assessment, Added Value and Applications Extended Abstracts of a WMO/WCRP-sponsored Regional-scale Climate Modelling Workshop. Lund University electronic reports in physical geography, Lund, Sweden.

Bielli, S. and Laprise, R. (2007). Time mean and variability of the scale decomposed atmospheric water budget in a 25-year simulation of the Canadian regional climate model over North America. *Clim Dyn*, 29:763–777.

Boer, G. and Lazare, M. (1988). Some results concerning the effect of horizontal resolution and gravity-wave drag on simulated climate. *J Clim*, 1:789–806.

Boville, B. (1991). Sensitivity of simulated climate to model resolution. *J Clim*, 4:469–485.

Boyle, J. (1993). Sensitivity to dynamical quantities to horizontal resolution for a climate simulation using the ECMWF (cycle 33) model. *J Clim*, 6:796–815.

Bresson, R. and Laprise, R. (2009). Scale-decomposed atmospheric water budget over north america as simulated by the Canadian regional climate model for current and future climates. *Clim Dyn*, 36(1-2):365–384.

Castro, C. L., Pielke, R. A., and Leoncini, G. (2005). Dynamical downscaling: An assessment of value added using a regional climate model. *J Geophys Res*, 110:D05108.

Caya, D. and Laprise, R. (1999). A semi-implicit semi-lagrangian regional climate model: The Canadian RCM. *Mon Wea Rev*, 127(3):341–362.

Chen, C.-T. and Knutson, T. (2008). On the verification and comparison of extreme rainfall indices from climate models. *J Clim*, 21:1605–1621.

Christensen, J., Hewitson, B., Busuioc, A., Chen, A., Gao, X., Held, I., Jones, R., Kolli, R., Kwon, W.-T., Laprise, R., Rueda, V. M., Mearns, L., Menéndez, C., Räisänen, J., Rinke, A., Sarr, A., and Whetton, P. (2007). Regional climate projections. contribution of working group i to the fourth assessment report of the intergovernmental panel on climate change. In Solomon, S., Qin, D., Manning, M., Chen, Z., Marquis, M., Averyt, K., Tignor, M., and Miller, H., editors, *Climate Change 2007: The Physical Science Basis*, pages 847–940. Cambridge University Press, Cambridge, United Kingdom and New York, NY, USA.

Collins, W. D., Bitz, C. M., Blackmon, M. L., Bonan, G. B., Bretherton, C. S., Carton, J. A., Chang, P., Doney, S. C., Hack, J. J., Henderson, T. B., Kiehl, J. T., Large, W. G., McKenna, D. S., Santer, B. D., and Smith, R. D. (2006). The community climate system model version 3 (ccsm3). *J Clim*, 19:2122–2143.

Daly, C., Neilson, R., and Phillips, D. (1994). A statistical-topographic model for mapping climatological precipitation over mountainous terrain. *J Appl Meteor*, 33:140–158.

De Sales, F. and Xue, Y. (2011). Assessing the dynamic downscaling ability over South America using the intensity-scale verification technique. *Int J Climatol*, 31:1205–1221.

Denis, B., Laprise, R., Caya, D., and Côté, J. (2002). Downscaling ability of one-way nested regional climate models: The big-brother experiment. *Clim Dyn*, 18:627–646.

Déqué, M. and Somot, S. (2008). Extreme precipitation and high resolution with aladin. *Idöjaras Q J Hung Meteorol Serv*, 112(3-4):179–190.

Déqué, M., Somot, S., Sanchez-Gomez, E., Goodess, C. M., Jacob, D., Lenderink, G., and Christensen, O. B. (2011). The spread amongst ensembles regional scenarios: regional climate models, driving general circulation models and interannual variability. *Clim Dyn*.

Di Luca, A. (2009). Added value in the Canadian regional climate model: Comparison of precipitation at the scales of the Canadian global climate model. Master, Université du Québec à Montréal.

Di Luca, A., de Elía, R., and Laprise, R. (2011a). Potential for added value in precipitation simulated by high-resolution nested regional climate models and observations. *Clim Dyn.*

Di Luca, A., de Elía, R., and Laprise, R. (2011b). Potential for added value in RCM-simulated surface temperature. Submitted to Clim Dyn.

Diaconescu, E. P., Laprise, R., and Sushama, L. (2007). The impact of lateral boundary data errors on the simulated climate of a nested regional climate model. *Clim Dyn*, 28(4):333–350.

Dickinson, R., Errico, R., Giorgi, F., and Bates, G. (1989). A regional climate model for the western United States. *Clim. Change*, 15:383–422.

Duffy, P. B., Arritt, R. W., Coquard, J., Gutowski, W., Han, J., Iorio, J., Kim, J., Leung, L.-R., Roads, J., and Zeledon, E. (2006). Simulations of present and future climates in the western United States with four nested regional climate models. *J Clim*, 19:873–895.

Durman, C., Gregory, J., Hassell, D., Jones, R., and Murphy, J. (2001). A comparison of extreme European daily precipitation simulated by a global and a regional climate model for present and future climates. *Quart. J. R. Meteor. Soc.*, 127:1005–1015.

Dutton, J. (1976). *The Ceaseless Wind.* McGrawHill, New York, USA.

Efron, B. and Tibshirani, R. (1993). *An introduction to the bootstrap*, volume 57 of *Monographs on Statistics and Applied Probability.* Chapman and Hall., London.

Feser, F. (2006). Enhanced detectability of added value in limited-area model results separated into different spatial scales. *Mon Wea Rev*, 134:2180–2190.

Feser, F., Rockel, B., von Storch, H., Winterfeldt, J., and Zahn, M. (2011). Regional climate models add value to global model data: A review and selected examples. *Bull Am Meteorol Soc*.

Feser, F. and von Storch, H. (2005). Spatial two-dimensional discrete filters for limited area model evaluation purposes. *Mon Wea Rev*, 133:1774–1786.

Flato, G. and Boer, G. (2001). Warming asymmetry in climate change simulations. *Geophys. Res. Lett.*, 28:195–198.

Foley, A. (2010). Uncertainty in regional climate modelling: A review. *Progress in Physical Geography*, 34(5):647–670.

Gao, Y., Vano, J. A., Zhu, C., and Lettenmaier, D. P. (2011). Evaluating climate change over the colorado river basin using regional climate models. *J. Geophys Res*, page in press.

GFDL Global Atmospheric Model Development Team (2004). The new GFDL global atmosphere and land model am2–lm2: Evaluation with prescribed sst simulations. *Journal of Climate*, 17(24):4641–4673.

Giorgi, F. (2002). Dependence of the surface climate interannual variability on spatial scale. *Geophys Res Lett*, 29(23):16.1–16.4.

Giorgi, F. and Bates, G. (1989). The climatological skill of a regional model over complex terrain. *Mon Wea Rev*, 117:2325–2347.

Giorgi, F., Christensen, J., Hulme, M., von Storch, H., Whetton, P., Jones, R., Mearns, L., Fu, C., Arritt, R., Bates, B., Benestad, R., Boer, G., Buishand, A., Castro, M., Chen, D., Cramer, W., Crane, R., Crossly, J., Dehn, M., Dethloff, K., Dippner, J., Emori, S., Francisco, R., Fyfe, J., Gerstengarbe, F., Gutowski, W., Gyalistras, D., Hanssen-Bauer, I., Hantel, M., Hassell, D., Heimann, D., Jack, C., Jacobeit, J., Kato, H., Katz, R., Kauker, F., Knutson, T., Lal, M., Landsea, C., Laprise, R., Leung, L., Lynch, A., May, W., McGregor, J., Miller, N., Murphy, J., Ribalaygua, J., Rinke,

A., Rummukainen, M., Semazzi, F., Walsh, K., Werner, P., Widmann, M., Wilby, R., Wild, M., and Xue, Y. (2001). Regional climate information- evaluation and projections. In Houghton, J. T., editor, *Climate Change 2001: The Scientific Basis. Contribution of Working Group I to the Third Assessment Report of the Intergovernmental Panel on Climate Change*, pages 583–638. Cambridge University Press, Cambridge, United Kingdom and New York, USA.

Giorgi, F., Jones, C., and Asrar, G. (2009). Addressing climate information needs at the regional level: The CORDEX framework. *WMO Bulletin*, 58:175–183.

Giorgi, F., Marinucci, M., and Bates, G. (1993). Development of a second generation regional climate model (regcm2) i: Boundary layer and radiative transfer processes. *Mon Wea Rev*, 121:2794–2813.

Giorgi, F. and Marinucci, M. R. (1996). An investigation of the sensitivity of simulated precipitation to model resolution and its implications for climate studies. *Mon. Wea. Rev.*, 124:148–166.

Giorgi, F. and Mearns, L. (1991). Approaches to the simulation of regional climate change: A review. *Rev. Geophys.*, 29:191–216.

Giorgi, F., Mearns, L., Shields, C., and McDaniel, L. (1998). Regional nested model simulations of present day and 2xCO2 climate over the central great plains of the United States. *Clim. Change*, 40:457–493.

Gordon, C., Cooper, C., Senior, C., Banks, H., Gregory, J., Johns, T., Mitchell, J., and Wood, R. (2000). The simulation of sst, sea ice extents and ocean heat transports in a version of the Hadley Centre coupled model without flux adjustments. *Clim Dyn*, 16:147–168.

Grell, G., J. D. and Stauffer, D. R. (1993). *A description of the fifth-generation Penn State/NCAR mesoscale model (MM5)*. National Center for Atmospheric Research, ncar/tn-398 1 ia edition.

Gutowski, W., Kozak, K., Arritt, R., Christensen, J., Patton, J., and Takle, E. (2007). A possible constraint on regional precipitation intensity changes under global warming. *J Hydrometeorol*, 8:1382–1396.

Harris, D., Foufoula-Georgiou, E., Droegemeier, K., and Levit, J. (2001). Multiscale statistical properties of a high-resolution precipitation forecast. *J Hydrometeorol*, 2:406–418.

Higgins, R., Silva, V., Kousky, V., and Shi, W. (2008). Comparison of daily precipitation statistics for the United States in observations and in the NCEP climate forecast system. *J Clim*, 21:5993–6014.

Higgins, R. W., Shi, W., Yarosh, E., and Joyce, R. (2000). Improved United States precipitation quality control system and analysis. Technical report, NCEP/Climate Prediction Center Atlas 7, National Weather Service, NOAA, U.S. Department of Commerce.

Howell, J. and Mahrt, L. (1997). Multiresolution flux decomposition. *Bound Layer Meteorol*, 83:117–137.

IPCC (2007). *Contribution of Working Group I to the Fourth Assessment Report of the Intergovernmental Panel on Climate Change*. Cambridge University Press, Cambridge, United Kingdom and New York, NY, USA.

Jones, R. G., Noguer, M., Hassel, D. C., Hudson, D., Wilson, S. S., Jenkins, G. J., and Mitchell, J. F. B. (2004). Generating high resolution climate change scenarios using precis. Technical report, Met Office Hadley Centre.

Juang, H.-M. H., Hong, S.-Y., and Kanamitsu, M. (1997). The NCEP regional spectral model: an update. *Bull Am Meteorol Soc*, 78:2125–2143.

Kanamitsu, M., Ebisuzaki, W., Woollen, J., Yang, S.-K., Hnilo, J., Fiorino, M., and Potter, G. (2002). NCEP-DOE AMIP-II reanalysis (R-2). *Bull Am Meteorol Soc*, 83(11):1631–1643.

Kanamitsu, M. and Kanamaru, H. (2007). Fifty-seven-year California Reanalysis Downscaling at 10 km (CaRD10). Part i: System detail and validation with observations. *J Clim*, 20(22):5553–5571.

Knutti, R. (2008). Should we believe model predictions of future climate change ? *Philosophical Transactions of the Royal Society*, 366:4647–4664.

Laprise, R. (2005). A foreword to "High-resolution climate modelling: Assessment, added value and applications". In Bärring, L. and Laprise, R., editors, *High-resolution Climate Modelling: Assessment, Added Value and Applications Extended Abstracts of a WMO/WCRP-sponsored Regional-scale Climate Modelling Workshop*, pages 12–16, Lund, Sweden. Lund University electronic reports in physical geography.

Laprise, R., de Elía, R., Caya, D., Biner, S., Lucas-Picher, P., Diaconescu, E., Leduc, M., Alexandru, A., and Separovic, L. (2008). Challenging some tenets of regional climate modelling. *Meteor Atmos Phys*, 100, Special Issue on Regional Climate Studies(20):3–22.

Laprise, R., Jones, R., Kirtman, B., von Storch, H., and Wergen, W. (2002). Atmospheric regional climate models (RCMs): A multiple purpose tool? Technical report, Report of the Joint WGNE/WGCM ad hoc Panel on Regional Climate Modelling.

Leduc, M. and Laprise, R. (2009). Regional climate model sensitivity to domain size. *Clim Dyn*, 32(6):833–854.

Lenderink, G., van Ulden, A., van den Hurk, B., and Keller, F. (2007). A study on combining global and regional climate model results for generating climate scenarios of temperature and precipitation for the Netherlands. *Clim Dyn*, 29:157–176.

Leung, L., Done, J., Dudhia, J., Henderson, T., Vertenstein, M., and Kuo, B. (2005). Preliminary results of WRF for regional climate simulations. In *Workshop Research Needs and Directions of Regional Climate Modeling Using WRF and CCSM*, number 6, pages 833–854. Available from http://www.cs.berkeley.edu/~luca/cs278/notes/lecture09.pdf, Boulder, CO.

Liang, X.-Z., Kunkel, K. E., Meehl, G. A., Jones, R. G., and Wang, J. X. L. (2008). Regional climate models downscaling analysis of general circulation models present climate biases propagation into future change projections. *Geophys. Res. Leit.*, 35:L08709.

Lin, Y., Mitchell, K., Rogers, E., Baldwin, M., and DiMego, G. (1999). Test assimilations of the real-time, multisensor hourly precipitation analysis into the NCEP eta model. In *Eighth Conf. on Mesoscale Meteorology*, pages 341–344, Boulder, CO. Amer. Meteor. Soc.

Mallat, S. G. (1989). The theory of multiresolution signal decomposition: The wavelet representation. *IEEE Trans. Pattern Anal. Machine Intell.*, 7:674–693.

Maurer, E., Wood, A., Adam, J., Lettenmaier, D., and Nijssen, B. (2002). A long-term hydrologically-based data set of land surface fluxes and states for the conterminous United States. *J Clim*, 5(22):3237–3251.

Mearns, L., Gutowski, W., Jones, R., Leung, R., McGinnis, S., Nuñes, A., and Qian, Y. (2009). A regional climate change assessment program for north america. *Eos Trans. AGU*, 90(36):311.

Mesinger, F. (2000). Numerical methods: The arakawa approach, horizontal grid, global, and limited-area modeling. In Randall, D. A., editor, *General Circulation Model Development*, pages 373–419. Academic Press, San Diego, California, USA.

Mesinger, F., Brill, K., Chuang, H.-Y., DiMego, G., and Rogers, E. (2002). Limited area predictability: Can "upscaling" also take place? Technical Report 32, 5.30-5.31, Research Activities in Atmospheric and Oceanic Modelling, WMO, CAS/JSC WGNE, Geneva.

Mesinger, F., DiMego, G., Kalnay, E., Mitchell, K., Shafran, P., Ebisuzaki, W., Jovic, D., Woollen, J., Rogers, E., Berbery, E., Ek, M., Fan, Y., Grumbine, R., Higgins, W., Li, H., Lin, Y., Manikin, G., Parrish, D., and Shi, W. (2006). North american regional reanalysis. *Bull Am Meteorol Soc*, 87:343–360.

Oreskes, N., Stainforth, D., and Smith, L. (2010). Adaptation to global warming: Do climate models tell us what we need to know? *Philosophy of Science*, 77(5):1012–1028.

Orlanski, I. (1975). A rational subdivision of scales for atmospheric processes. *Bull Am Meteorol Soc*, 56(5):527–530.

Pielke, R., Wlako, R., Steyaert, L., Vidale, P., Liston, G., and Lyons, W. (1999). The influence of anthropogenic landscape changes on weather in south Florida. *Mon Wea Rev*, 127:1663–1673.

Pielke, R. A. (1991). A recommended specific definition of "resolution". *Bull Am Meteorol Soc*, 72(12):1914.

Pope, V. and Stratton, R. (2002). The processes governing horizontal resolution sensitivity in a climate model. *Clim Dyn*, 19:211–236. 10.1007/s00382-001-0222-8.

Prömmel, K., Geyer, B., Jones, J., and Widmann, M. (2010). Evaluation of the skill and added value of a reanalysis-driven regional simulation for alpine temperature. *Int J Climatol*, 30:760–773.

Randall, D., Wood, R., Bony, S., Colman, R., Fichefet, T., Fyfe, J., Kattsov, V., Pitman, A., Shukla, J., Srinivasan, J., Stouffer, R., Sumi, A., and Taylor, K. (2007). Climate models and their evaluation. In Solomon, S., Qin, D., Manning, M., Chen, Z., Marquis, M., Averyt, K., Tignor, M., and Miller, H., editors, *Climate Change 2007: The Physical Science Basis. Contribution of Working Group I to the Fourth Assessment Report of the Intergovernmental Panel on Climate Change*. Cambridge University Press, Cambridge, United Kingdom and New York, NY, USA.

Rauscher, S., Seth, A., Liebmann, B., Qian, J.-H., and Camargo, S. (2007). Regional climate model-simulated timing and character of seasonal rains in South America. *Mon Wea Rev*, 135:2642–2657.

Rockel, B., Arritt, R., Rummukainen, M., and Hense, A. (2010). The 2nd Lound regional-scale climate modelling workshop. *Meteorol. Z.*, 19(3):223–224.

Roebber, P. J. and Gyakum, J. R. (2003). Orographic influences on the mesoscale structure of the 1998 ice storm. *Mon Wea Rev*, 131(1):27–50.

Rummukainen, M. (2010). State-of-the-art with regional climate models. *WIRE (Wiley Interdisciplinary Reviews: Climate Change) Advanced Review*, 1(1):82–96.

Sanchez-Gomez, E., Somot, S., and Déqué, M. (2009). Ability of an ensemble of regional climate models to reproduce weather regimes over Europe-Atlantic during the period 1961-2000. *Clim Dyn*, 33:723–736.

Seneviratne, S., Corti, T., Davin, E., Hirschi, M., Jaeger, E., Lehner, I., Orlowsky, B., and Teuling, A. (2010). Investigating soil moisture-climate interactions in a changing climate: A review. *Earth-Science Reviews*, 99(3-4):125–161.

Separovic, L., de Elía, R., and Laprise, R. (2008). Reproducible and irreproducible components in ensemble simulations with a regional climate model. *Mon. Wea. Rev.*, 136:4942–4961.

Seth, A., Rauscher, S., Camargo, S., Qian, J.-H., and Pal, J. (2007). Regcm regional climatologies for South America using reanalysis and ECHAM model global driving fields. *Clim Dyn*, 28:461–480.

Shepard, D., editor (1984). *Computer mapping: The SYMAP interpolation algorithm.* Spatial Statistics and Models. D. Reidel Publishing Company, Dordrecht, Netherlands.

Sotillo, M., Aznar, R., and Valero, F. (2005). The 44-year mediterranean hipocas wind database: A useful tool to analyse offshore extreme wind events from a long-term regional perspective. *Coast Eng*, 55(11):930–943.

Stull, R. (1988). *An Introduction to Boundary Layer Meteorology.* Kluwer Acad Publ, Morwell, USA.

Suklitsch, M., Gobiet, A., Truhetz, H., Awan, N. K., Göttel, H., and Jacob, D. (2011).

Error characteristics of high resolution regional climate models over the alpine area. *Clim Dyn*, 37(1-2):377–390.

Trenberth, K., Dai, A., Rasmussen, R., and Parsons, D. (2003). The changing character of precipitation. *Bull Am Meteorol Soc*, 84:1205–1217.

Veljovic, K., Rajkovic, B., Fennessy, M. J., Altshuler, E. L., and Mesinger, F. (2010). Regional climate modeling: Should one attempt improving on the large scales? Lateral boundary condition scheme: Any impact? *Meteorol Z*, 19(3):237–246.

Vickers, D. and Mahrt, L. (2002). The cospectral gap and turbulent flux calculations. *J. of Atmospheric and Ocean. technology*, 20:660–672.

von Storch, H. (2005). Models of global and regional climate. In Anderson, M., editor, *Encyclopedia of Hydrological Sciences, Part 3. Meteorology and Climatology*, pages 478–490. J. Wiley, Chichester, West Sussex, England ; Hoboken, NJ.

von Storch, H. and Zwiers, F. (1999). *Statistical Analysis in Climate Research*. Cambridge Univesity Press.

Wang, Y., Leung, L., McGregor, J., Lee, D.-K., Wang, W.-C., Ding, Y., and Kimura, F. (2004). Regional climate modeling: Progress, challenges, and prospects. *J. Meteor. Soc. Japan*, 82(6):1599–1628.

Wilby, R., Charles, S., Zorita, E., Timbal, B., Whetton, P., and Mearns, L. (2004). Guidelines for use of climate scenarios developed from statistical downscaling methods. Technical report, IPCC Task Group on data and scenario support for Impact and Climate Analysis (TGICA).

Wilks, D. (2010). Sampling distributions of the Brier score and Brier skill score under serial dependence. *Q J R Meteorol Soc*, 136:2109–2118.

Winterfeldt, J., Geyer, B., and Weisse, R. (2011). Using quikscat in the added value assessment of dynamically downscaled wind speed. *Int J Climatol*, 31:1028–1039.

Winterfeldt, J. and Weisse, R. (2009). Assessment of value added for surface marine wind speed obtained from two regional climate models. *Mon Wea Rev*, 137:2955–2965.

Zepeda-Arce, J., Foufoula-Georgiou, E., and Droegemeier, K. K. (2000). Space-time rainfall organization and its role in validating quantitative precipitation forecasts. *J Geophys Res*, 105:10129–10146.